DIGITAL TRANSMISSION THROUGH SATELLITE CHANNELS: PERFORMANCE ANALYSIS AND RECEIVER SYNTHESIS

by

(C) NIMAL EKANAYAKE, B.Sc., M.Sc.

A Thesis

Submitted to the School of Graduate Studies

in Partial Fulfilment of the Requirements

for the Degree

Doctor of Philosophy

McMaster University

September , 1979

DIGITAL TRANSMISSION THROUGH SATELLITE CHANNELS

DOCTOR OF PHILOSOPHY (1979)
(Electrical Engineering)

McMASTER UNIVERSITY
Hamilton, Ontario

TITLE: Digital Transmission Through Satellite Channels: Performance Analysis and Receiver Sythesis

AUTHOR: Mudiyanselage Nimal Ekanayake
B.Sc. (University of Ceylon)
M.Sc. (University of London)

SUPERVISOR: Dr. D.P. Taylor

NUMBER OF PAGES: xiv,176

ABSTRACT

This thesis examines the transmission and reception of coherent phase shift keyed signals (CPSK) over band-limited nonlinear satellite channels in a noisy environment. First, we analyzed the performance of M-ary CPSK signals transmitted over band-limited nonlinear satellite channels in the presence of uplink additive Gaussian noise and downlink additive Gaussian noise. An expression for evaluating the exact probability of error is derived for the case of a general satellite transponder model and then this expression is applied to specific transponder models to obtain numerical results.

Secondly, we have derived bounds on the symbol error probability for binary CPSK signals transmitted over band-limited satellite channels in the presence of uplink and downlink thermal noise. These bounds can be evaluated using previously known error probabilities for wideband channels. Numerical results are evaluated and compared with those results computed using the exact error probability expressions. The advantage of these bounds is that they can be evaluated knowing only the peak value and variance of the intersymbol interference (ISI), and the bounds appear to

yield reasonably accurate approximations to the exact error probabilities when ISI is not too large. Also, a computationally efficient technique is derived to evaluate the error probabilities for binary CPSK signals transmitted over a wideband piece-wise smooth saturating channels.

Finally, the optimal reception of binary CPSK signals over band-limited nonlinear satellite channels is investigated. A receiver structure, similar to a decision feedback receiver for linear channels, is derived to combat the ISI effect. The performance is evaluated by computer simulation techniques and it is shown that the receiver performs significantly better than the single sample sign detector. Also, it is shown that the single sample sign detector yields optimum decisions for wideband hard-limited channels.

ACKNOWLEDGEMENTS

I gratefully acknowledge the assistance and guidance given by Dr. D.P. Taylor during the course of my studies and preparation of this thesis.

Also, sincere acknowledgement is extended to Dr. J.B. Anderson, Dr. S.S. Haykin and Dr. C.R. Riehm for serving in the supervisory committee. Thanks are also due to Miss P. Dillon of the Word Processing Centre for typing this thesis.

Last, but not least, I wish to extend my great appreciation to my wife, Malini, for the innumerable sacrifices she made during my studies at McMaster University and to my son, Namal, for the many sacrifices he made unknowingly.

TABLE OF CONTENTS

TABLE OF CONTENTS (continued)

TABLE OF CONTENTS (continued)

LIST OF ILLUSTRATIONS

LIST OF ILLUSTRATIONS (continued)

LIST OF ILLUSTRATIONS (continued)

LIST OF TABLES

LIST OF PRINCIPAL SYMBOLS

Symbol	Representation
AM-AM	Amplitude modulation to amplitude modulation
AM-PM	Amplitude modulation to phase modulation
BW	Bandwidth
b_m	Coefficients of the power series expansion
CPSK	Coherent phase shift keying
CR/BTR	Carrier recovery and bit timing recovery
CSC	Common signalling channel
CNR	Carrier power to noise power ratio
DA	Demand assignment
DASS	Demand assignment signalling and switching
DSI	Digital signal interpolation
EIRP	Effective isotropic radiated power
E[.]	Expectation with respect to a random variable
erf(.)	Error function
erfc(.)	Complementary error function
FM	Frequency modulation
FDM	Frequency division multiplex
FDMA	Frequency division multiple access
${}_1F_1(.,.;.)$	Confluent Hypergeometric function
f(.)	AM-AM conversion
HPA	High power amplifier
$H_n(.)$	n th order Hermite polynomial
IF	Intermediate frequency
ISI	Intersymbol interference
$I_n(.)$	n th order modified Bessel function
MA	Multiple access
N_o^u	Uplink thermal noise spectral density
N_o^d	Downlink thermal noise spectral density

LIST OF PRINCIPAL SYMBOLS (continued)

Symbol	Representation
$n_c^u(t)$	Inphase component of uplink thermal noise
$n_s^u(t)$	Quadrature component of uplink thermal noise
$n_c^d(t)$	Inphase component of downlink thermal noise
$n_s^d(t)$	Quadrature component of downlink thermal noise
$p(.)$	Probability density function
QPSK	Quadrature phase shift keying
RF	Radio frequency
SPADE	Single channel per carrier, pulse code modulation, multiple access, demand assignment equipment
TDMA	Time division multiple access
UW	Unique word
$\Gamma(.)$	Gamma function

CHAPTER 1

INTRODUCTION

1.1 A Brief Introduction to Satellite Communication Techniques [1-9]

In this thesis we are concerned with the performance analysis and receiver synthesis for digitally phase modulated signals transmitted over bandwidth limited satellite channels. More specifically, the performance of bandlimited coherent phase-shift-keyed (CPSK) signals transmitted over nonlinear satellite channels in additive Gaussian noise is analyzed. In addition, a receiver structure suitable for combating the effect of bandlimitation of binary CPSK signals is derived and its performance is evaluated. Since the analysis is particularly applicable to satellite communication systems, in the following paragraphs we briefly describe current satellite communication techniques, highlighting important features, in order to enhance readability of the thesis.

The first communications satellite Score was launched in 1958. This success was followed by the launch of the Telstar satellite in 1962 and the first synchronous satellite Syncom in 1963. The first commercially

operational system was initiated in 1965 with the launch of the Early Bird (Intelsat I) satellite, which was a modified version of Syncom. With this began a new era in communications. Early Bird's 240 voice channels not only provided a greater capacity than all of the cables laid between the United States and Europe over the previous ten years, but for the first time it was technically possible to provide direct, reliable, high quality voice, television and data communication between distant points. To keep up with the ensuing rapid traffic growth, which has been between 15% and 25% per year, the rest of the Intelsat series of satellites has been introduced, with a larger capacity being achieved almost every two years; i.e. Intelsat II in 1967, Intelsat III in 1968, Intelsat IV in 1971 and Intelsat IV A in 1978.

Early Bird was designed primarily to meet traffic requirements between Europe and the United States, and it featured a hard-limiting transponder as the on-board satellite amplifier. In addition, the frequency division multiple access (FDMA) technique was used to access the satellite and therefore, only two earth stations could access it simultaneously if channel capacity was to be maintained. For this reason, even though there were three earth stations in Europe, only one could access the satellite during any one time period and hence, to

accommodate the traffic from the other two countries, a preassigned multidestination frequency division multiplex/ frequency modulation (FDM/FM) system, as in terrestrial microwave or undersea cable point to point systems, was used.

Although, the Early Bird system provided a great deal of experience in general satellite operation, it did not provide the full capability of a direct communications system among more than two countries. The major reason for this lay in the use of the preassigned carrier system which is ideally suited only if there is heavy traffic between two points. Since no single country has the requirement for such a large number of channels, in order to exploit the full capability of a satellite system, it must be feasible for a large number of countries (i.e. earth stations) to simultaneously interconnect their voice, data, facsimile and telecommunication links. This is known as multiple access (MA). There are several schemes of multiple access currently being used.

One widely used scheme known as frequency division multiple access (FDMA) was used in Intelsat II, Intelsat III and Intelsat IV. It was possible to accommodate FDMA more effectively on these satellites since the satellites were able to operate their transponders in the linear region in contrast to the hard-limiter used in the Early Bird. Thus

many FM carriers from a multiplicity of earth stations could simultaneously access the satellite. In FDMA, the available transponder bandwidth is devided into a number of non-overlapping frequency bands with bandwidth dependent upon the traffic transmitted on each carrier. The traffic is assembled in FDM form and then the composite baseband is used to frequency modulate the RF carrier. This method is widely used in power limited commercial satellites and its efficiency lies in spreading the power over the available bandwidth.

Furthermore, FDMA is easy to incorporate because many terrestrial microwave links use FDM/FM. Since there are several carriers simultaneously accessing the satellite, it is necessary to operate the satellite's travelling wave tube amplifier (TWTA) in the linear region, that is 'backed off' from saturation, to avoid intermodulation distortion and crosstalk. This in turn reduces the available effective isotropic radiated power (EIRP) of the satellite. In addition, all earth stations transmitting to the satellite need to control and monitor their output powers so that the satellite transponder operates only within the linear region. To further reduce intermodulation, guard bands between adjacent channels are necessary and careful spacing of the carriers is required. These requirements cause a reduction in available satellite transponder capacity. As

the number of carriers simultaneously accessing the transponder increases, the channel capacity still decreases, but not nearly as quickly as for a hard-limiting satellite such as Early Bird. Table 1.1 shows the FDM/FM/FDMA capacity of a Intelsat IV Global beam transponder [1,2]. A major disadvantage of the FDM/FM/FDMA scheme is the difficulty in reconfiguring the system when needed in order to satisfy dynamic traffic requirements.

With wider acceptance of the satellite as an efficient communication system, more and more countries wish to access the satellite simultaneously. But most of these countries have light traffic requirements and can not justify the assignment of permanent carriers. For example, approximately one hundred countries use the Intelsat system, but the majority of these users need 12 voice channels or less. Under these circumtances, FDM/FM/FDMA can not perform efficiently since it is basically a preassigned scheme, and for this reason Comsat developed a new technique known as demand assignment (DA).

One of the demand assignment schemes, which is an extension of FDMA known as SPADE, (Single channel per carrier, Pulse code modulation, multiple Access, Demand assignment Equipment) was developed and implemented on Intelsat IV in mid 1971. This scheme is of particular interest to us, because digital modulation techniques were

RF bandwidth per carrier MHz	Voice channe--ls per carrier	Accesses per transponder	Voice channels/ transponder
2.5	24	14	336
5	60	7	420
10	132	3.5*	456
36	900	1	900

* Three carriers at 10 MHz and one carrier at 5 MHz

Table 1.1

Intelsat IV global beam characteristics [1,2]

used for the first time in a commercial satellite system.

In this scheme, each channel accesses the satellite via an independent carrier assigned from a shared pool of frequencies. Since each carrier is associated with only one channel, there is no multiplexing of channels. Pulse code modulation is used for channel encoding and four phase coherent phase shift keying (QPSK) is used for modulating each carrier. A control algorithm known as DASS (Demand Assignment Signalling and Switching) allocates frequencies from an available pool of frequencies to any earth station requesting a carrier, and once the call is completed, the carrier is returned to the available pool. No carrier is permanently allocated to any earth station. The DASS units and earth stations communicate with one another over a common signalling channel (CSC). By monitoring the CSC all DASS units can update their available frequency pools and all earth stations know the frequency allocations available for outgoing and incoming calls.

A voice activated carrier on/off feature is incorporated to allow 800 voice activated channels at any one time in the system. Table 1.2 [2] gives some important technical characteristics of the SPADE system. Figure 1.1 shows the frequency spectrum arrangement of the SPADE system in a 36 MHz bandwidth transponder as implemented in Intelsat IV [1]. It is noted that the allowed bandwidth for a

Channel encoding	PCM
Modulation	QPSK (coherent)
Bit rate	64 Kb/Sec
Bandwidth per channel	38 KHz
Channel spacing	45 KHz
Stability requirement	± 2 KHz (with AFC)
Bit error rate at threshold	10^{-4}
TDMA Common Signalling Channel (CSC)	
Bit rate	128 Kb/Sec
Modulation	Binary PSK
Frame length	50 mS
Burst length	1 mS
Number of accesses	50
Bit error rate	10^{-7}

Table 1.2

Some technical characteristics of the SPADE system

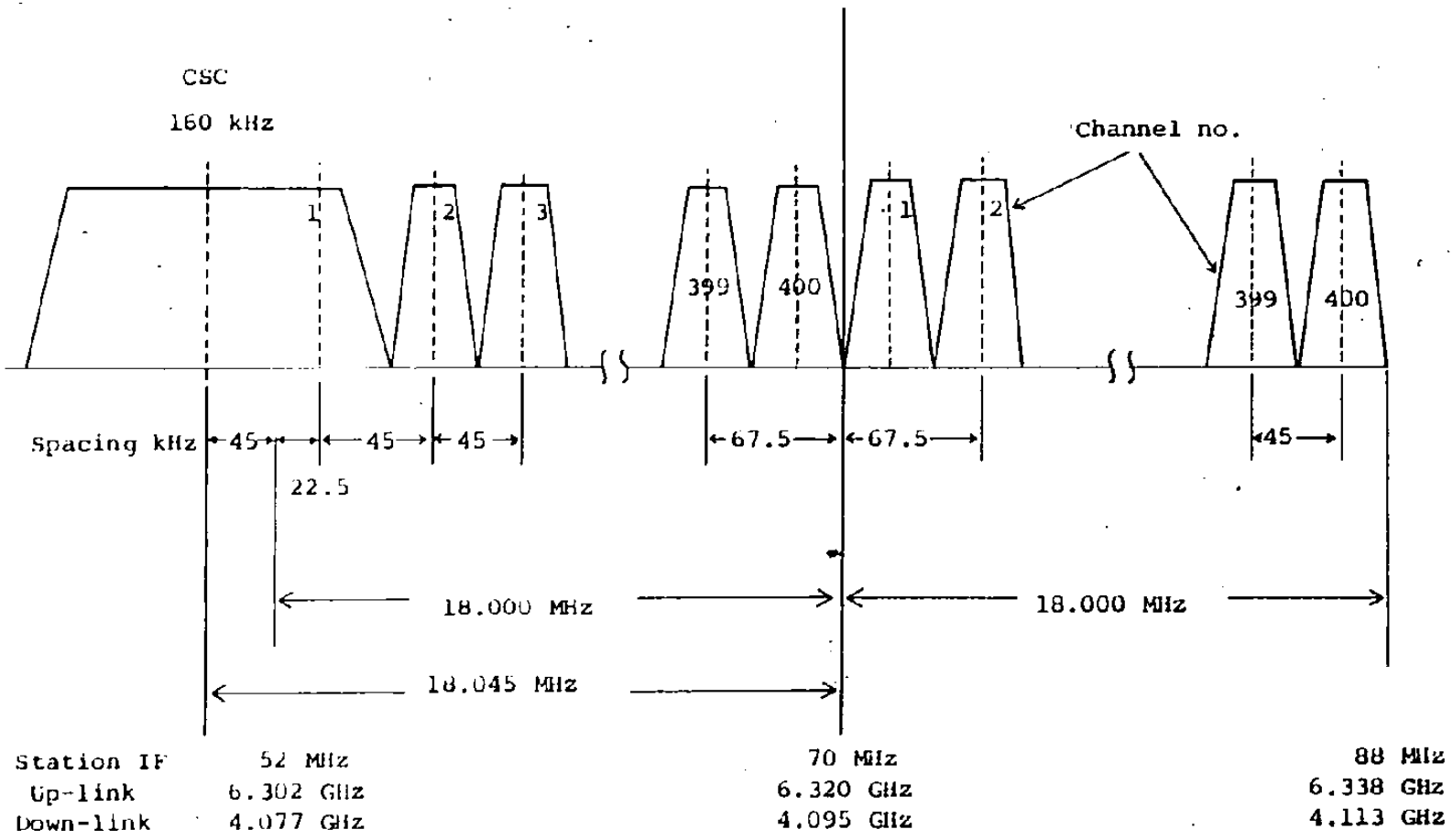

Fig. 1.1 SPADE multichannel frequency-allocation spectrum

channel is 38 KHz and channel spacing is 45 KHz, allowing a 7 KHz guard band between channels. Another notable feature from our point of view is that the CSC is operated in the time division multiple access mode. The time division multiple access (TDMA) is another multiple access scheme, which we shall discuss later on in this section in detail, but for the time being we outline only the important features of CSC. The frame length of the CSC of the SPADE system is 50 mS and the access time is 1 mS allowing fifty stations to simultaneously access the channel. The operating bit rate is 128 k bits/sec and in order to maintain high reliability of this channel binary CPSK modulation is used. Also, this channel radiates at a level 7 dB higher than a normal voice channel thus providing a bit error rate of better than 1×10^{-7}. It is noted that the CSC in SPADE was the first operational example of a TDMA system.

An inherent disadvantage of FDMA in satellite communication is its inability to make full use of the available transponder power since the transponder must be operated in the linear region in order to avoid intermodulation distortion. Table 1.1 shows that if one carrier uses the transponder exclusively, then 900 channel capacity per transponder can be attained but this decreases rapidly as the number of carriers increases. To exploit the

large capacity of a single carrier system, time division multiple access was developed. It is a single carrier technique and we discuss its features briefly in the following paragraphs.

In TDMA, the earth stations transmit their information in bursts rather than continously and these bursts are synchronized such that they enter the satellite in non overlapping time slots. Since only one earth station accesses the satellite during any one time slot, there is no generation of intermodulation products in the nonlinear transponder. This makes it possible to operate the transponder in the saturation region, thus increasing the EIRP of the satellite. TDMA is a completely digital communication technique. By incorporating digital signal interpolation (DSI) techniques, the channel capacity per transponder in Intelsat IV can be increased to approximately 1800 channels.

Figure 1.2 shows a typical TDMA frame [2,3] and burst format. Each earth station transmits bursts periodically, and the collection of bursts consisting of only one burst from each station forms a frame. The basic frame length for standard PCM voice channels is 125 μS. The bursts are separated by a time spacing of about 100 nS to 200 nS, called guard time, in order to avoid overlapping due to errors in the time reference. Each burst contains a

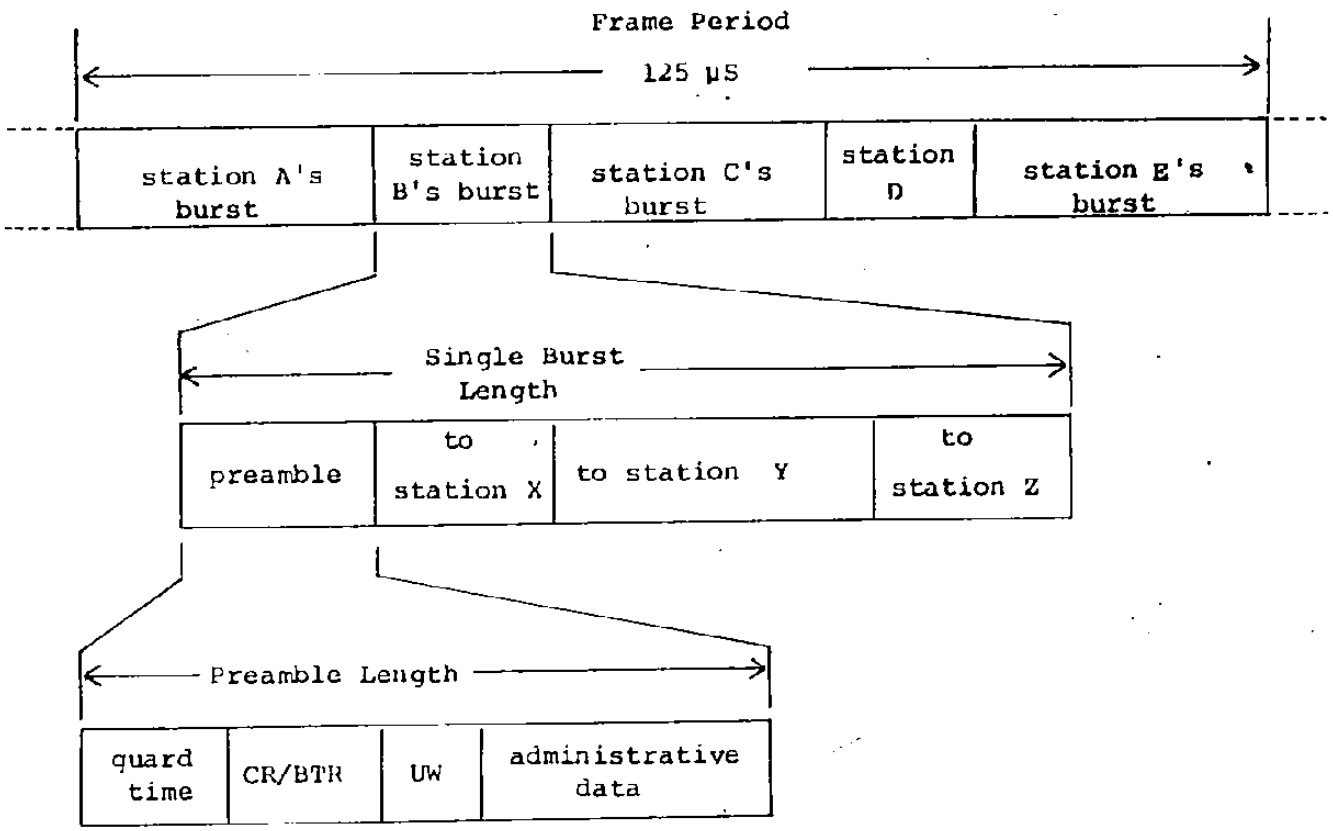

Fig. 1.2 Format structure of a typical TDMA system

preamble consisting of carrier recovery and bit timing (CR/BTR) data followed by a data pattern known as the unique word (UW) to establish an absolute time reference. The UW plays an important role in TDMA. If it is not correctly detected, the data burst is completely lost. Therefore, in order to maintain high reliability, the CR/BTR and UW data are often restricted to binary CPSK modulation. The rest of the preamble contains other administrative information. The frame length, preamble length and the number of accesses or bursts per frame determine the transmission efficiency of a TDMA system. Typically 95% transmission efficiency can be achieved.

In general, TDMA is not effective for earth stations with very light total transmitted traffic and typically is found to be optimum for earth stations transmitting a total of 20 voice channels or more per burst. There are several other multiple access techniques being proposed and currently under implementation. Some of these systems use frequency reuse techniques, spot beam techniques and spread spectrum techniques. Another technique being actively developed includes the incorporating of a time division switching capability on board the satellite itself. We do not intend to go into a detailed description of these in this brief introduction and more details can be found in [2].

1.2 Digital Modulation Techniques

The frequency modulation (FM) technique is used almost exclusively in current commercial communication satellite systems, except for a few cases such as SPADE and parts of the Canadian Domestic or Anik satellite system. The major reasons for the use of FM have been

(a) The available output power of a satellite repeater has up to now been very limited but the available bandwidth has been ample.

(b) FM is a very well established technique so that the cost and effort required to develop satellite systems have been reduced to a minimum.

Nevertheless, the current trend is toward the use of digital modulation techniques and most future satellite systems will use digital modulation techniques. Also, with the advent of high power TWTA's and the involvement of a large number of countries in satellite communication, future satellites are expected to be bandwidth limited in contrast to the current power limited satellites. Digital methods offer increased capacity, network flexibility and reliability. Figure 1.3 shows a capacity comparison of FM/FDMA and PCM/PSK/TDMA techniques [9]. Although any comparison strictly depends on the assumptions made in evaluating performance, in general, it can be concluded that

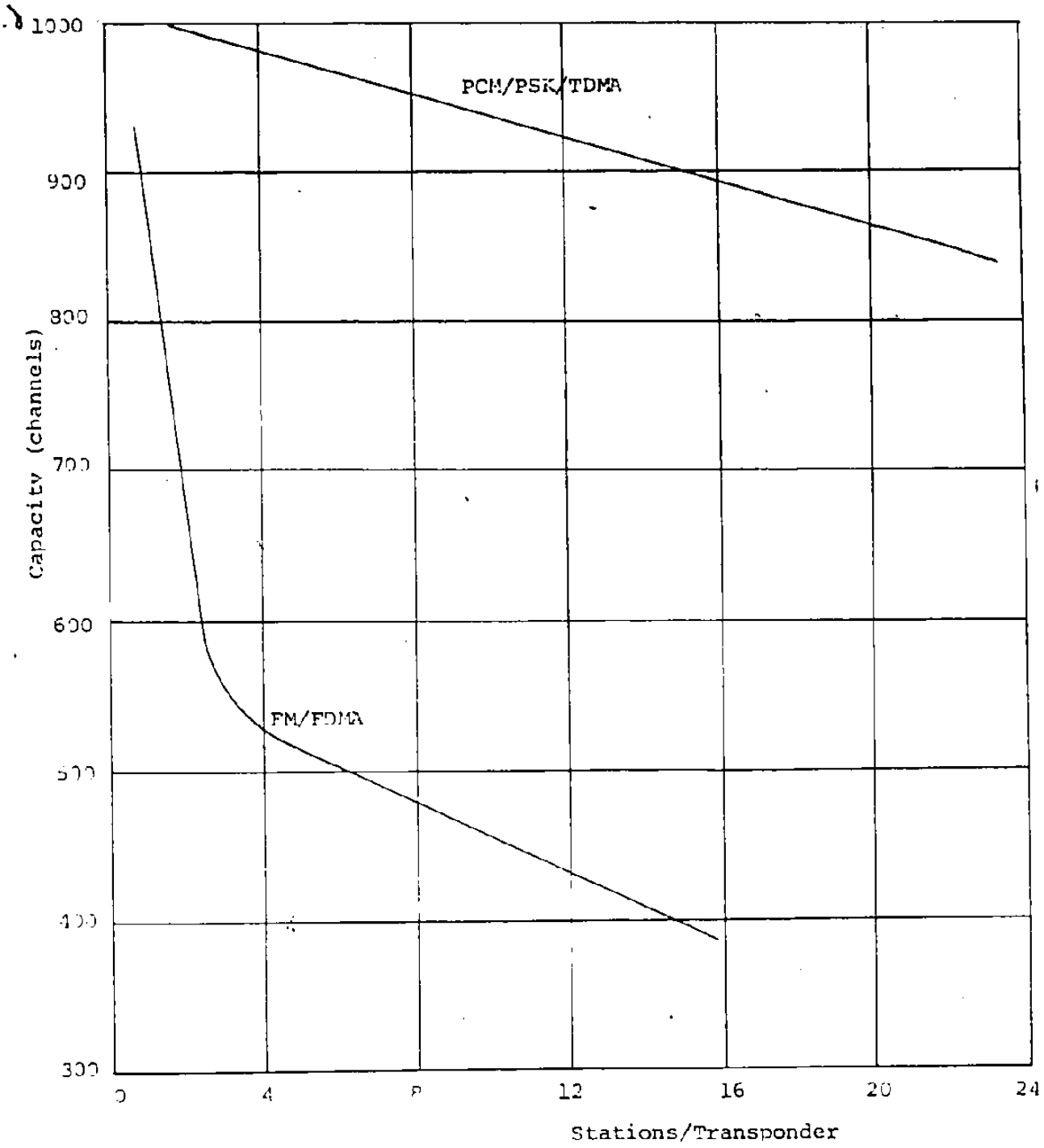

Fig. 1.3 Effects of FM/FDMA and PCM/PSK/TDMA techniques on satellite transponder capacity [9]

PCM/PSK/TDMA is preferable to FM/FDMA for the bandwidth-limited class of satellites. With digital modulation techniques, the bandwidth efficiency can be attained by using multi-level modulation methods. For example, in the SPADE scheme filtered QPSK is used to reduce the required bandwidth from 64 KHz to 38 KHz per channel.

Figure 1.4 [6] shows a comparison of digital modulation systems based on average power. It is seen that PSK has advantages over conventional modulation schemes except for combined amplitude and phase modulation (APK) techniques. Because of the nonlinear amplitude characteristic of the satellite transponder, APK cannot be used in satellite communication systems. In PSK modulation, another advantage is that by increasing the number of levels to four from two, the channel capacity can be approximately doubled without any expense of bandwidth. Also, PSK has the advantage of relatively low suceptibility to interference as compared to analog FM [4,6].

In general, in satellite communications, digital modulation methods have the following advantages:

(1) Increased transponder capacity in a multiple access mode.

(2) The capability of achieving any prescribed amount of error control in single as well as cascade channels.

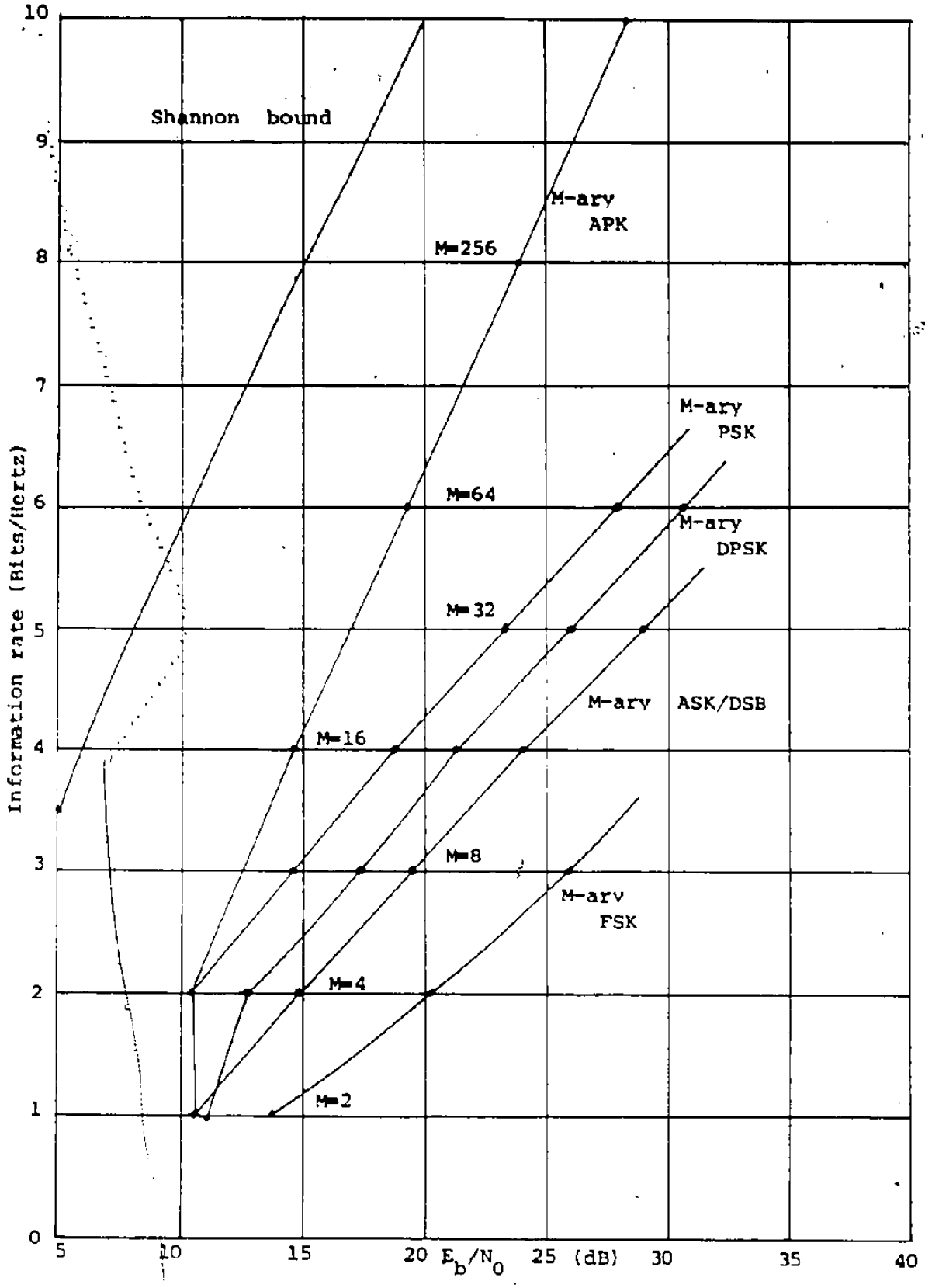

Fig. 1.4 Comparison of digital modulation systems based on average power [6]

(3) Efficient trade off between bandwidth and signal to noise ratio (SNR) permitting processing gains higher than those attainable with analog systems.

(4) Flexibility in message handling such as multiplexing signals with different characteristics, adding and dropping channels, routing, switching and storing, and regenerating signals.

(5) Signal processing capability to give spectrum conservation through source encoding, redundancy reduction and data compression.

(6) Flexibility of low cost digital hardware implementation using microprocessors and large-scale integrated circuits.

1.3 Sources of Interference and Noise in Digital Satellite Channels

A typical satellite channel consists of two communication links separated by a satellite repeater as shown in Figure 1.5. Earth station A transmits signals to the satellite, which amplifies the signals and retransmits them. Earth station B receives the signals transmitted from the satellite. The earth stations A and B are located at different geographical locations, and typically no point to point contact could be established in the absence of a satellite. The link from earth station A to the satellite

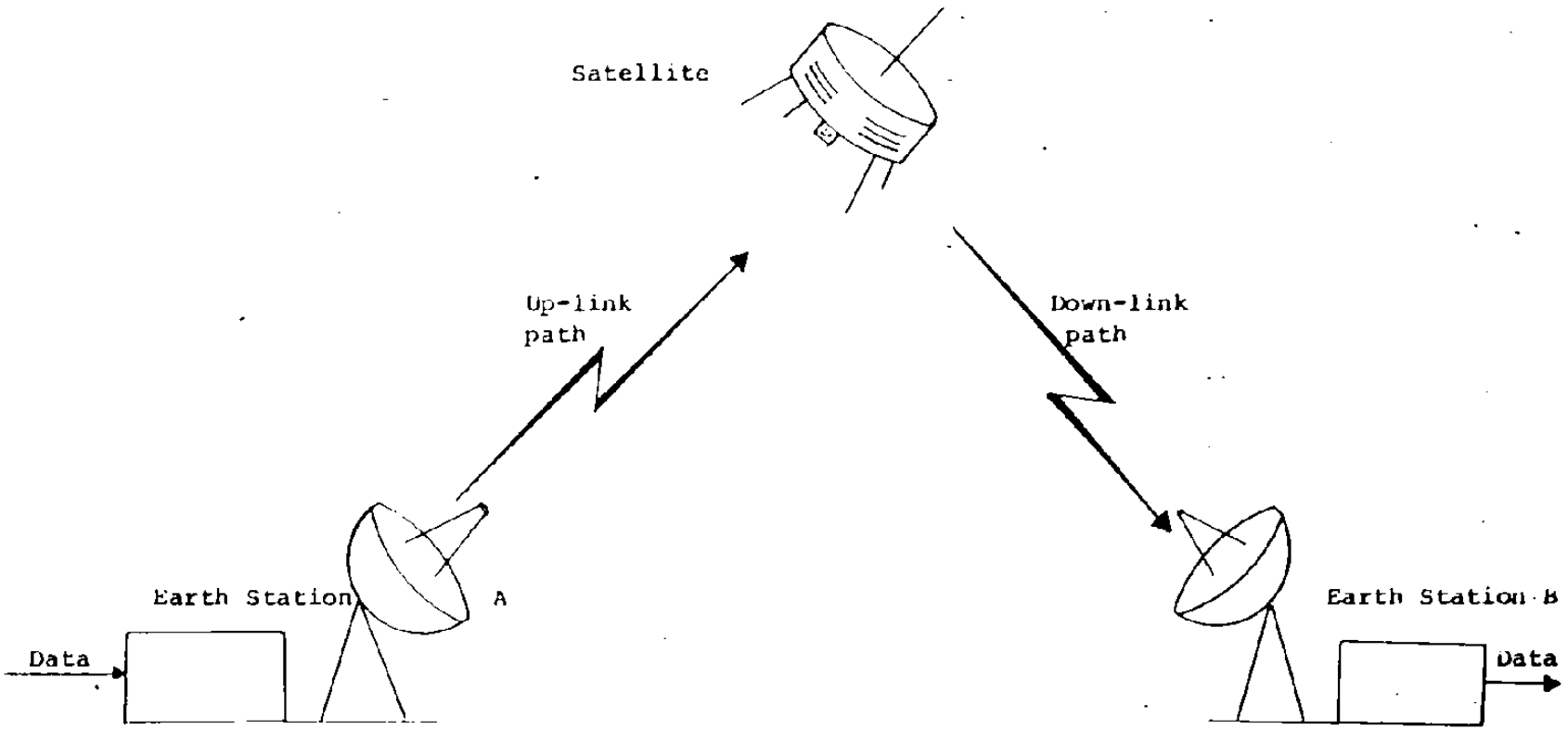

Fig. 1.5 Typical satellite communication link

is called the uplink path and 6 GHz with 500 MHz bandwidth is the carrier frequency and available bandwidth used in current Intelsat satellites on the uplink path.

The satellite repeater consists of a low noise receiver, an intermediate frequency (IF) converter and TWT high power amplifier (HPA). The link from the satellite to earth station B is usually referred to as the downlink path and the carrier frequency and bandwidth being used in the Intelsat system are 4 GHz and 500 MHz respectively. Next, we consider each of these communication subsystems separately and examine the possible sources of noise and interference.

(a) Transmitting Earth Station

Figure 1.6 shows the basic stages of a transmitting earth station. Digital data is modulated on to the uplink carrier and bandlimited to restrict the frequency range to the allowed bandwidth. Then the signal is power amplified using either a Klystron HPA or a wideband TWTA and fed to the antenna. In some cases, the modulation is done in two stages using the double conversion principle in IF/RF (radio frequency) signal processing to provide 500 MHz BW. The bandlimiting filter is required in order to avoid adjacent channel interference. For example, the need for filtering is clearly seen from the SPADE frequency plan shown in

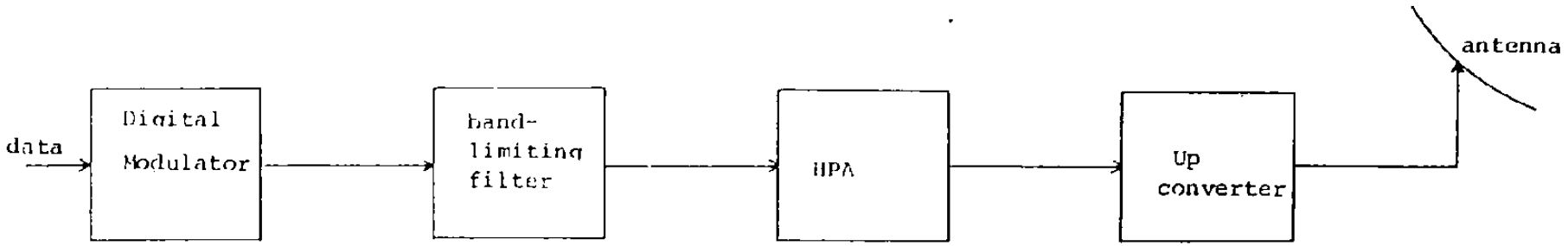

Fig. 1.6 Basic stages of a transmitting earth station

Figure 1.1. Using standard PCM, i.e. 8 KHz sampling rate and 8 bit channel encoding, the BW required is 64 KHz. Using filtered QPSK, BW can be reduced to 32 KHz. Because sharp filtering is not practicable, 38 KHz is used as the channel BW and the channel separation is selected as 45 KHz. On the other hand, at 32 K Baud rate, the QPSK signal with constant envelope has a frequency spectrum much wider than the allowed 38 KHz BW per channel, causing adjacent channels to interfere with one another. The spectrum of QPSK signals is shown in Figure 1.7. Therefore, before transmitting, the QPSK signals have to be bandlimited so that the spectrum is limited to the required 38 KHz bandwidth.

On the other hand, after band-limitation, the pulses do not remain rectangular or restricted to their time intervals, but instead are spread in time causing interference with adjacent pulses. The smearing of pulses due to band-limitation is known as intersymbol interference (ISI) and this is one of the major causes of system performance degradation.

Figure 1.8 provides a pictorial view of the ISI effect. The pulse spreading usually diminishes with time and in well controlled practical systems, there is no significant contribution beyond more than a couple of bauds or signalling intervals. There are other types of distortion introduced due to filtering in IF stages such as

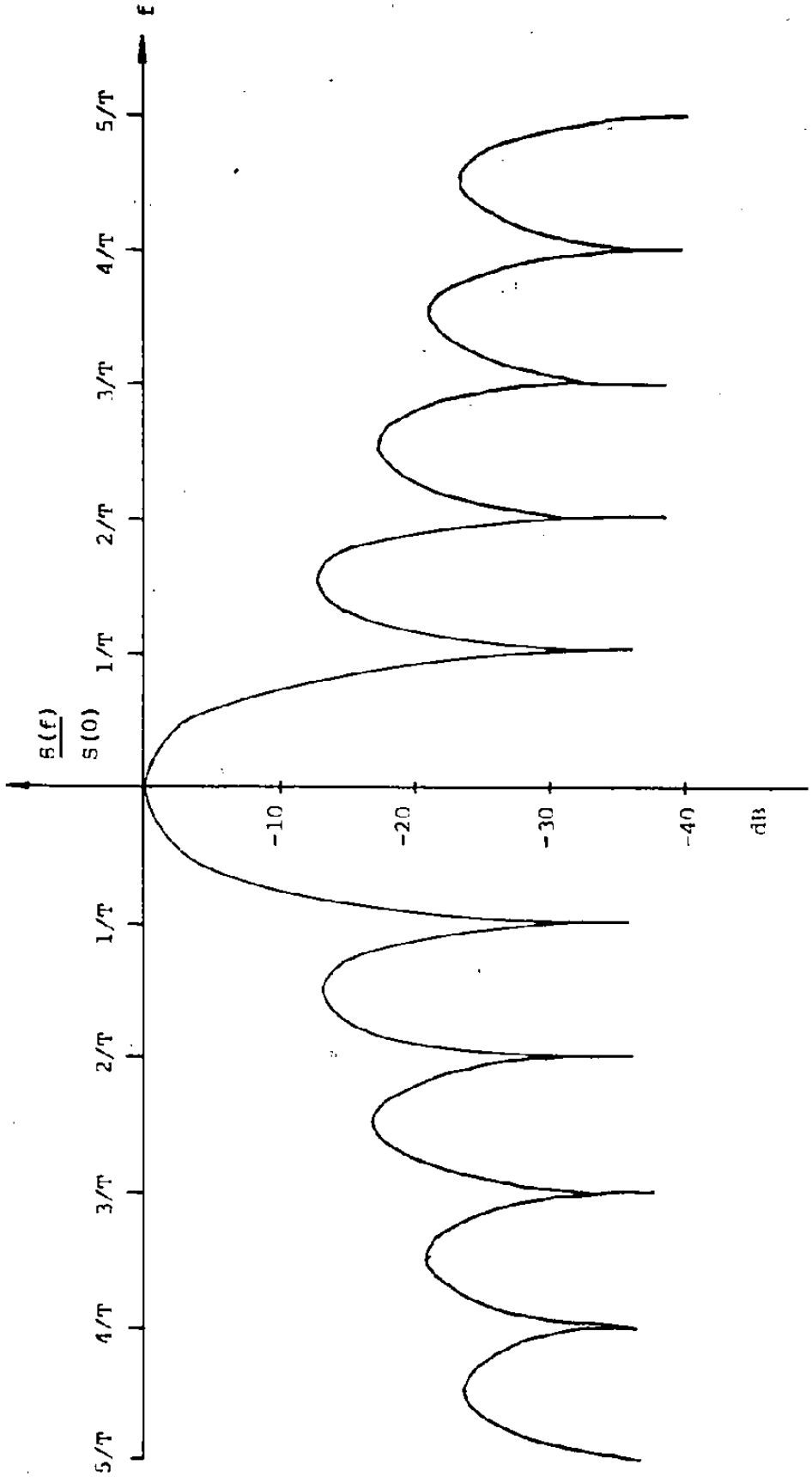

Fig. 1.7 Power spectrum of PSK signals

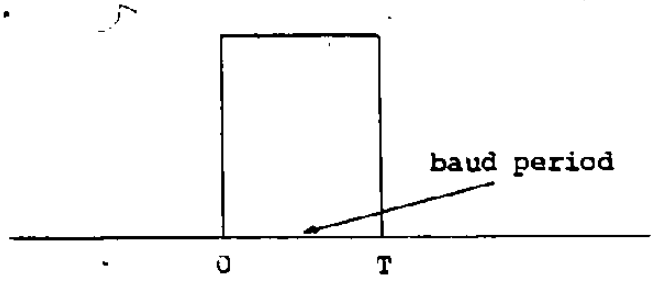

before band-limiting

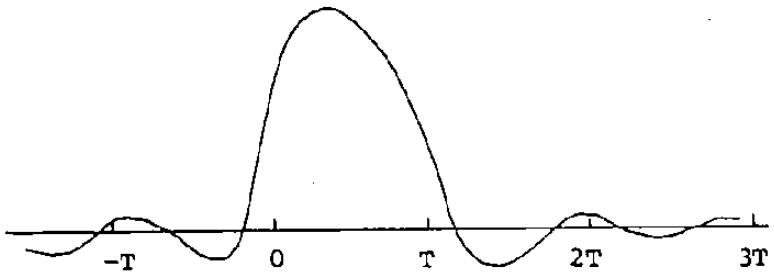

After band-limiting

Fig. 1.8 Illustration of pulse spreading due to band-limitation

pulse shape distortion and phase distortion due to the non uniform amplitude characteristics and nonlinear phase characteristics of the filters respectively, but we are not concerned with these distortions. Usually, these types of distortion can be equalized by phase and amplitude equalizers and any residual interferences become second order effects when compared to the ISI due to band-limitation.

As far as this thesis is concerned, the main source of interference in the system is ISI. We assume high power amplification at the transmitter to be ideal.

(b) Satellite Repeater

The signal received by the antenna of the satellite is fed to a bandpass filter and a low noise amplifier, frequency translated to the downlink carrier frequency and transmitted back to the earth.

The second major source of interference is uplink thermal noise generated by the transmitting earth station electronic equipments and those equipments on board the satellite up to the input of the TWTA. All other interferences such as fading, interference from other satellites, non ideal filtering and frequency translation errors etc. are disregarded for our analysis of satellite system performance. In practice, these types of

interference tend to be second order effects when compared to the ISI, thermal noise and the satellite transponder nonlinearity which we shall describe in the following paragraphs. The uplink thermal noise power density N_o^u due to the thermal noise is given as kT watts/Hz where k is Boltzmann's constant and T is the equivalent noise temperature of the system at the TWTA input in degrees Kelvin. The uplink thermal noise normally has a white (constant) frequency spectrum and Gaussianly distributed amplitude values.

The bandlimited signal and the thermal noise are amplified by the TWTA without regeneration, i.e. we assume that there is no processing capability on board satellite. The TWTA is being exclusively used as a power amplifier or transponder. In Intelsat IV, there are 12 such transponders each with 36 MHz BW. The reasons for using TWTA's as on board satellite power amplifiers are

(i) their inherent ability to provide the highest gain-bandwidth product over octave bandwidths compared to any other component available

(ii) their reliability and long life span suitable for space applications.

In spite of all these advantages, the TWTA has one major disadvantage as far as communications systems are

concerned, in that it exhibits a nonlinear input power to output power transfer characteristic and a nonlinear input power to output signal phase transfer characteristic. The transfer characteristics of the Hughes 261-H TWTA (used in Intelsat IV) is shown in Figure 1.9. In single carrier operation, the power transfer characteristics cause amplitude compression or soft-limiting of any input amplitude modulation (known as AM-AM conversion), and in addition convert input signal amplitude variations or modulation to output signal phase modulation (known as AM-PM conversion). For low power amplification the TWT can be considered approximately as a linear device, but in high power amplification as used in satellites the transfer characteristics exhibit severe nonlinear behaviour. In multi-carrier operation such as in FDMA, the effect of the nonlinear behaviour is to produce intermodulation distortion. In this thesis, we are primarily concerned with the AM-AM conversion and AM-PM conversion effects in single carrier operation and in the subsequent analysis we consider the effect of the TWT nonlinearity on bandlimited PSK signal transmission.

Between the TWTA and satellite transmitting antenna we assume ideal conditions in the sense that no additional distortions or interferences other than those due to the TWTA nonlinearity are introduced.

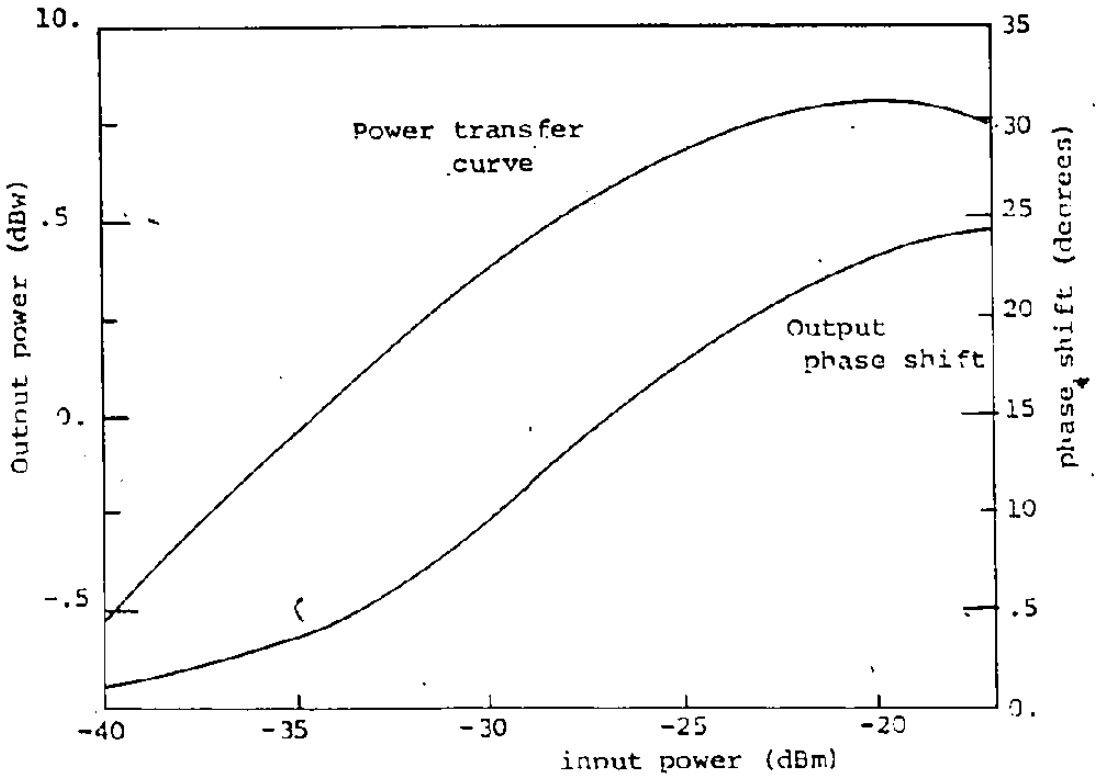

Fig. 1.9 Transfer characteristics of Hughes 261-H TWT

(c) Receiving Earth Station

The signals received by the antenna of the receiving earth station (B) are bandpass filtered to reduce the out of band noise, amplified by low noise amplifiers, coherently demodulated, sampled and then processed to recover the transmitted data. Thermal noise is generated in electronic equipment on the downlink path primarily in the input stages of the earth station receiver, and is considered as the main source of noise in the downlink path. The downlink thermal noise has properties similar to those of the uplink thermal noise. Since the satellite EIRP is comparatively much lower than the transmitting earth station power, the downlink thermal noise tends to be a dominant factor in degrading system performance. For this reason, it is preferable to have cooled low noise amplifiers at the receiving station. Again, as before, we ignore all other interferences which normally tend to be second order effects in well designed satellite systems.

Figure 1.10 is a simplified model of a satellite system derived from Figure 1.5, and indicates the main sources of noise and interference mentioned so far and of primary concern to us in this thesis. Throughout our analysis in the rest of the thesis, we refer to this as our communication model.

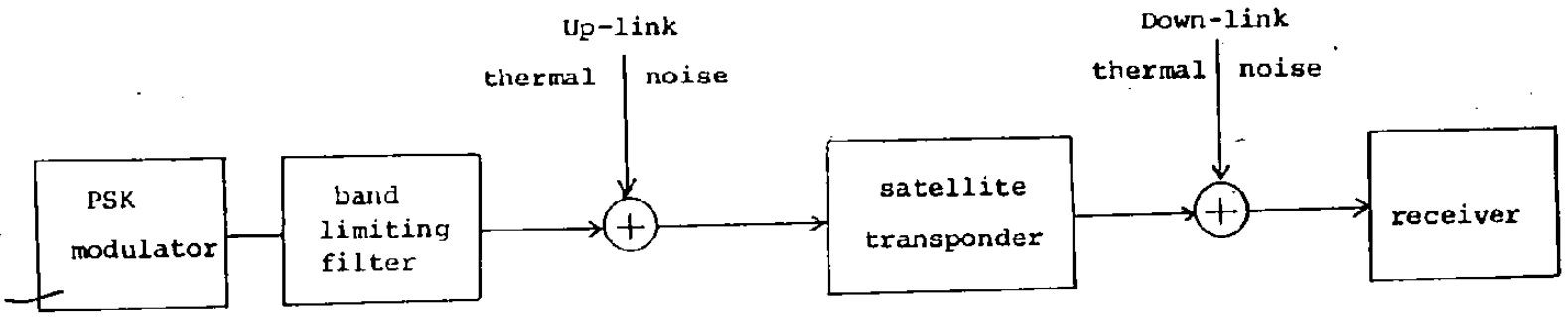

Fig. 1.10 Communication system model

1.4 Purpose and Scope of the Thesis

In designing a communication system, system engineers need to know the system degradation caused by various types of interference. In the absence of exact methods to evaluate performance degradation due to various types of interference, one has had to resort to computer simulation techniques or allow sufficient safety margin to account for the unknown degradations. Computer simulation techniques, often used in the absence of exact analysis, are not only time consuming and costly, but do not give much physical insight to the problem. The latter solution often leads to high cost due to over designing of the system. Therefore, it is preferable to have at least approximate analytical solutions wherever possible in order to ease the designer's task and to reduce the system cost.

Because of the high cost of satellites and ground stations, it is also desirable to process the signal at the receiver to minimize the effect of various interferences and to yield the maximum probability of correct decision as much as possible. By using receivers which yield minimum error probability it is possible to obtain maximum efficiency from small earth stations as well as large earth stations without sacrificing satellite EIRP.

In this thesis we address both these problems. First we shall carry out a performance analysis of the system in

the presence of additive thermal noise and intersymbol interference and secondly, we shall investigate means of processing signals at the receiving earth station to yield minimum probability of error. Throughout the thesis we shall consider phase shift keying modulated signal transmission only. Also, it is assumed that perfect carrier phase recovery is available at the receiver (previously referred to as coherent demodulation).

In Chapter 2, we treat the evaluation of symbol error probability for M-ary CPSK signals transmitted over bandlimited nonlinear channels in additive thermal noise. The various channel models commonly found in the communications literature are used to represent the satellite transponder nonlinearity including an AM-AM and AM-PM conversion model. In each case, to illustrate the applicability of the technique, a numerical example is considered.

For a system designer, it is sometimes as useful to have approximations to the exact solution of the system performance as much as the exact result itself. In communications parlance, these approximations are referred to as bounds. This is the subject of Chapter 3 in which we develop error rate bounds for binary CPSK transmission. Upper and lower bounds are derived and a numerical example is considered in order the compare the results with those

obtained in Chapter 1.

The second question, that of signal processing, is addressed in Chapter 4. The analysis is restricted to binary CPSK reception and a decision feedback receiver structure is derived for a channel containing a TWT nonlinearity and time invariant bandlimiting filter. The receiver structure is applied to a hard-limiting channel to obtain a mathematical tractable expression for the decision statistic and some interesting conclusions are drawn. We evaluated the performance of this receiver by Monte Carlo simulation techniques. Two numerical examples are considered for the simulation studies.

Finally in Chapter 5, we conclude the thesis with a discussion of the results obtained, the conclusions reached and a brief discussion of some of the remaining unsolved problems in this field.

CHAPTER 2

EXACT ANALYSIS OF PERFORMANCE OF M-ARY CPSK TRANSMISSION

2.1 Introduction

The performance evaluation of digitally modulated signals transmitted over nonlinear satellite channels has been the subject of extensive research during the last two decades [10-17]. In these analyses, the satellite transponder nonlinearity has been represented by various models such as a hard-limiter, a piece-wise smooth soft limiter and actual TWT models with both AM-AM and AM-PM conversion [10,15,16,17] included. But all these analyses have been limited to transmission of digitally modulated wideband signals with no consideration of band limitation effects. As explained in Chapter 1, in practice this assumption need not be true, especially since current satellites tend to be bandwidth limited, in contrast to earlier power-limited satellites. Therefore, it is of considerable importance to evaluate the performance of digitally modulated bandlimited signal transmission not only in satellite channels but in any other digital communications system whether linear on nonlinear.

The accurate evaluation of probability of error for various digitally modulated signals in linear channels has received considerable attention [18-20]. The major difficulty in analyzing bandlimited channels is our inability to obtain the probability density of the inter-symbol interference [ISI]. One obvious way to evaluate the probability of error is to enumerate the probabilities of error for all possible combinations of ISI terms and then average all these probabilities to obtain the required probability of error. But this is a rather impracticable technique when the number of interfering pulses become large and is not considered even for linear channels. For example, if we consider a binary modulated system when there are 10 interference terms, 1024 ($= 2^{10}$) direct enumerations are required. Since the number of computations grows exponentially with the number of interference terms, direct enumeration becomes impracticable.

The use of a power series expansion of the ISI statistic has been adopted effectively [18-20] to overcome this difficulty and with this method the probability of error of an M-ary CPSK system can be evaluated to any desired accuracy with a reasonable computational effort. Although, one can assume that this problem has been completely analyzed for the linear systems, little or no effort has been made to analyze nonlinear systems. An

additional difficulty with nonlinear system is that the nice properties of linear systems such as algebraic addition and linear superposition are not applicable to nonlinear systems. For this reason even in the absence of band limitation, the analysis of nonlinear channels remains a difficult task.

In this chapter we provide a technique for exactly evaluating the error probability of bandlimited CPSK signals transmitted in nonlinear satellite channels. As for the linear channels, a series expansion of the ISI probability density is adapted to evaluate the probability of error. We consider both uplink and downlink thermal noise in our model and various known models are used to represent the satellite nonlinearity. Even though we are concerned mainly with satellite channels, the analysis can be readily applied to most other bandpass nonlinear systems such as digital radio systems in which the TWTA is used for power amplification. Numerical examples are considered using a 4-pole Chebyshev bandlimiting filter in each case to illustrate the applicability of the technique.

2.2 Performance Analysis

2.2.1 Mathematical Formulation

A stream of carrier phase modulated data can be expressed as

$$S(t) = \sum_{k=-\infty}^{+\infty} p(t-kT) \cos (\omega_c t - \phi_k) \qquad (2.1)$$

where

$$p(t-kT) = \begin{cases} 1 & (k-1)T \leq t < kT \\ 0 & \text{elsewhere} \end{cases}$$

ω_c = carrier frequency

$\phi_k \in \{\frac{\pi}{M}(2i+1);\ i = 0, 1, \ldots, (M-1)\}$

representing the M-ary data symbols

M = Number of modulation levels

T = Baud period or symbol duration

Also, we assume the data to be equally likely and identically distributed and therfore the ϕ_k are identically distributed and equally probable.

It is noted that since each p(t-kT) is nonzero only during its signalling interval, there is no interference among pulses. Next, S(t) is subjected to bandlimiting filtering.

The output of the filter is

$$S_b(t) = \{S(t)\} * \{2\, h(t) \cos \omega_c t\} \qquad (2.2)$$

where 2 h(t) Cos ω_ct is the impulse response of the bandlimiting filter which we consider here to have a frequency spectrum symmetrical about the carrier and $\{\cdot\} * \{\cdot\}$ indicates convolution.

Simplifying (2.2), after substituting for S(t) from

(2.1), we get

$$S_b(t) = \sum_{k=-\infty}^{+\infty} \text{Cos}\ (\omega_c t + \phi_k) \int_{-\infty}^{+\infty} p(\tau-kT)\ h(t-\tau)d\tau$$

$$= \sum_{k=-\infty}^{k=+\infty} \{p(t-kT)*h(t)\}\ \text{Cos}\ (\omega_c t + \phi_k)$$

$$= \sum_{k=-\infty}^{k=+\infty} q(t-kT)\ \text{Cos}\ (\omega_c t + \phi_k) \qquad (2.3)$$

where

$$q(t-kT) \triangleq p(t-kT) * h(t)$$

We notice that the pulse-shapes q(t-kT) of the band-limited signal are no longer restricted to single symbol intervals, and instead are smeared into adjacent pulses. A geometrical interpretation of the smearing of pulses is shown in Figure 2.1(a).

We now concentrate on a particular baud interval, say the (k+1)th. During this interval, we can algebraically add all the interfering pulses together to form a new pulse as shown in Figure 2.1(b). Extending this procedure to all baud interval we get a new stream of pulses as,

$$S_b(t) = \sum_{k=-\infty}^{k=+\infty} A(t-kT)\ \text{Cos}\ [\omega_c t + \rho(t-kT)] \qquad (2.4)$$

where

$$A(t-kT)\ \text{Cos}\ \rho(t-kT) = \sum_n q(t-nT)\ \text{Cos}\ \phi_n \qquad (2.5)$$

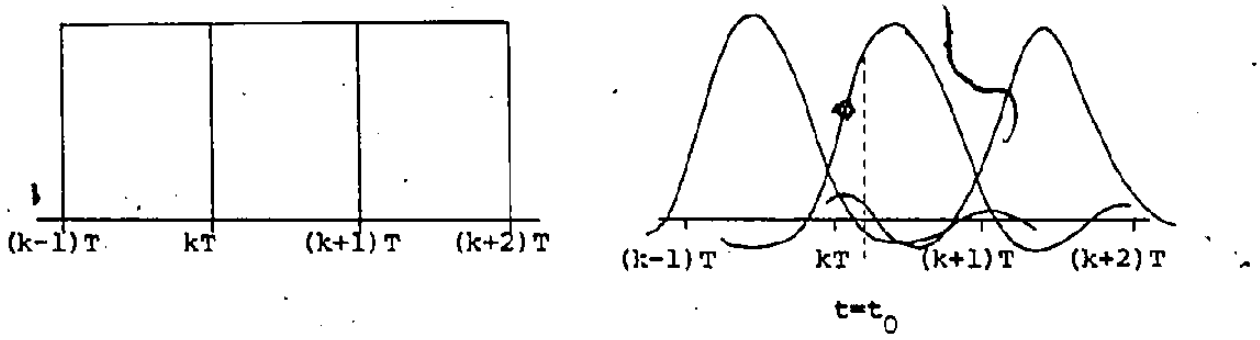

before bandlimiting after bandlimiting

(a)

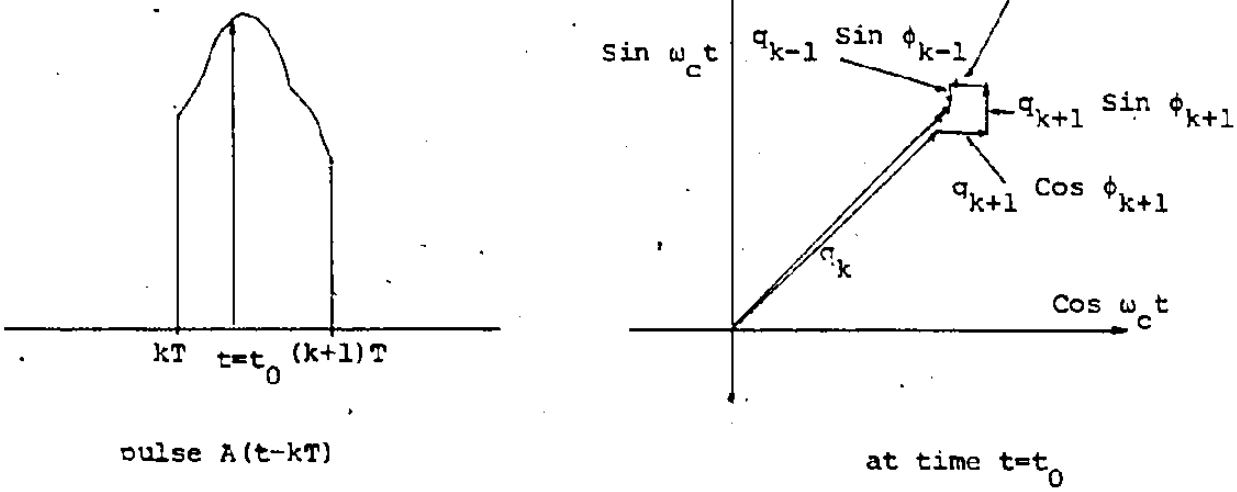

pulse A(t-kT) at time t=t0

(b)

Fig. 2.1 (a) Effect of band-limitation and
(b) Construction of new pulses

$$A(t-kT)\ \text{Sin}\ \rho(t-kT) = \sum_n q(t-nT)\ \text{Sin}\ \phi_n \qquad (2.6)$$

where the summation in n is taken over all interfering pulses in the (k+1)th baud interval.

According to the definition of A(t-kT) we note that

$$A(t-kT) \begin{cases} \neq 0 & (k-1)T \leq t < kT \\ = 0 & \text{elsewhere} \end{cases}$$

The signal $S_b(t)$ is transmitted to the satellite and is corrupted by additive Gaussian noise on the uplink path. The signal appearing at the input to the TWT is

$$S_t(t) = S_b(t) + n_c^u(t)\ \text{Cos}\ \omega_c t - n_s^u(t)\ \text{Sin}\ \omega_c t \qquad (2.7)$$

where $n_c^u(t)$ and $n_s^u(t)$ are the uplink thermal noise components. Here we have adopted the narrow-band representation of Gaussian noise. Both components have zero mean and variance $\sigma_u^2 = N_o^u B$ watts where B is the bandwidth of the satellite receiving filter and N_o^u is the power spectral density of the uplink thermal noise. The satellite receiving filter bandwidth is considered to be much larger than the signal bandwidth.

Combining equations (2.4) through (2.7) we get

$$S_t(t) = R(t)\ \text{Cos}\ [\omega_c t + \lambda(t)] \qquad (2.8)$$

where

$$R(t) = X^2(t) + Y^2(t)$$

$$\lambda(t) = \tan^{-1} [Y(t)/X(t)]$$

$$X(t) \triangleq \sum_k A(t-kT) \text{ Cos } \rho(t-kT) + n_c^u(t) \qquad (2.9)$$

$$Y(t) \triangleq \sum_k A(t-kT) \text{ Sin } \rho(t-kT) + n_s^u(t) \qquad (2.10)$$

When $S_t(t)$ is power amplified by the TWT, it is subjected to AM-AM and AM-PM conversion. The output of the TWT is transmitted to earth. Let $S_d(t)$ be the downlink signal. Then,

$$S_d(t) = f(R(t)) \text{ Cos } \{\omega_c t + \lambda(t) + \rho(R(t))\} \qquad (2.11)$$

where

$f(\cdot) \triangleq$ AM-AM conversion

$\rho(\cdot) \triangleq$ AM-PM conversion

At the receiving earth station $S_d(t)$ is received combined with the additive downlink thermal noise. The received signal $S_r(t)$ is

$$S_r(t) = S_d(t) + n_c^d(t) \text{ Cos } \omega_c t - n_s^d(t) \text{ Sin } \omega_c t \qquad (2.12)$$

where $n_c^d(t)$ and $n_s^d(t)$ are the downlink narrow-band thermal noise components. Again, we assume n_c^d and n_s^d to be zero mean and of variance $\sigma_d^2 = N_o^d B^d$ where N_o^d is the spectral density of the downlink thermal noise and B^d is the bandwidth of the earth station receiving filter.

At the receiver, the signal is coherently demodulated

by multiplying it by two quadrature carriers as shown in Figure 2.2. The resultant signal components are low-pass filtered and sampled at some time instant, say $t = t_o$, when the baseband pulse is expected to be a maximum in the absence of noise and interferences.

From equation (2.12) we obtain the sample values as,

$$x(t_o) = f(R(t_o)) \text{ Cos } [\lambda(t_o) + \rho(R(t_o))] + n_c^d(t_o)$$
$$y(t_o) = f(R(t_o)) \text{ Sin } [\lambda(t_o) + \rho(R(t_o))] + n_s^d(t_o) \quad (2.13)$$

We are interested in finding the average probability of error in receiving any symbol. Since the symbols are equally likely, without loss of generality we can consider only the symbol transmitted during the interval $k = 0$. Also, because of the symmetry of the signal set, we may assume that the phase transmitted in this interval to be π/M.

For notational convenience we drop the time dependence in the rest of the analysis. That is,

$$f \triangleq f(R(t_o)); \quad \lambda \triangleq \lambda(t_o)$$

and

$$\rho \triangleq \rho(R(t_o))$$

The probability of making a correct decision in the $k = 0$ baud interval conditioned on R and λ is then,

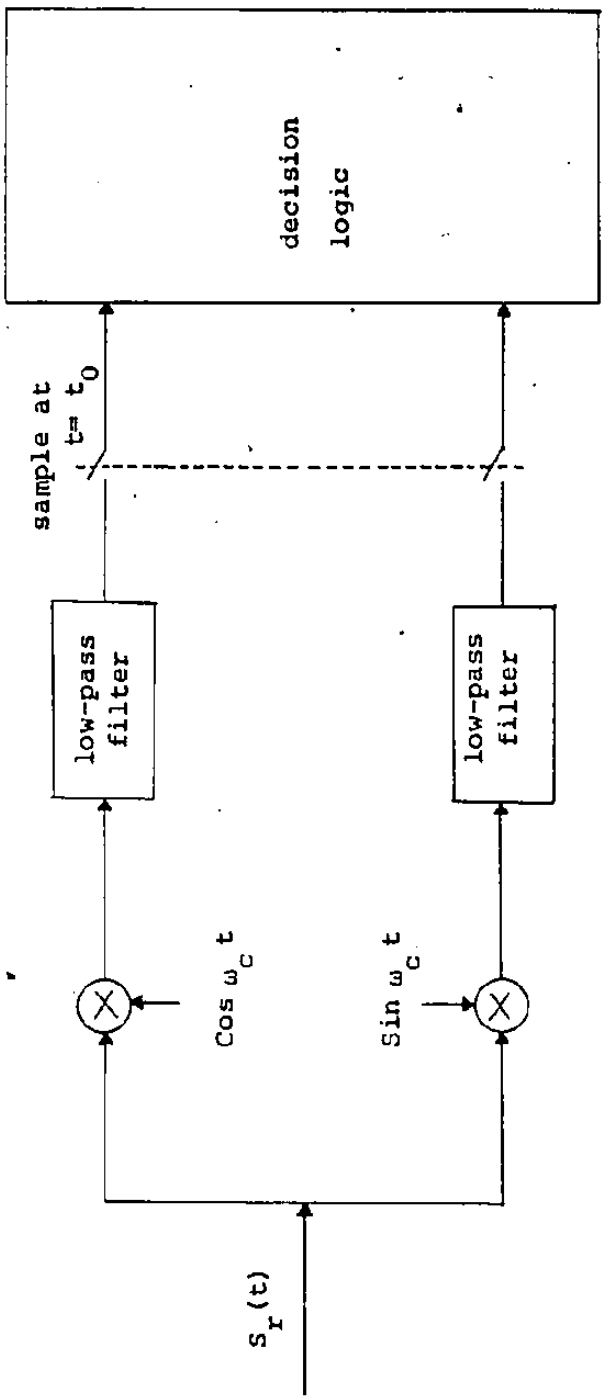

Fig. 2.2 Single sample receiver

$$P_c\big|_{R,\lambda} = \frac{1}{2\pi\sigma_d^2} \int_0^{y'} \int_{x'}^{\infty} e^{-[x-f\ \mathrm{Cos}(\lambda+\rho)]^2/2\sigma_d^2} . e^{-[y-f\ \mathrm{Sin}(\lambda+\rho)]^2/2\sigma_d^2} \, .dx.dy \qquad (2.14)$$

For $M = 2 \quad x' = -\infty \quad y' = +\infty$

$M > 2 \quad x' = 0 \quad y' = x \tan \frac{\pi}{M}$

Equation (2.14) can be simplified using Confluent Hypergeometric functions to obtain [see Appendix A],

$$P_c\big|_{R,\lambda} = \frac{1}{M} + \frac{1}{\pi} \sum_{n=1}^{\infty} \frac{\Gamma(\frac{n}{2})}{n!} \left(\frac{f}{\sqrt{2}\ \sigma_d}\right)^n {}_1F_1\left(\frac{n}{2}, n+1, -\frac{f^2}{2\sigma_d^2}\right) .$$

$$. \mathrm{Sin}\left(\frac{n\pi}{M}\right) \mathrm{Cos}\ n\left(\rho + \lambda - \frac{\pi}{M}\right) \qquad (2.15)$$

where

$\Gamma(\cdot)$ = Gamma function

${}_1F_1(\cdot,\cdot,\cdot)$ = Confluent Hypergeometric function

Alternatively, for some special cases of interest, i.e. binary PSK (M=2) and QPSK (M=4), we can use the error function to evaluate (2.14) in closed form as

For M=2 $$P_c\big|_{R,\lambda} = \frac{1}{2}\left\{1 + \mathrm{erf}\left[\frac{f\ \mathrm{Cos}(\lambda+\rho)}{\sqrt{2}\ \sigma_d}\right]\right\} \qquad (2.16)$$

For M=4

$$P_c\big|_{R,\lambda} = \frac{1}{4}\left\{1 + \mathrm{erf}\left[\frac{f\ \mathrm{Cos}(\lambda+\rho)}{\sqrt{2}\ \sigma_d}\right]\right\}\left\{1 + \mathrm{erf}\left[\frac{f\ \mathrm{Sin}(\lambda+\rho)}{\sqrt{2}\ \sigma_d}\right]\right\} \qquad (2.17)$$

where

$$\mathrm{erf}(t) = \frac{2}{\sqrt{\pi}} \int_0^t e^{-t^2}\, dt$$

The derivation of equation (2.15) is given in Appendix A. In order to now find the unconditional probability of error we must average equation (2.15) over R and λ.

2.2.2 Expression for the Joint Probability Density Function of R and λ

Considering only the k = 0 baud interval and combining equations (2.5), (2.6), (2.9) and (2.10) we can write, using the notation

$$q_k \triangleq q(t_o - kT)$$

$$X \triangleq q_o \cos \phi_o + \sum_n{}' q_n \cos \phi_n + n_c^u = a_o + \alpha + n_c^u \qquad (2.18)$$

$$Y \triangleq q_o \sin \phi_o + \sum_n{}' q_n \sin \phi_n + n_s^u = b_o + \beta + n_s^u \qquad (2.19)$$

where

$$\alpha \triangleq \sum_n{}' q_n \cos \phi_n; \quad \beta \triangleq \sum_n{}' q_n \sin \phi_n$$

$$a_o \triangleq q_o \cos \phi_o ; \quad b_o \triangleq q_o \sin \phi_o$$

and $\sum'$ denotes the summation over all interfering terms excluding the n = 0 term α and β are the inphase and quadrature components of the ISI and (a_o, b_o) are the desired signal components. Since the ϕ_n are random variables, the ISI components α and β are also random variables. If the interfering pulses extend over L baud

intervals, then each of the random variables α and β can have M^L possible values. Since α and β represent discrete random variables we proceed from the joint characteristic function of α and β, given as

$$\phi_{x,y}(u,v) = E[e^{j(a_o+\alpha+n_c^u)u} \cdot e^{j(b_o+\beta+n_s^u)v}]$$

where $E[\cdot]$ denotes the expectation of the argument. Using the statistical independence of the ISI and the Gaussian noise variables, we get

$$\phi_{x,y}(u,v) = e^{j(a_o u+b_o v)} \; e^{-\sigma_u^2 (u^2+v^2)/2} \; E[e^{j(u\alpha+v\beta)}] \quad (2.20)$$

The expectation of (2.20) can be easily shown [18], on taking into account the symmetrical properties of the signal set, to be

$$\phi_{\alpha,\beta}(u,v) = E[e^{j(u\alpha+v\beta)}] = \prod_n{}' \left\{\frac{2}{M} \sum_{j=0}^{M/2-1} \cos\left[q_n u \cos\frac{\pi}{M}(1+2j) + q_n v \sin\frac{\pi}{M}(1+2j)\right]\right\} \quad (2.21)$$

where $\prod'$ indicates the product of n terms excluding the n=0 term.

The joint probability density function of x and y is the inverse Fourier transform of $\phi_{x,y}(u,v)$.

Hence we get

$$p(x,y) = \left(\frac{1}{2\pi}\right)^2 \int_{-\infty}^{+\infty}\int_{-\infty}^{+\infty} e^{j(a_o u + b_o v)} e^{-\sigma_u^2 (u^2+v^2)/2} \cdot \phi_{\alpha,\beta}(u,v) \cdot$$

$$\cdot e^{-j(ux+vy)}\, du \cdot dv \qquad (2.22)$$

To evaluate the integral in (2.22), a power series expansion is used for the characteristic function $\phi_{\alpha,\beta}(u,v)$ as shown by Shimbo et al. [18]. We do not give any details of the expansion which can be found in [18]. As given in [18], we use the following expansion for $\phi_{\alpha,\beta}(u,v)$.

$$\phi_{\alpha,\beta}(u,v) = \sum_{\ell}\sum_{m} b_{\ell,m}\, u^{\ell}\, v^{m} \triangleq \sum_{\ell,m} b_{\ell,m}\, u^{\ell}\, v^{m} \qquad (2.23)$$

where $\sum_{\ell,m}$ denotes the summation over all even ℓ and m. Substituting (2.23) into (2.22), then after some manipulation we get [see Appendix A]

$$p(x,y) = \sum_{\ell,m} b_{\ell,m} \frac{(-1)^{\ell+m/2}}{(\sqrt{2}\,\sigma_u)} \frac{1}{2\pi\,\sigma_u^2} H_{\ell}\left(\frac{x-a_o}{\sqrt{2}\,\sigma_u}\right) \cdot H_m\left(\frac{y-b_o}{\sqrt{2}\,\sigma_u}\right) \cdot$$

$$\cdot e^{-(x-a_o/\sqrt{2}\sigma_u)^2} \cdot e^{-(y-b_o/\sqrt{2}\sigma_u)^2} \qquad (2.24)$$

where $H_n(\cdot)$ is the nth order Hermit polynomial defined by

$$H_n(x) = (-1)^n e^{x^2} \frac{d^n}{dx^n}\left(e^{-x^2}\right)$$

and obeys the recursion relation

$$H_{n+1}(x) = 2x\, H_n(x) - 2n\, H_{n-1}(x) \qquad (2.25)$$

$$\text{for } n \geq 1$$

Since we have derived an expression for the joint probability density of (x,y), then by transforming to polar co-ordinates (R,λ), we can obtain the joint probability density function of R and λ.

2.2.3 Derivation of the Symbol Probability of Error

To find the probability of error we find the expectation of $P_{c/R,\lambda}$ given in (2.15) with respect to the p(x,y) given in (2.24). This expectation may be written as

$$P_c = \int_{-\infty}^{+\infty} \int_{-\infty}^{+\infty} P_{c|R,\lambda} \cdot p(x,y)\, dx \cdot dy \qquad (2.26)$$

or

$$P_c = \frac{1}{M} + \frac{1}{\pi} \sum_{n=1}^{\infty} \frac{\Gamma(n/2)}{n!} \operatorname{Sin}\left(\frac{n\pi}{M}\right) \cdot \sum_{\ell,m} \frac{b_{\ell,m}}{(\sqrt{2}\,\sigma_u)^{\ell+m}} \frac{(-1)^{\ell+m/2}}{2\pi\,\sigma_u^2}$$

$$\cdot \int_{-\infty}^{+\infty} \int_{-\infty}^{+\infty} \left(\frac{f}{\sqrt{2}\,\sigma_d^2}\right)^n , F, \left(\frac{n}{2}, n+1, -\frac{f^2}{2\sigma_d^2}\right) \cdot$$

$$\cdot \operatorname{Cos} n\left[\rho + \tan^{-1}\left(\frac{y}{x}\right) - \frac{\pi}{M}\right] \cdot H_\ell \left(\frac{x-a_o}{\sqrt{2}\,\sigma_u}\right) \cdot H_m \left(\frac{y-b_o}{\sqrt{2}\,\sigma_u}\right)$$

$$\cdot e^{-(x-a_o/\sqrt{2}\sigma_u)^2} e^{-(y-b_o/\sqrt{2}\sigma_u)^2} \cdot dx \cdot dy \qquad (2.27)$$

We recall that

$$f = f(R) = f(\sqrt{x^2+y^2})$$

$$\rho = \rho(R) = \rho(\sqrt{x^2+y^2})$$

Even though the expression in (2.27) appears to be rather complex, it can, in particular cases of the transponder, be simplified further. We do so by considering special cases of the modulation, e.g. M=2, M=4 and M>4.

Case I M=2, i.e. binary CPSK modulation

In this case $\phi_k = \frac{\pi}{2}$ or $\frac{3\pi}{2}$

Inspecting equations (2.18) and (2.19) we see that the ISI component α vanishes in this case. Also, $a_o = 0$, and (2.18) and (2.19) reduce to

$$X = n_c^u$$
$$Y = q_o + \sum_n{}' q_n \operatorname{Sin} \phi_n + n_s^u \tag{2.28}$$

so that

$$\phi_\beta(v) = \prod{}' \operatorname{Cos}(q_n v) = \sum_m b_m v^m$$

As shown in Appendix A, P_c can then be expressed in a much simpler form as

$$P_c = \frac{1}{2} + \frac{1}{\pi} \sum_{n=o}^{\infty} \frac{\Gamma(n+1/2)}{(2n+1)!} (-1)^n \sum_m \frac{b_m}{(\sqrt{2}\,\sigma_u)^m} (-1)^{m/2} \cdot$$
$$\cdot \int_0^{\infty} \left(\frac{f_1}{\sqrt{2}\,\sigma_d}\right)^{2n+1} \cdot {}_1F_1\left(n+\frac{1}{2}, 2n+2, -\frac{f^2}{2\sigma_d^2}\right) \cdot$$
$$\cdot s\, e^{-s^2} \operatorname{Cos}(n\rho_1) \cdot \frac{\partial^m}{\partial q^m} \left[e^{-q^2} I_n(2sq)\right] \cdot ds \tag{2.29}$$

where $q^2 \triangleq q_o^2/2\sigma_u^2$ is the uplink carrier power to noise power ratio (CNR) and $I_n(\cdot)$ is the nth order modified Bessel function.

Also,

$$f_1 \triangleq f(\sqrt{2}\,\sigma_u\, s);\ \rho_1 \triangleq \rho(\sqrt{2}\,\sigma_u\, s)$$

It can easily be shown that

$$\frac{\partial^m}{\partial q^m}\left[e^{-q^2} I_n(2sq)\right] = e^{-q^2} \sum_{p=0}^{m} {}^{m}C_p\, (-1)^p\, H_p(q)\, s^{m-p} \cdot \sum_{k=0}^{m-p} {}^{m-p}C_k \cdot I_{n-m+p+2k}(2sq)$$

where

$${}^{\ell}C_n = \frac{\ell!}{(\ell-n)!\ n!}$$

We note that when there is no ISI, only the term for m=0 remains. Equation (2.29) then reduces to that obtained by Forsey et al. [16], which is the error probability in the presence of uplink and downlink thermal noise only.

If the ISI is small, the number of terms of the second series required is typically less than 6. In this case, expression (2.29) can be used for evaluating the error probability efficiently. But when the ISI is large, a larger number of terms of the second series is required. In this case it becomes difficult to evaluate the integral numerically because of the difficulty in evaluating the mth order derivative.

Therefore for large ISI, we give an alternate

expression for the error probability. Combining equations (2.16) and (2.24) we get

$$P_c = \sum_m \frac{b_m}{(\sqrt{2}\,\sigma_u)^m} \frac{(-1)^{m/2}}{2\pi\,\sigma_u^2} \int_{-\infty}^{+\infty}\int_{-\infty}^{+\infty} \frac{1}{2}\{1 + \operatorname{erf}[\frac{f\,\cos(\lambda+\rho)}{\sqrt{2}\,\sigma_d}]\} \cdot$$

$$H_\ell\,(\frac{x-a_o}{\sqrt{2}\,\sigma_u}) \cdot H_m\,(\frac{y-b_o}{\sqrt{2}\,\sigma_u}) \cdot e^{-(x-a_o/\sqrt{2}\sigma_u)^2}$$

$$\cdot\, e^{-(y-b_o/\sqrt{2}\sigma_u)^2} \cdot dx \cdot dy$$

$$= \sum_m \frac{b_m}{(\sqrt{2}\,\sigma_u)^m} \frac{(-1)^{m/2}}{2\pi} \int_{-\infty}^{+\infty}\int_{-\infty}^{+\infty} \{1 + \operatorname{erf}[\frac{f\,\cos(\lambda+\rho)}{\sqrt{2}\,\sigma_d}]\} \cdot$$

$$\cdot\, H_\ell(r) \cdot H_m(s) \cdot e^{-r^2}\, e^{-s^2}\, dr \cdot ds \qquad (2.30)$$

where

$$f \triangleq f(t) \text{ and } \rho \triangleq \rho(t)$$

$$t^2 \triangleq (\sqrt{2}\,\sigma_u)^2\,[(r+q)^2 + (s+q)^2]$$

$$\lambda \triangleq \tan^{-1}\,[\frac{q + s\sqrt{2}}{q + r\sqrt{2}}]$$

$$q \triangleq \frac{q_o^2}{2\sigma_u^2}$$

The double integral in equation (2.30) can be easily evaluated using the Cartesian products of Gauss-Hermite formulas. This expression is preferable to expression (2.29) for computational purposes, even though the former

contains only a one dimensional integral.

Case II M=4, i.e. QPSK Modulation

In this case

$$\phi_k = \frac{\pi}{4}, \frac{3\pi}{4}, \frac{5\pi}{4}, \frac{7\pi}{4}$$

$$a_o = \frac{q_o}{\sqrt{2}}; \quad b_o = \frac{q_o}{\sqrt{2}}$$

Both the components of ISI, α and β then appear in (2.18) and in (2.19), but the characteristic function $\phi_{\alpha,\beta}(u,v)$ reduces from (2.21) to

$$\phi_{\alpha,\beta}(u,v) = \pi \cos\left(\frac{q_n}{\sqrt{2}} u\right) \cdot \pi \cos\left(\frac{q_n}{\sqrt{2}} v\right) \qquad (2.31)$$

Following the arguments used in obtaining (2.29) we can derive a similar expression for the error probability in this case too, but the resulting expression is extremely difficult to evaluate numerically. Instead we use the alternate expression of $P_{c/R,\lambda}$ given in (2.17) to obtain the probability of error as

$$P_c = \frac{1}{4} \sum_{\ell,m} \frac{b_{\ell,m}}{(\sqrt{2}\,\sigma_u)^{\ell+m}} \frac{(-1)^{\ell+m/2}}{2\pi\,\sigma_u^2} \int_{-\infty}^{+\infty}\int_{-\infty}^{+\infty} \{1 + \text{erf}\,[\frac{f\,\text{Cos}(\lambda+\rho)}{\sqrt{2}\,\sigma_d}]\}$$

$$\cdot \{1 + \text{erf}\,[\frac{f\,\text{Sin}(\lambda+\rho)}{\sqrt{2}\,\sigma_d}]\} \cdot H_\ell\left(\frac{x-a_o}{\sqrt{2}\,\sigma_u}\right) H_m\left(\frac{y-b_o}{\sqrt{2}\,\sigma_u}\right)$$

$$\cdot e^{-(x-a_o/\sqrt{2}\sigma_u)^2} e^{-(y-b_o/\sqrt{2}\sigma_u)^2} dx \cdot dy \qquad (2.32)$$

where

$$f \triangleq f(\sqrt{x^2+y^2}); \quad \rho \triangleq \rho(\sqrt{x^2+y^2}); \quad \lambda = \tan^{-1}\left(\frac{y}{x}\right)$$

with the substitutions

$$r = \frac{x}{\sqrt{2}\,\sigma_u} - \frac{a_o}{\sqrt{2}\,\sigma_u}$$

and

$$s = \frac{y}{\sqrt{2}\,\sigma_u} - \frac{b_o}{\sqrt{2}\,\sigma_u}$$

(2.32) can be expressed in the form,

$$P_c = \frac{1}{4} \sum_{\ell,m} \frac{b_{\ell,m}}{(\sqrt{2}\,\sigma_u)^{\ell+m}} \frac{(-1)}{4\pi} \int_{-\infty}^{+\infty}\int_{-\infty}^{+\infty} \{1 + \operatorname{erf}\left[\frac{f\,\cos(\lambda+\rho)}{\sqrt{2}\,\sigma_d}\right]\}$$

$$\{1 + \operatorname{erf}\left[\frac{f\,\sin(\lambda+\rho)}{\sqrt{2}\,\sigma_d}\right]\} \cdot H_\ell(r)\, H_m(S)\, e^{-r^2}\, e^{-s^2}\, dr\, ds \qquad (2.33)$$

where

$$f \triangleq f(t) \text{ and } \rho \triangleq \rho(t)$$

$$t^2 \triangleq (\sqrt{2}\,\sigma_u)^2\,[(r+q)^2 + (s+q)^2]$$

and

$$\lambda = \tan^{-1}\left[\frac{q + s\sqrt{2}}{q + r\sqrt{2}}\right]$$

$$q^2 = \frac{q_o^2}{2\sigma_u^2} \text{ is the uplink CNR}$$

The double integral appearing in equation (2.33), can be easily evaluated using the Cartesian products of Gauss-Hermite formulas [21]. Since at high CNR, the convergence of the Confluent Hypergeometric function is slow, the

computational time required in using expression (2.33) to evaluate error probability is less than that required for evaluating error probability expressed in terms of Hyper-geometric functions as given in equation (2.27).

Case III $M > 4$

In this case the general expression given in (2.27) can not be simplified further.

In the following section we apply the expressions derived to different nonlinear channel models and obtain numerical results. In Appendix A, the evaluation of the coefficients $b_{\ell,m}$ is shown for BPSK and QPSK systems. For the general case, $M > 4$, a detailed derivation is given in ref. [18].

2.3 Application to Different Channel Models

2.3.1 Hard-limiting Channel [54]

The hard-limiting channel model is often used to model satellite transponder nonlinearity mainly because it leads to tractable mathematical expressions, making it easier to obtain numerical results. Also, the TWTA operating at saturation, can be approximately modelled as a hard-limiter, if we ignore the AM-PM conversion effect. This is the case for the TDMA mode of operation of a phase compensated TWTA. Figure 2.3(a) shows the input-output amplitude characteristic of a hard-limiter which can be

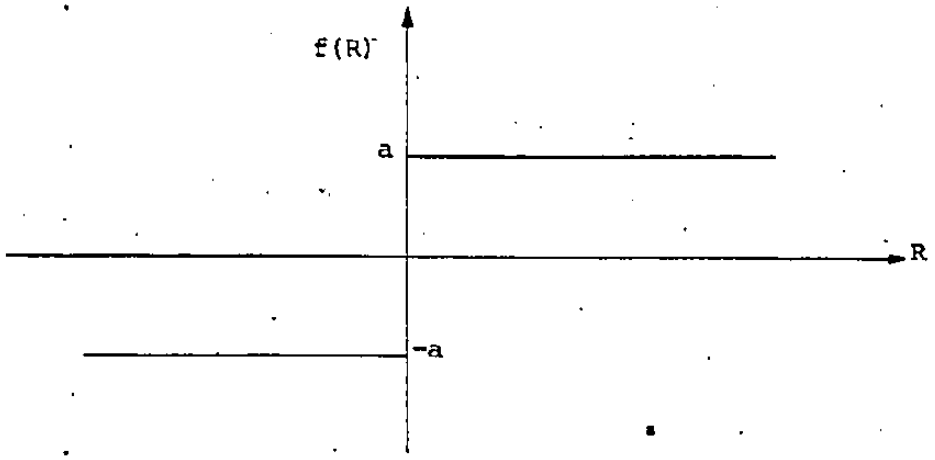

(a)

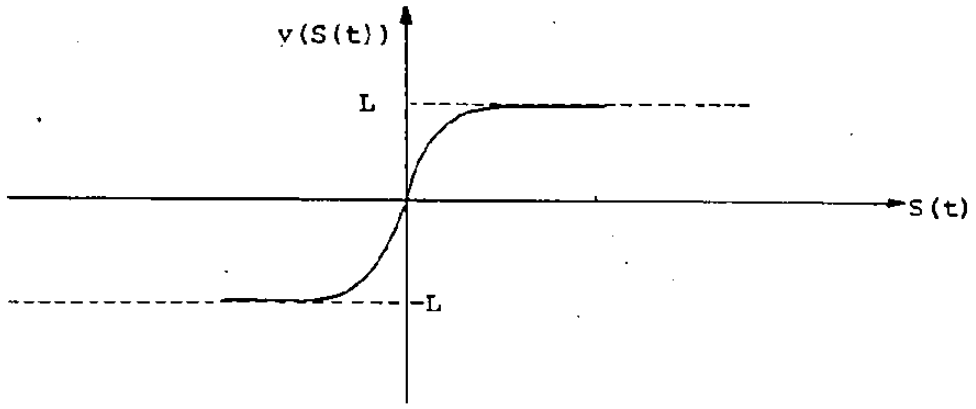

(b)

Fig. 2.3 (a) Characteristics of a hard-limiting channel
(b) Characteristics of a soft-limiting channel

expressed mathematically as

$$f(R(t)) = \begin{cases} a & R(t) \geq 0 \\ -a & R(t) < 0 \end{cases}$$

$$\rho(R(t)) = 0 \quad \text{for } -\infty \leq R(t) \leq +\infty$$

Making these substitution in (2.29) it can be shown that (Appendix A),

for M = 2, i.e. binary PSK modulation

$$P_c = 1-P_c = \frac{1}{2} - \frac{1}{\pi} \sum_{n=0}^{\infty} (-1)^n \frac{\Gamma(n/2+1)}{(2n+1)!} \rho_d^{2n+1} \, {}_1F_1(n+1/2, 2n+2, -\rho_d^2) \sum_m \frac{b_m}{(\sqrt{2}\,\sigma_u)^m} (-1)^{m/2} \frac{\Gamma(n+3/2)}{(2n+1)!} \frac{\partial^m}{\partial q^m} \{q^m \, {}_1F_1(n+1/2, 2n+2, -q^2)\} \tag{2.34}$$

For M = 4, i.e. QPSK modulation, we use expression (2.33) to obtain

$$P_e = 1 - \frac{1}{4} \sum_{\ell,m} \frac{b_{\ell,m}}{(\sqrt{2}\,\sigma_u)^{\ell+m}} \frac{(-1)^{\ell+m/2}}{4\pi} \int_{-\infty}^{+\infty} \int_{-\infty}^{+\infty} [1+\operatorname{erf}(\rho_d \cos\rho)] [1 + \operatorname{erf}(\rho_d \sin\rho)] H_\ell(r) H_m(s) e^{-r^2} e^{-s^2} dr\, ds \tag{2.35}$$

For M > 4, the general expression (2.27) reduces to

$$P_e = \frac{M-1}{M} - \frac{1}{\pi} \sum_{n=1}^{\infty} \frac{\Gamma(n/2)}{n!} \sin\left(\frac{n\pi}{M}\right) \sum_{\ell,m} \frac{b_{\ell,m}}{(\sqrt{2}\,\sigma_u)^{\ell+m}} \frac{(-1)^{\ell+m/2}}{2\pi}$$

$$\cdot \rho_d^2 \,, F, \left(\frac{n}{2}, n+1, -\rho_d^2\right) \int_{-\infty}^{+\infty} \int_{-\infty}^{+\infty} \cos n\left(\theta - \frac{\pi}{M}\right) \cdot H_\ell(r) \cdot H_m(s) \cdot$$

$$\cdot e^{-r^2} \cdot e^{-s^2} \, dr \, ds \qquad (2.36)$$

where

$$\theta = \tan^{-1}\left[\frac{q + s\sqrt{2}}{q + r\sqrt{2}}\right]$$

In (2.4) through (2.36), $\rho_d^2 \triangleq a^2/2\sigma_d^2$ is the downlink carrier power to downlink noise power ratio $(CNR)_d$.

To obtain numerical results we consider a 4-pole Chebyshev filter [15] with impulse response given as,

$$h(t) = A_1 \cos(\omega_1 |t|/T_o - \phi_1) \exp(-\alpha_1' |t|/T_o)$$

$$+ A_2 \cos(\omega_2 |t|/T_o - \phi_2) \exp(-\alpha_2' |t|/T_o) \qquad (2.37)$$

with

$$A_1 = 0.4023 \qquad A_2 = 0.7163$$

$$\omega_1 = 2.839 \qquad \omega_2 = 1.176$$

$$\phi_1 = 0.7553 \qquad \phi_2 = 0.1602$$

$$\alpha_1' = 0.4587 \qquad \alpha_2' = 1.107$$

We consider two different values of (T/T_o) which is proportional to time-bandwidth product, namely

$T/T_o = 2$ 20 interfering terms considered

$T/T_o = 1$ 34 interfering terms considered

The numerical results are shown in Figures 2.4, 2.5, 2.6 and 2.7 for the cases M=2 and M=4.

2.3.2 Application to Soft-limiting Channel

The soft-limiting channel model gives a better approximation to the TWTA but still ignores AM-PM conversion. Also, this model makes it possible to investigate the operation of the TWTA below the saturation region. The nonlinearity in this case is defined by the equation [24],

$$y(t) = L \text{ erf } \left(\frac{K\sqrt{\pi}}{2L} S_d(t)\right)$$

where $S_d(t)$ is the input to the soft-limiter;

K is the slope of the nonlinearity at $S_d(t) = 0$

and L is the maximum output signal level.

Figure 2.3(b) shows the transfer function of an erf (·) type limiter. Since we are interested only in the fundamental component of the output signal, using a series expansion for error function [11] and making substitution for $S_d(t)$ from (2.11) we get

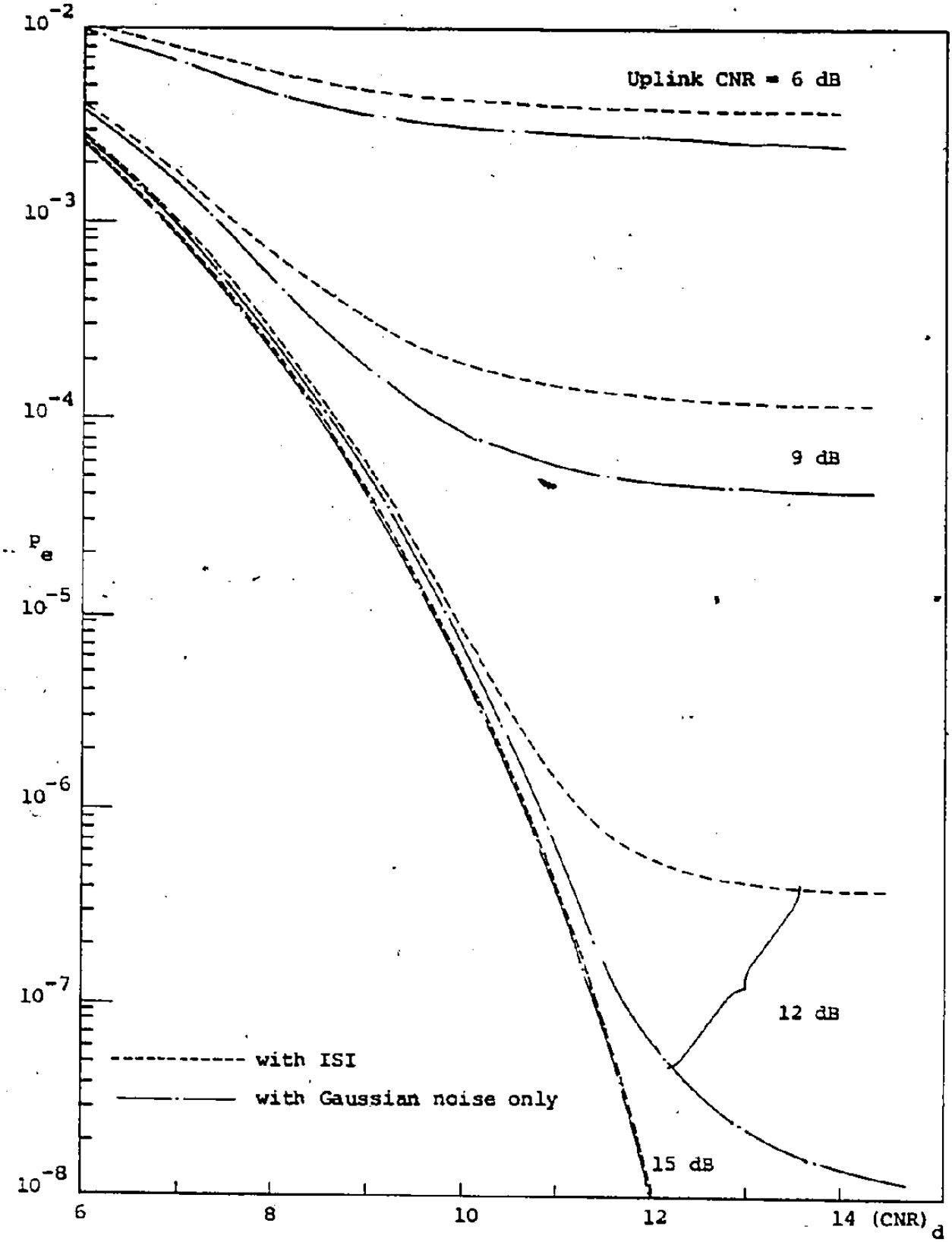

Fig. 2.4 Error probability of binary CPSK system, hard-limiting channel, $T/T_0=2$

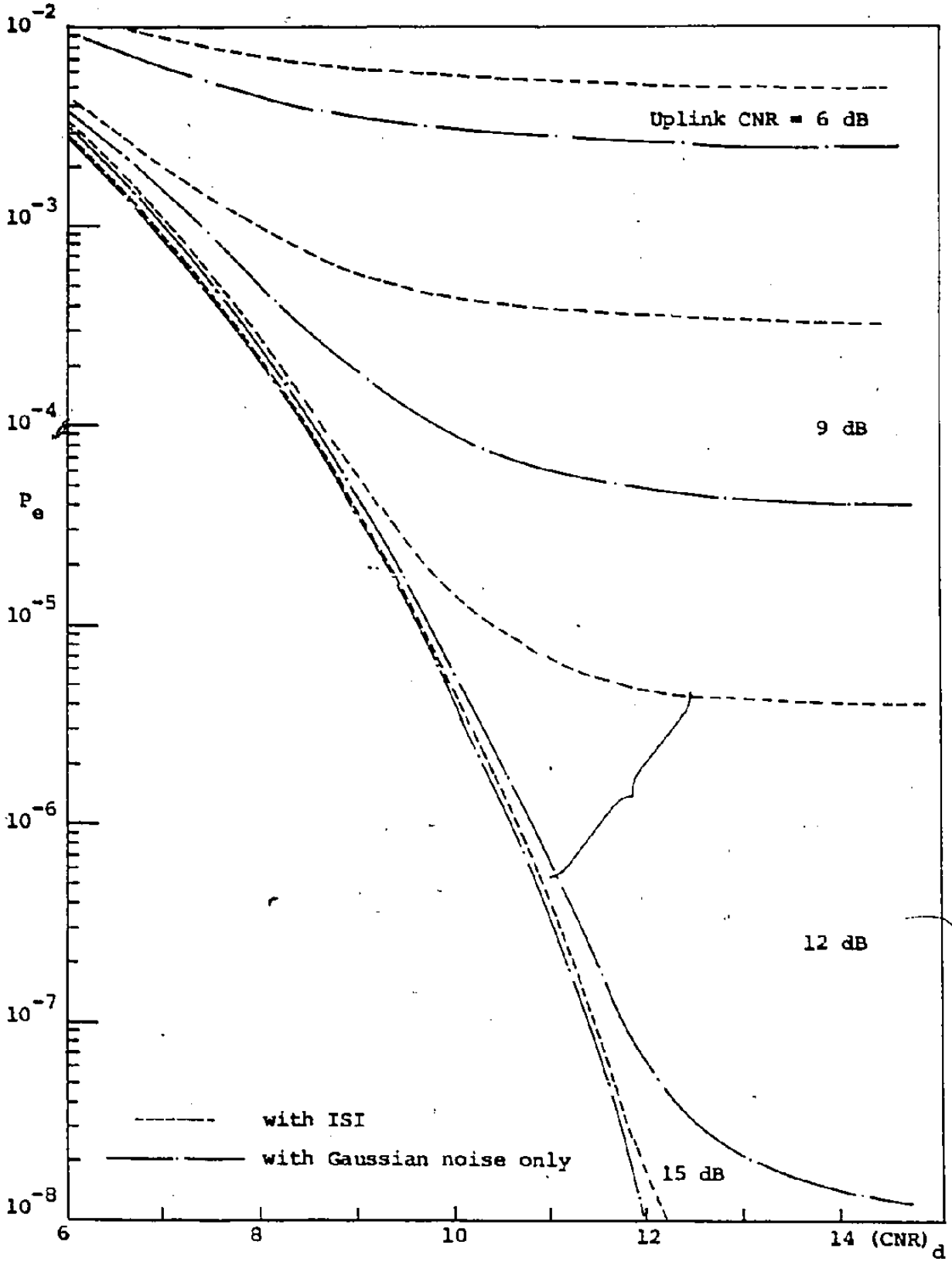

Fig. 2.5 Error probability of binary CPSK system, hard-limiting channel, $T/T_0=1$

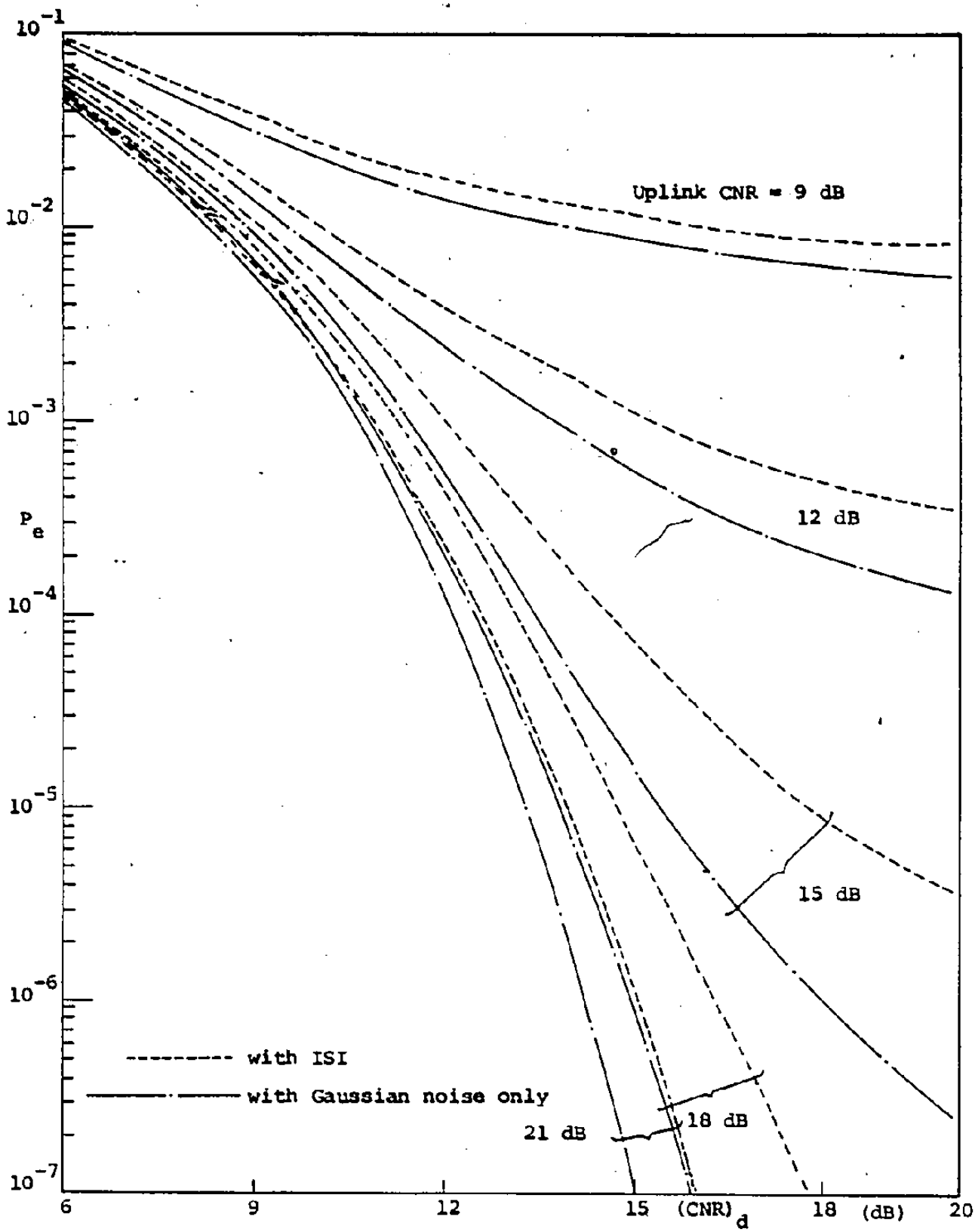

Fig. 2.6 Error probability of QPSK system, hard-limiting channel, $T/T_0=2$

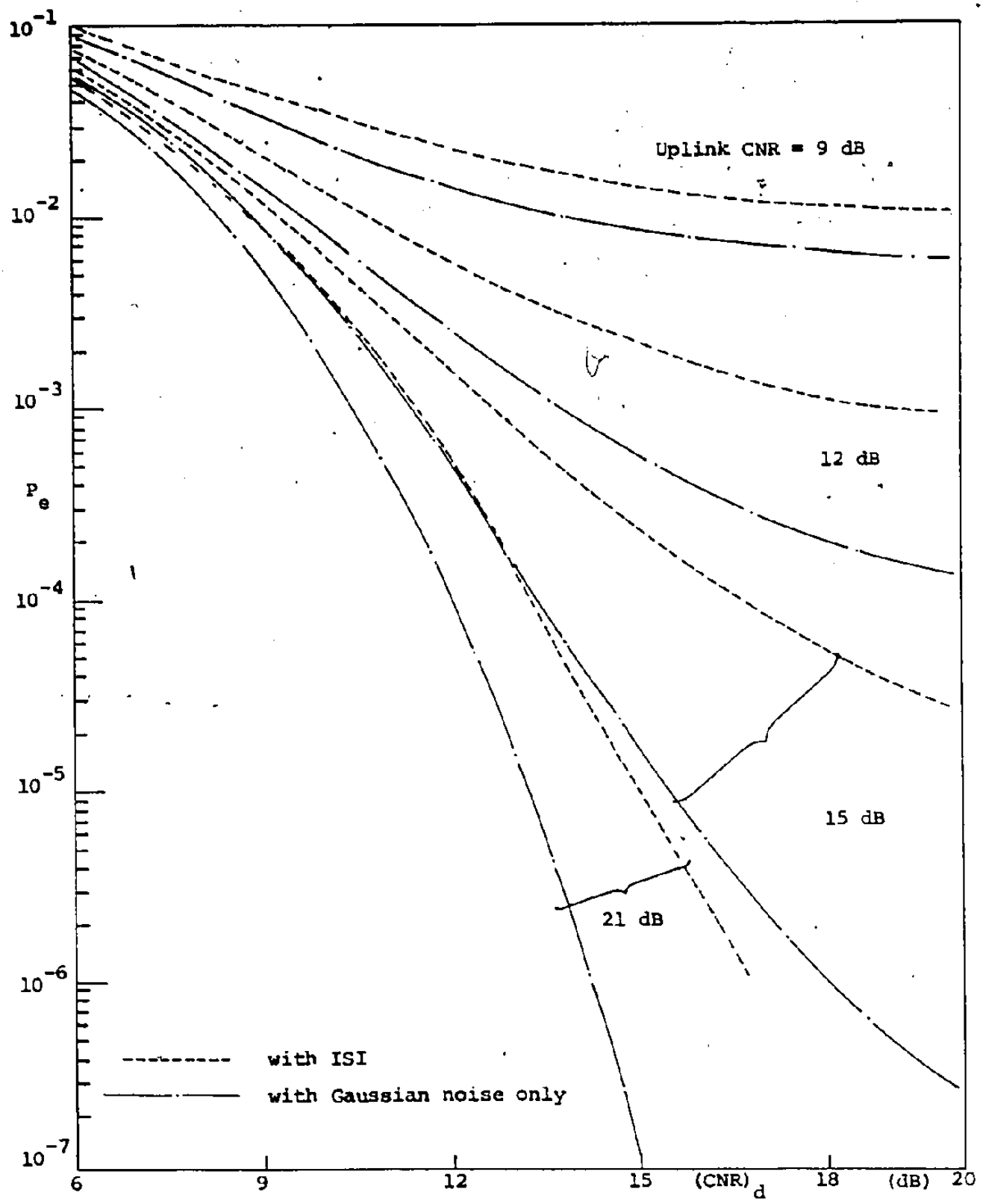

Fig. 2.7 Error probability of QPSK system, hard-limiting channel, $T/T_0=1$

$$y(t) = \frac{2}{\sqrt{\pi}}\,\gamma\, e^{-\gamma^2/2}\,\left[I_o\left(\frac{\gamma^2}{2}\right) + I_1\left(\frac{\gamma^2}{2}\right)\right] \cos\left[\omega_c t + \lambda(t)\right]$$

where $\gamma = \frac{k\sqrt{\pi}}{2L} R(t)$

From this expression it is clear that the AM-AM conversion of a soft-limiting channel is

$$f(R(t)) = \frac{2}{\sqrt{\pi}}\,\gamma\, e^{-\gamma^2/2}\,\left[I_o\left(\frac{\gamma^2}{2}\right) + I_1\left(\frac{\gamma^2}{2}\right)\right] \qquad (2.38)$$

and the AM-PM conversion

$$\rho(R(t)) = 0 \quad \text{for all } R(t).$$

With these values for $f(\cdot)$ and $\rho(\cdot)$, we can evaluate expressions (2.29) and (2.32).

To obtain numerical results we have considered the same bandlimiting filter as given in section 2.3.1. The results are shown in Figures 2.8-2.11.

In this case the downlink average carrier power to downlink thermal noise power is defined as,

$$(CNR)_d \triangleq \frac{E[f^2(R(t))]}{2\sigma_d^2}$$

where

$$E[f^2(R(t))] = \Sigma\, \frac{b_{\ell,m}}{(\sqrt{2}\,\sigma_u)^{\ell+m}}\, \frac{(-1)^{\ell+m/2}}{2\pi\,\sigma_u^2} \int_{-\infty}^{+\infty}\int_{-\infty}^{+\infty} f^2(\sqrt{x^2+y^2})$$

$$H_\ell\left(\frac{x-a_o}{\sqrt{2}\,\sigma_u}\right) H_m\left(\frac{y-b_o}{\sqrt{2}\,\sigma_u}\right) e^{-(x-a_o/\sqrt{2}\sigma_u)^2} e^{-(y-b_o/\sqrt{2}\sigma_u)^2}\, dx\, dy \qquad (2.40)$$

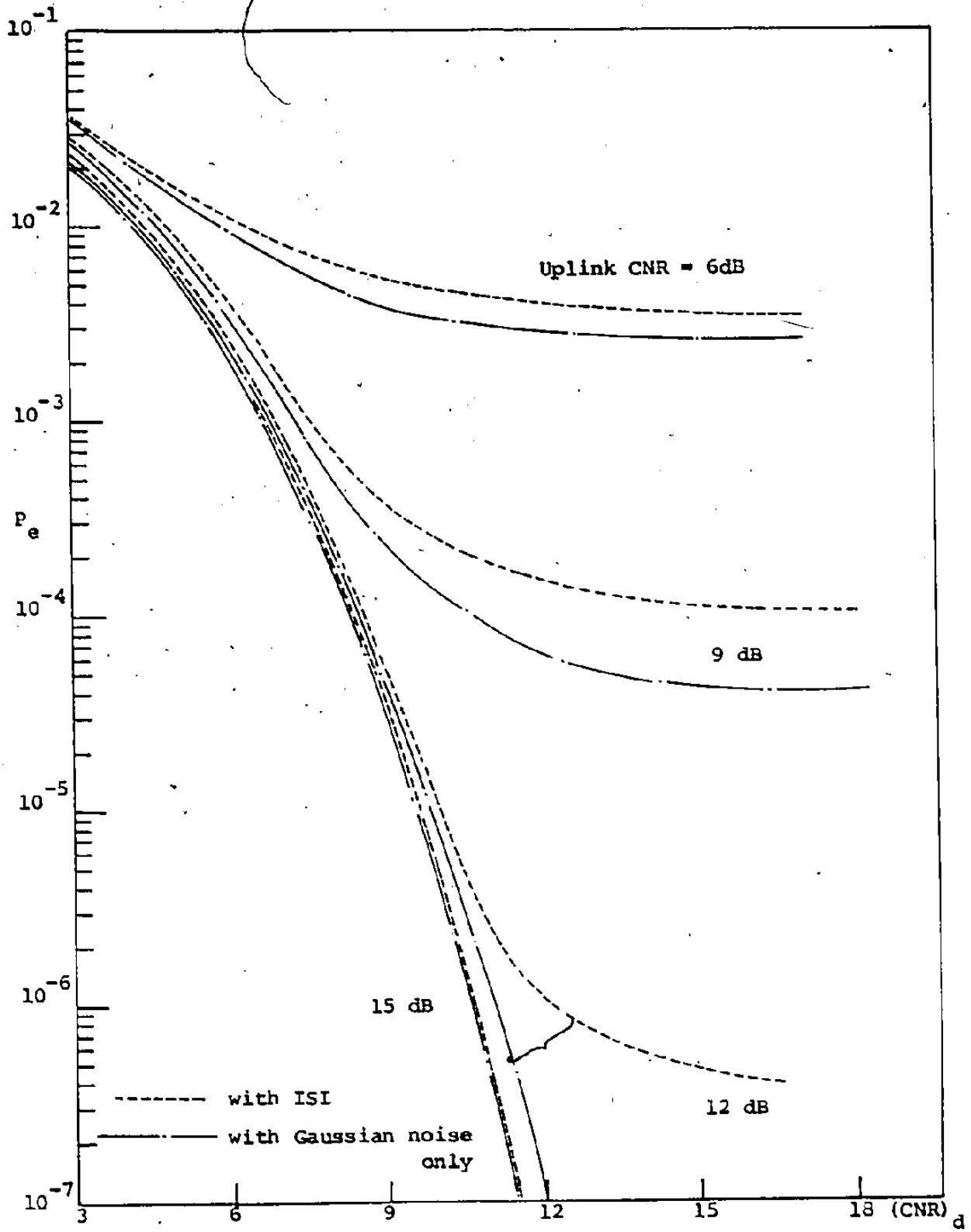

Fig. 2.8 Error probability of binary CPSK system, soft-limiting channel, $T/T_0=2$

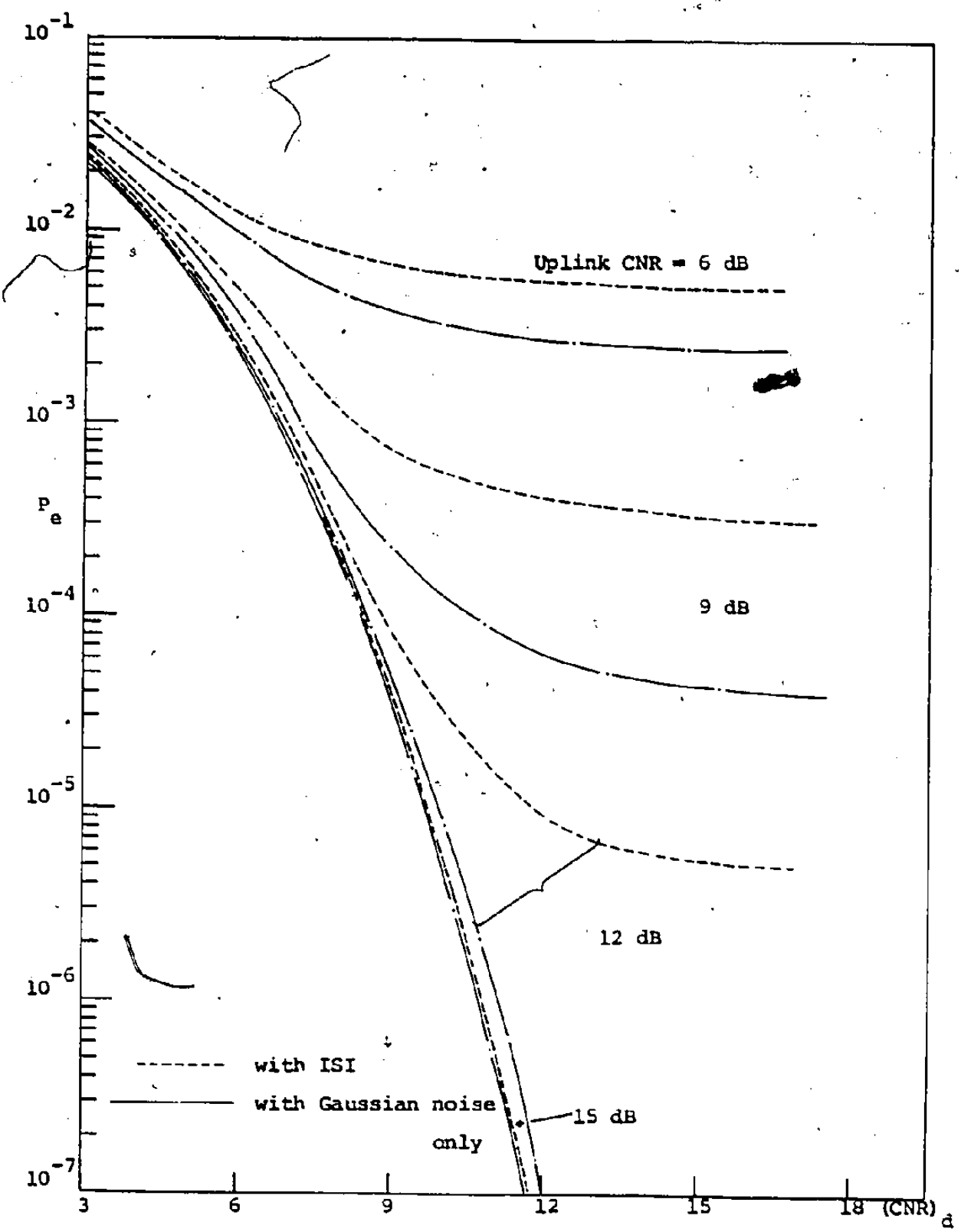

Fig. 2.9 Error probability of binary CPSK system, soft-limiting channel, $T/T_0=1$

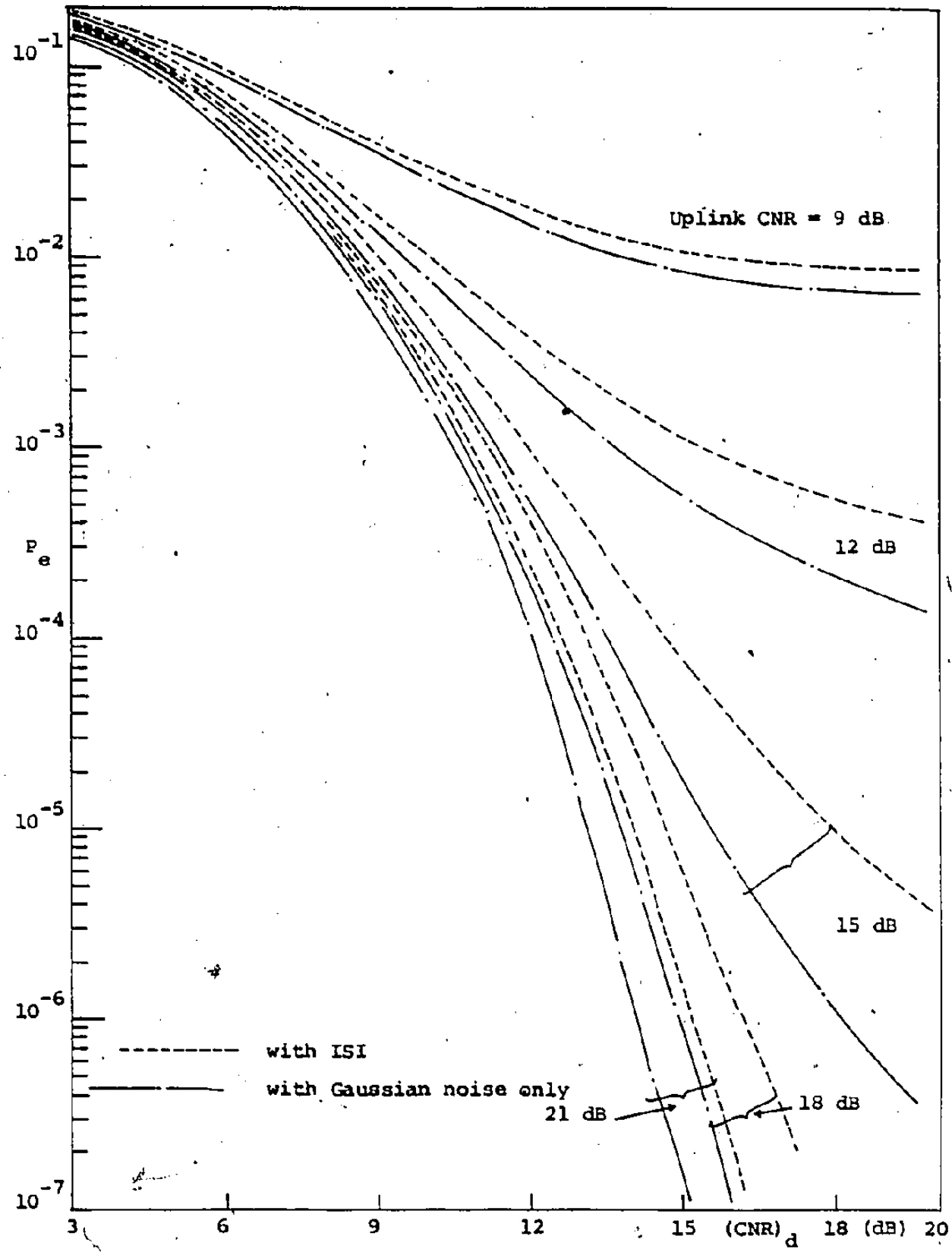

Fig. 2.10 Error probability of QPSK system, soft-limiting channel, $T/T_0=2$

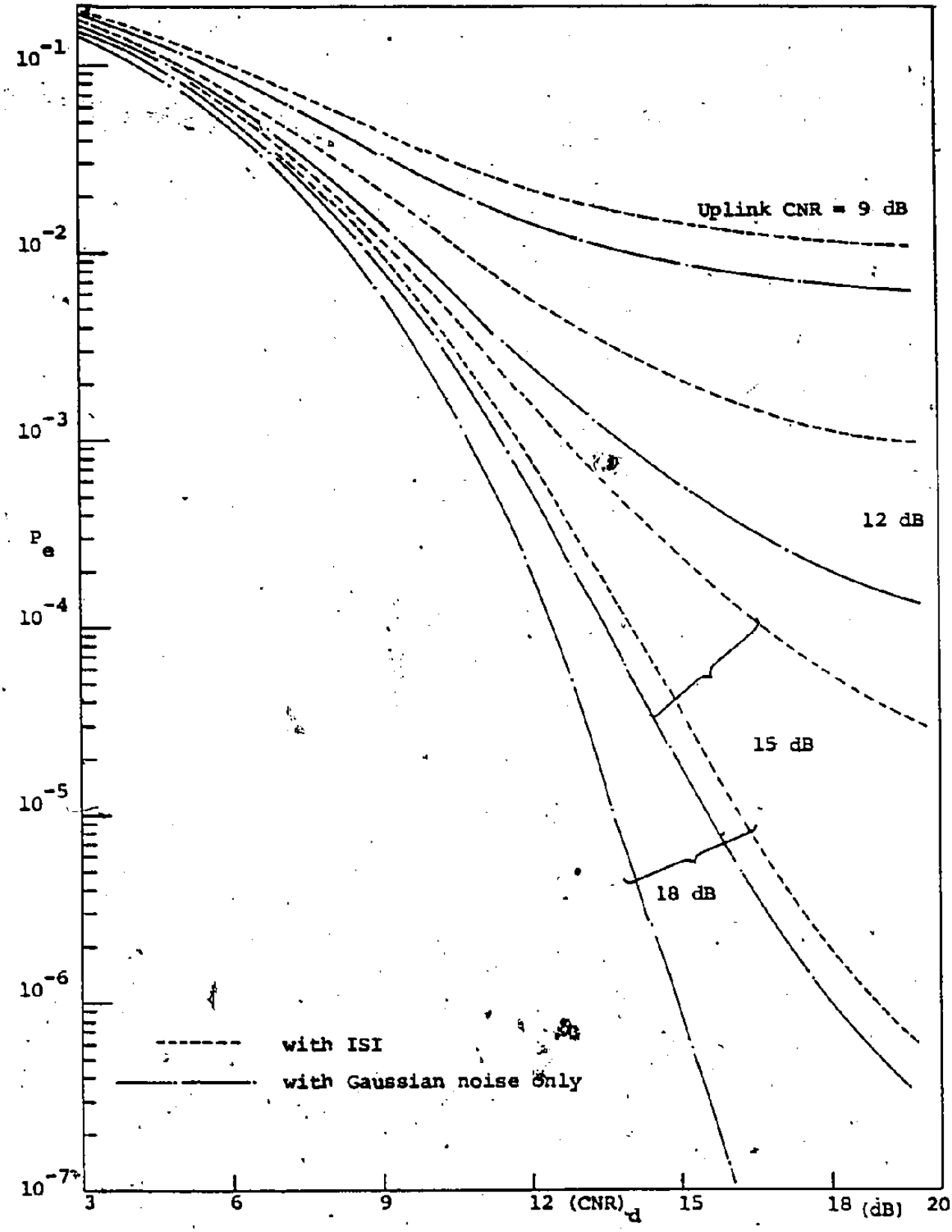

Fig. 2.11 Error probability of QPSK system, soft-limiting channel, $T/T_0=1$

Again, as before, the double intergral appearing in (2.40) is evaluated using Cartesian products of Gauss-Hermite formulas.

2.3.3 TWT Channel

In this case, we consider the effect of both AM-AM conversion and AM-PM conversion using a model of the actual TWT characteristic of a Hughes 261-H TWTA as used in the Intelsat IV satellite. The AM-AM and AM-PM conversions can be approximated by different methods [10,15,23]. In our example we use the quadrature model given by Hethrakal et al. [10,15]. With this model, the nonlinearities are expressed as

$$f^2(R) = z_p^2(R) + z_q^2(R)$$

$$\rho(R) = \tan^{-1}\left[\frac{z_p(R)}{z_q(R)}\right]$$

where

$$z_p(R) = C_1 R e^{-c_2 R^2} I_o (C_2 R^2)$$

$$z_q(R) = S_1 R e^{-s_2 R^2} I_1 (S_2 R^2)$$

$$c_1 = 1.61245; \quad c_2 = .053557$$

$$s_1 = 1.71850; \quad s_2 = .242218$$

To obtain numerical results we use the same filter as

given in section 2.3.1 and the results are shown in Figures 2.12-2.19.

In evaulating performance, we have considered three cases.

Case 1 TWTA driven at saturation. Therefore, the main sample value q_o = 4.5 mV.

Case 2 TWTA driven at saturation but with a phase compensated receiver. In this case we assume a carrier recovery loop tracks the AM-PM conversion effect (substracts 22.8^o from AM-PM conversion which is the AM-PM conversion at the saturation level if there is no uplink noise and interference).

Case 3 TWTA is operated at 6 dB input power back off from the saturation level.

Therefore, the main sample value q_o = 2.25 mV.

2.4 Conclusions

In this chapter we have analyzed the performance of M-ary CPSK transmission over bandlimited nonlinear channels. We have derived several expressions for the error probability. In deriving these expressions our objective was to obtain computationally efficient expressions for the error probability. One disadvantage of using the Confluent Hypergeometric functions is that at high CNR's the convergence of these functions becomes very slow. For

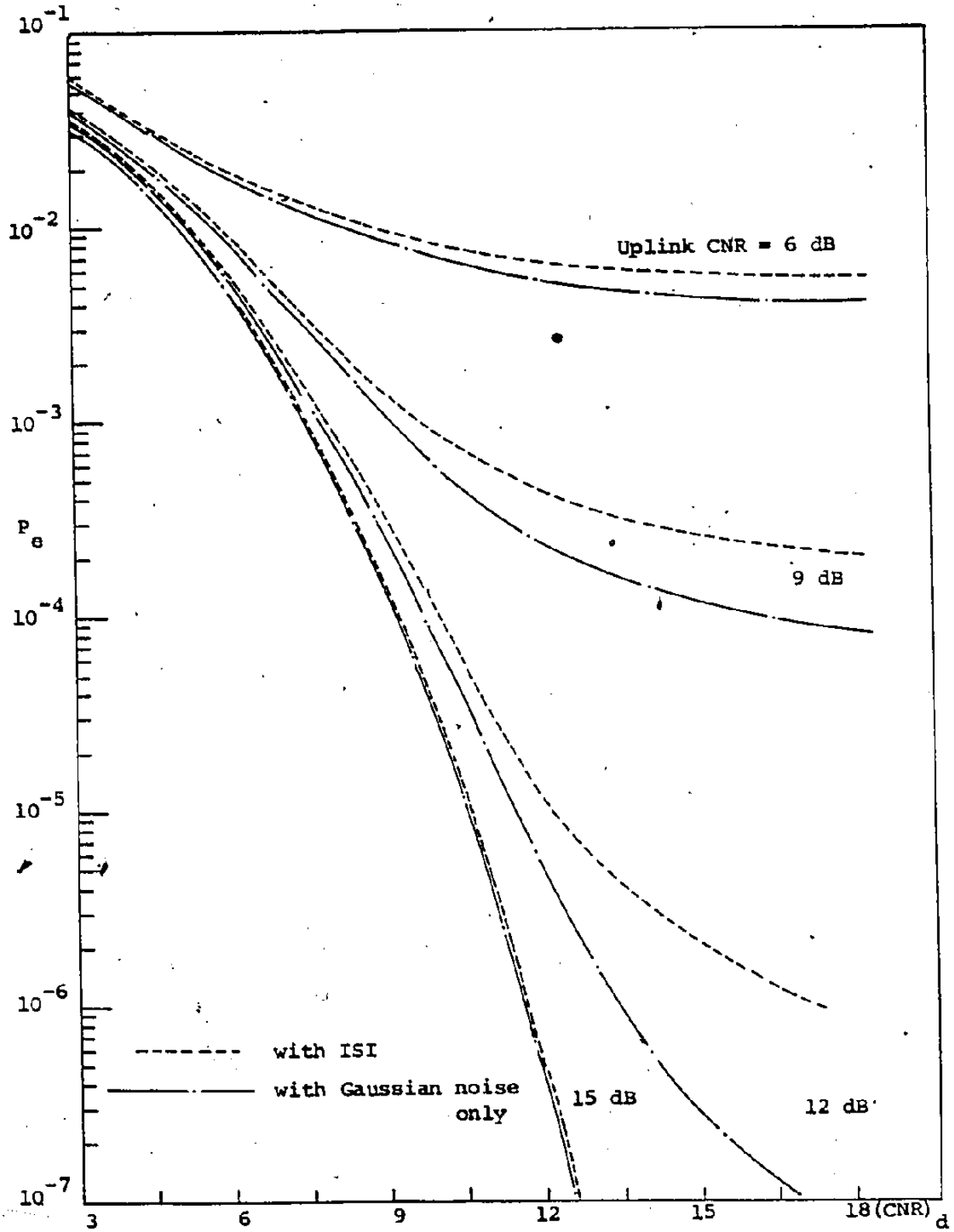

Fig. 2.12 Error probability of binary CPSK system, TWT channel (at saturation), $T/T_0=2$

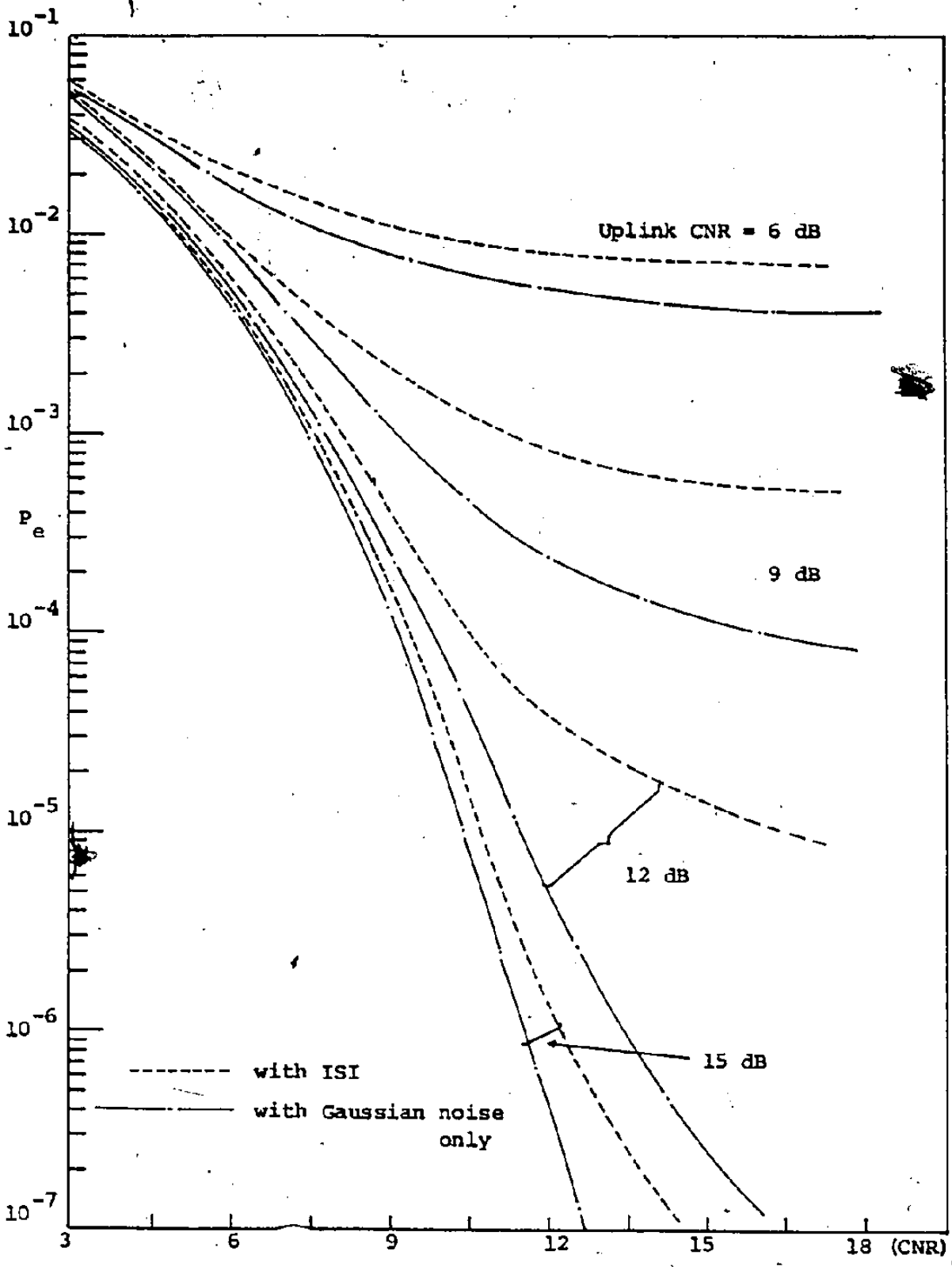

Fig. 2.13 Error probability of binary CPSK system, TWT channel (at saturation), $T/T_0=1$

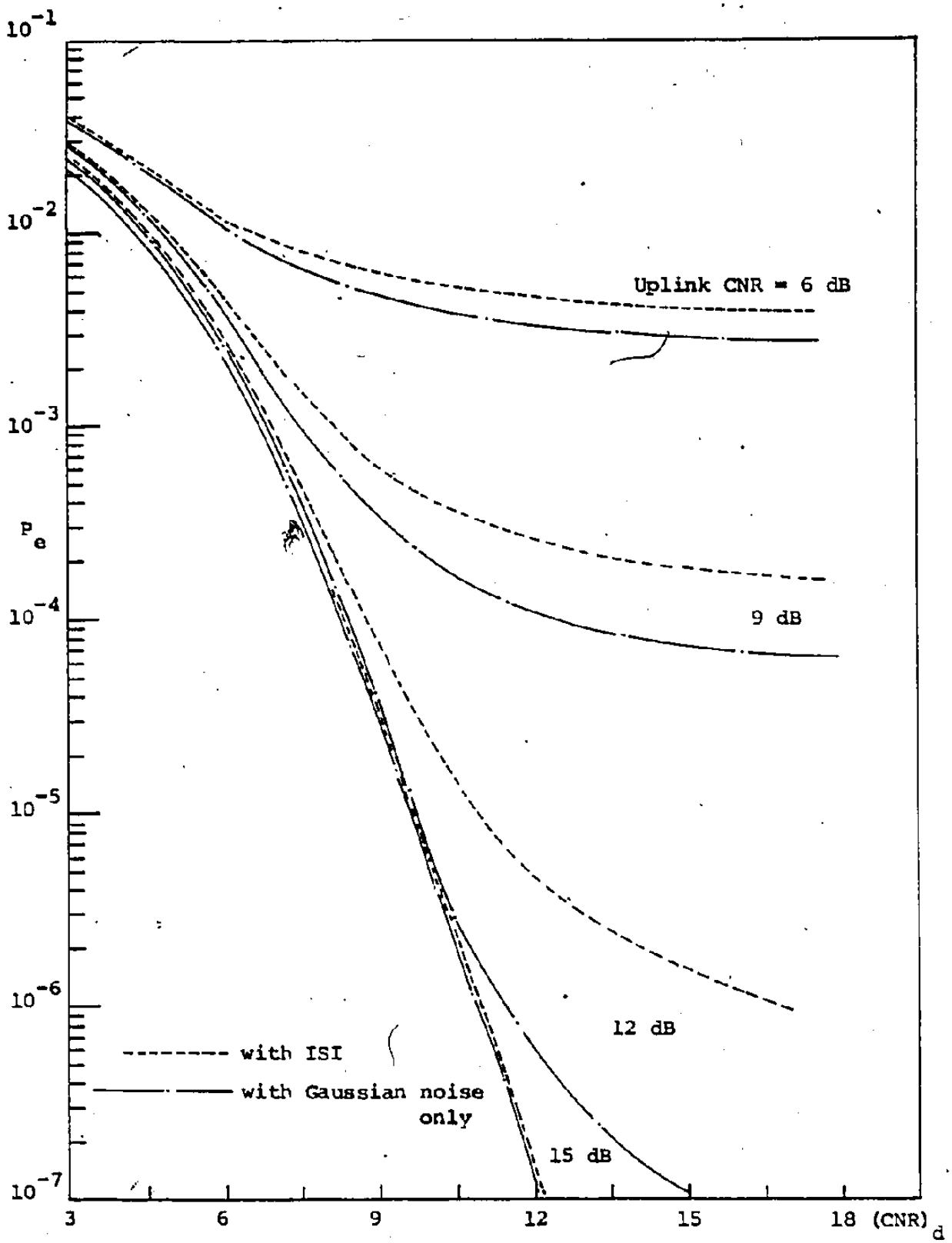

Fig. 2.14 Error probability of binary CPSK system, TWT channel (at saturation) with a phase compensated receiver, $T/T_0=2$

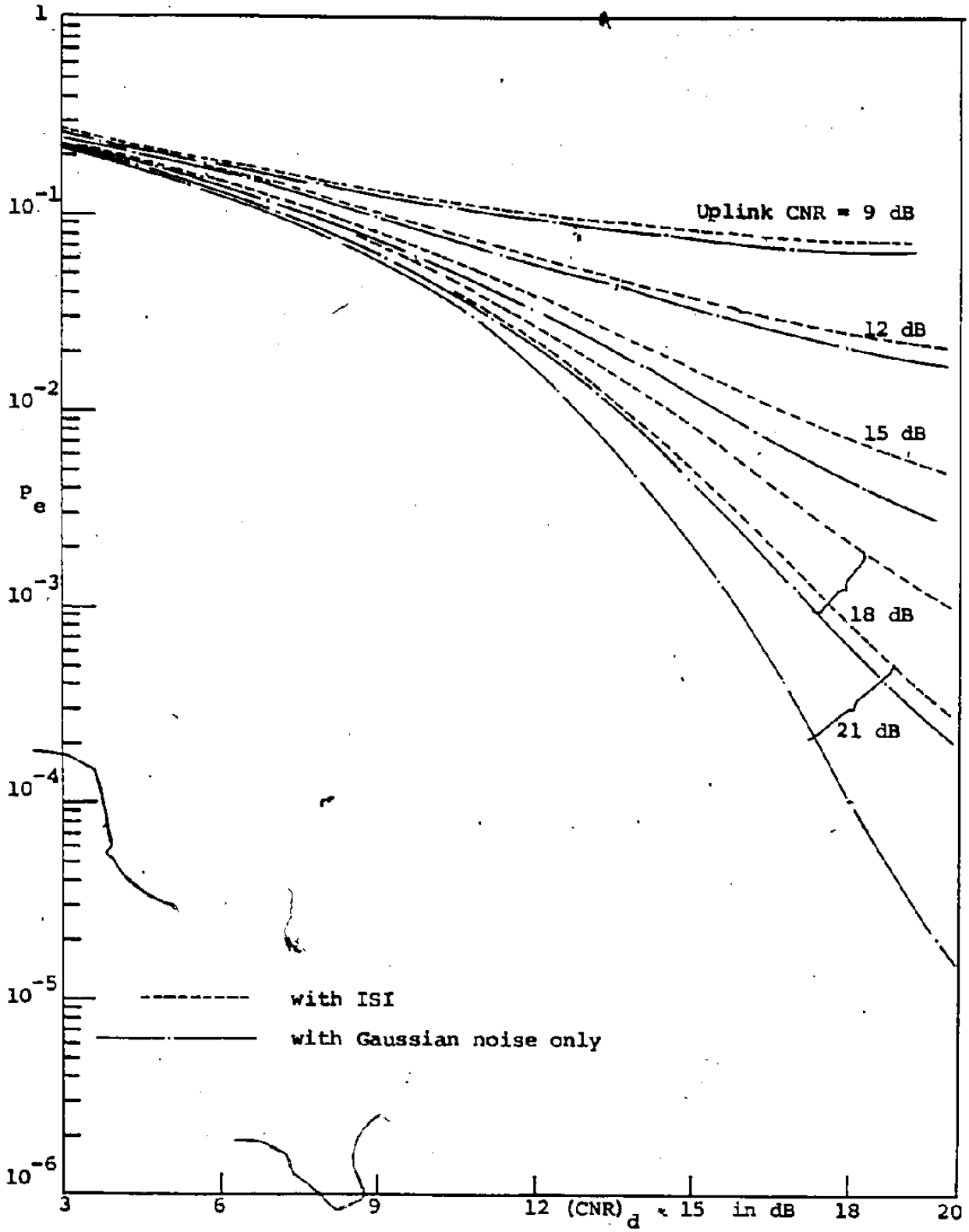

Fig. 2.15 Error probability of QPSK system, TWT channel (at saturation) $T/T_0=2$

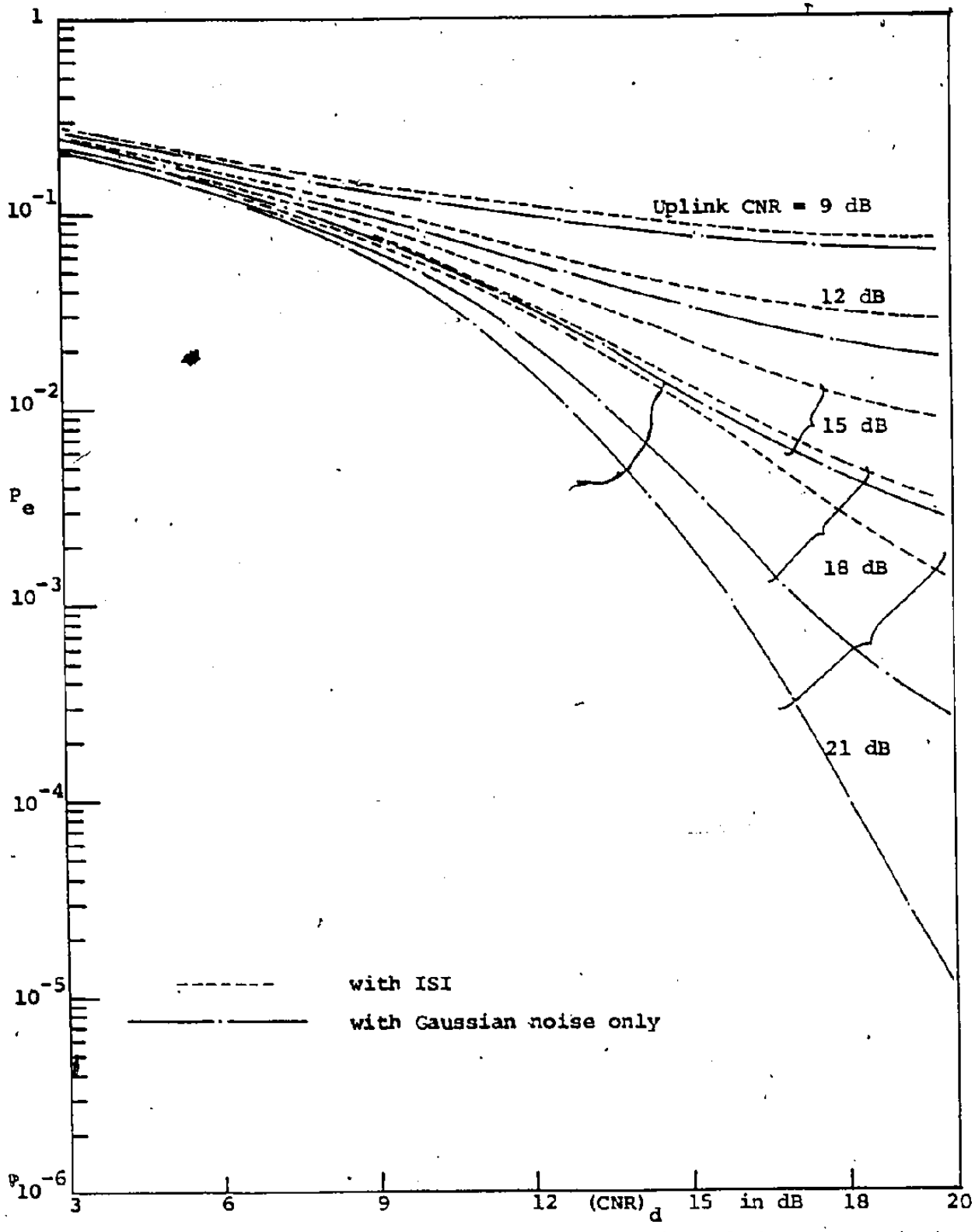

Fig. 2.16 Error probability of QPSK system, TWT channel (at saturation), $T/T_0=1$

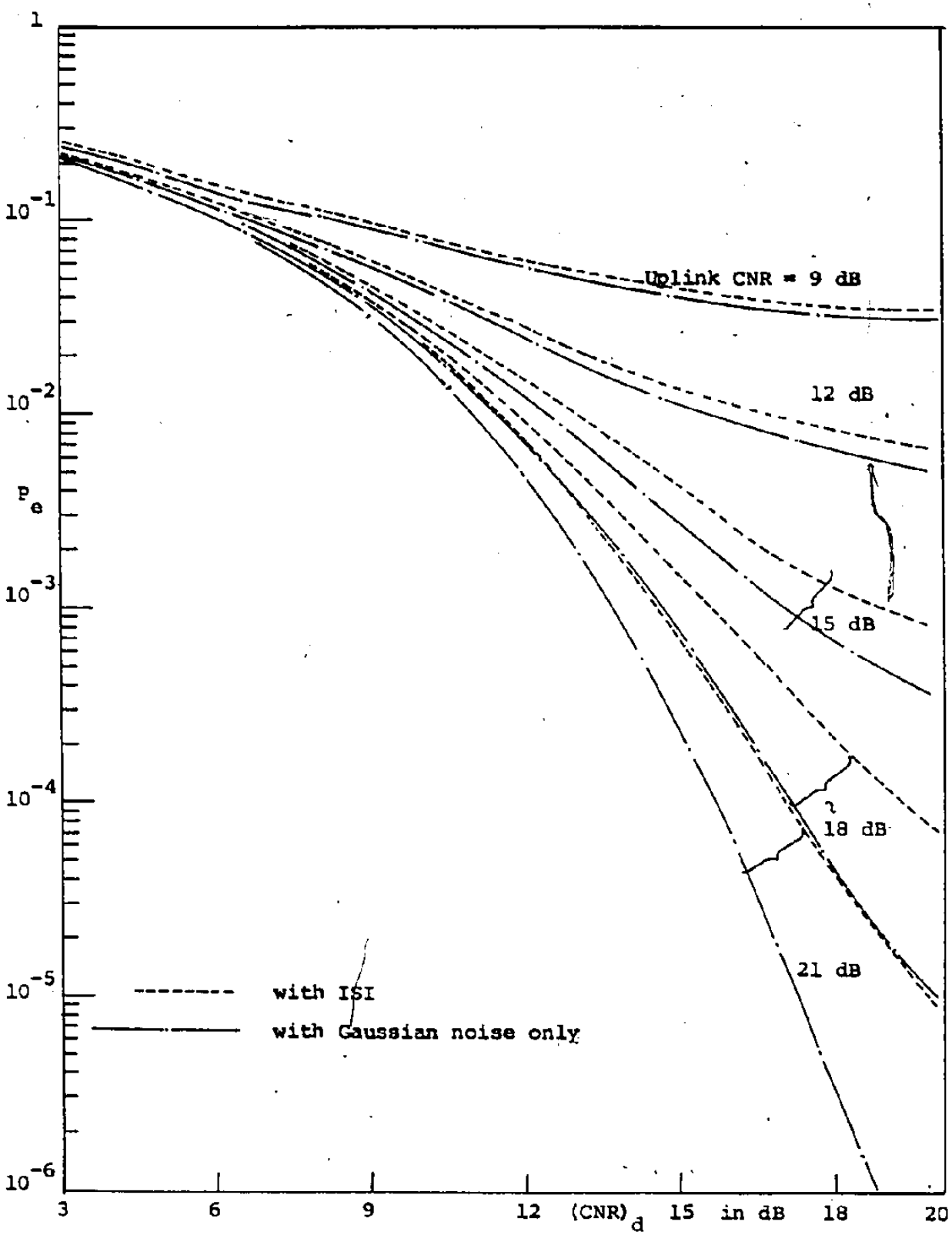

Fig. 2.17 Error probability of QPSK system, TWT channel (6 dB input power back off), $T/T_0=2$

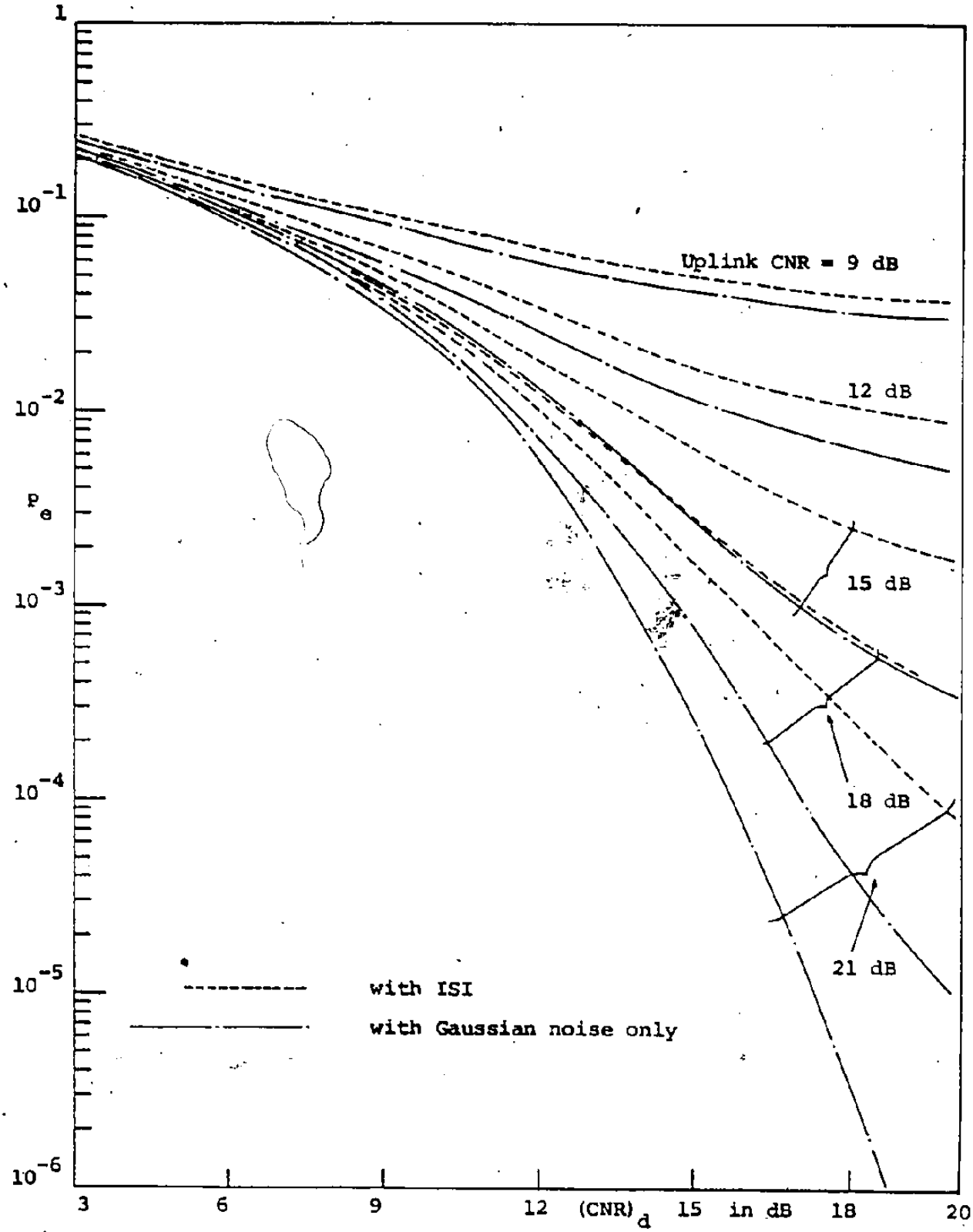

Fig. 2.18 Error probability of QPSK system, TWT channel (6 dB input power back off), $T/T_0=1$

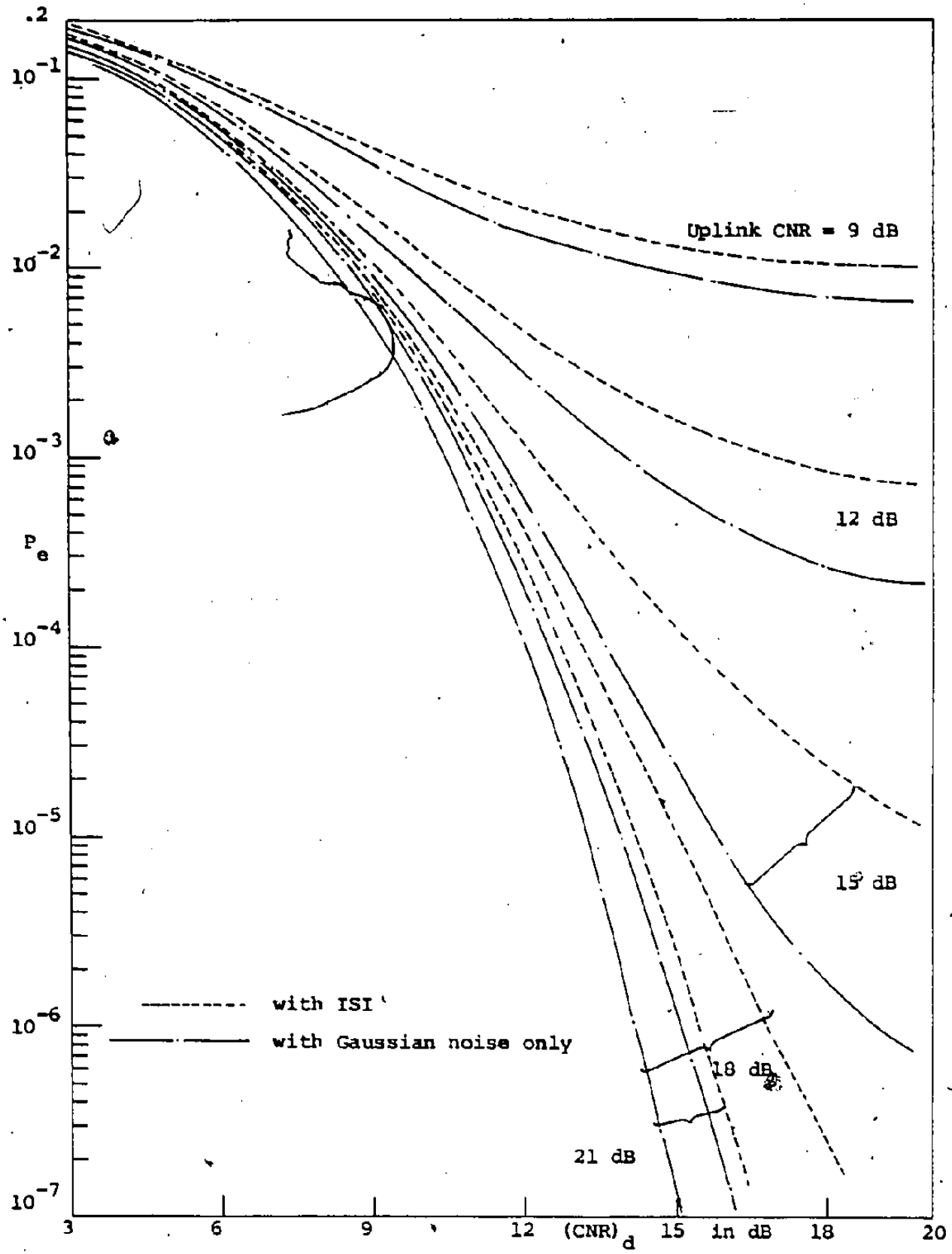

Fig. 2.19 Error probability of QPSK system, TWT channel (at saturation) with a phase compensated receiver, $T/T_0=2$

example when the CNR > 12 dB, we need typically 40 to 50 terms to attain any significant accuracy, and even when the CNR < 12 dB, it needs at least 30 terms. Therefore, numerical integration of the double integral of eqn. (2.33) in evaluating error probability expressions needs less time than that required for the previous case mentioned (eqn. 2.27). The reason for this is that the weighting function of the double integral is separable and therefore the Cartesian products of the Gauss-Hermite formulas can be efficiently employed. In all the cases we have considered, a 64 point Gauss-Hermite quadrature formula was sufficient for the CNR's we are interested in and at low CNR's even a 44 point formula was sufficient. The Confluent Hypergeometric function method has an advantage only in the case of binary PSK transmission over a hard-limiting channel. Obviously, when M > 4, the probability of error expression in terms of the Confluent Hypergeometric functions has to be used since it was not possible to obtain alternate expressions.

Examining the results for the hard-limiter, it can be concluded that the ISI degrades the performance only in the range of moderate downlink and uplink CNR's. At very high uplink CNR's, the ISI does not cause any significant system degradation. The reason for this is that at high uplink CNR's, the hard-limiter tends to restore the original pulse,

thus eliminating the ISI completely. At low downlink CNR's the system degradation is caused mainly by the downlink noise rather than the ISI. Also, at low uplink CNR's, the degradation is mainly due to the uplink thermal noise. The ISI plays a significant role only if it is comparable with the downlink and uplink noise powers.

The error rate curves for the soft-limiter are very similar to those of the hard-limiting channel since there is no AM-PM conversion in both cases. In the case of a TWT channel, the more significant factor in degrading performance is the AM-PM conversion, both at saturation and 6 dB input power backoff. But in binary PSK modulation, the AM-PM conversion does not cause any significant degradation. This is clearly seen from Figures 2.12 and 2.14. Therefore intersymbol interference causes the main degradation in system performance. Since AM-PM conversion has no significant effect on the performance degradation, we have not considered the 6 dB input power backoff case for binary PSK modulation.

As mentioned before, for QPSK modulation the significant factor in limiting the performance is AM-PM conversion. This can be seen from Figures 2.15 and 2.19. But at high uplink CNR, the ISI effect causes some noticeable degreadation as seen from Figures 2.15 and 2.16. In order to study the effect of input power backoff, we need

to compare the Figures 2.15 and 2.16 with 2.17 and 2.18. But in comparing these figures, it should be noted that we have to account for the different noise power densities, since for example, a 6 dB uplink CNR at saturation is not the same as a 6 dB uplink CNR at the 6 dB input power backoff point. Therefore, to make a proper comparison, any curve shown in Figure 2.15 or 2.16 should be compared with the appropriate curve in Figure 2.17 or 2.18, such that the uplink CNR is reduced by 6 dB. For example, the 18 dB uplink CNR curves in Figures 2.15 and 2.16 should be compared with the 12 dB uplink CNR curves in Figures 2.17 and 2.18, respectively, but ignoring any changes in downlink CNR which can be neglected.

Comparing the curves in this way it can be concluded that the performance at saturation is better than the performance at the 6 dB input power backoff point. The error rate curves for a phase compensated receiver are very similar to those of a soft limiter, again as before. In this case, the ISI causes system performance degradation significantly as expected since a major part of the AM-PM conversion is removed by the carrier tracking loop.

CHAPTER 3

PERFORMANCE BOUNDS FOR BINARY CPSK TRANSMISSION

3.1 Introduction

Although, exact evaluation of the error probabilities of CPSK modulated systems in the presence of Gaussian noise and ISI is of both practical and theoretical interest, often it is desirable to have approximate results which can be evaluated with minimal computational effort. The major reason for this is that the exact results may not be totally accurate in practical systems since the assumptions made in deriving the analytical results need not hold in real life systems. Since theoretically derived accurate results become approximate results for a practical system, one may seek alternate methods to obtain approximate results via mathematically simple, less complicated expressions that need little computational effort.

We address this problem in this chapter. Again, we make use of the analysis previously done [26-32] in evaluating performance bounds for linear digital systems. The research work on the derivation of bounds on performance extends over more than a quarter century and an extensive list of references can be found in [32]. Yao and Tobin [32]

demonstrated a general method of deriving bounds, and interestingly enough, most of the bounds derived previously could be derived using their technique. Yao and Tobin made use of the properties and inequalities of moment space as analyzed by Dresher [31] in deriving their bounds.

In general, the evaluation of error probabilities in the presence of ISI or in any other interference can be posed as the evaluation of the expected value of a function with respect to a random variable. That is, if $f(\alpha)$ is the error probability under the assumption that α is known, then the unconditional error probability becomes

$$P_e = \int f(\alpha)\, d\, F(\alpha) \tag{3.1}$$

where $F(\alpha)$ is the cumulative distribution of the interfering random variable α. In our case, the interference variable α is the intersymbol interference. To include discrete probability densities, we have used the Stieltjes integral in (3.1). If $F(\alpha)$ is known, P_e can be evaluated at least in the theoretical sense. But in the case of ISI, $F(\alpha)$ is almost always not known in closed form, and this holds true for most of the interferences encountered in communication systems. Instead, in most cases at least some of the moments of the ISI can be evaluated easily, so that our object is to derive

$$\sup_{F(\alpha)} P_e = \sup_{F(\alpha)} \int f(\alpha)\, d\, F(\alpha)$$

and

$$\inf_{F(\alpha)} P_e = \inf_{F(\alpha)} \int f(\alpha)\, d\, F(\alpha)$$

where the supremum and infimum are taken over all possible distribution functions $F(\alpha)$ which obey the given moment conditions. There is well documented research literature on this subject [38, 39] but in this chapter we make use of moment space techniques only.

Dresher [31] addressed the problem of deriving inequalities of a function as given in the form of (3.1). To state briefly his work, let us assume that $f_1(\alpha)$, $f_2(\alpha)$, ..., $f_m(\alpha)$ are continuous functions in the interval $I = [a,b]$. Then the moments $m_i(F)$ of $F(\alpha)$ are defined by

$$m_i(F) = \int_I f_i(\alpha)\, d\, F(\alpha)$$

The m-th moment space R^m is defined as the set of points $m = (m_1, \ldots, m_m)$ in m-dimensional Euclidean space whose coordinates are the moments $m_1(F), \ldots, m_m(F)$ of at least one distribution function $F(\alpha)$. Then R^m is closed, bounded and convex. Let C^m be defined as the curve traced out in m-dimensional space by $m_i = f_1(\alpha)$, $(i = 1, \ldots, m)$ as α varies between a and b. Let H be the convex hull of C^m. Then

$$H = R^m$$

Detailed description and proof of the above statement can be

found in reference [31].

To apply this work to our problem and restricting ourselves to 2-dimensional moment space R^2 for mathematical tractability, we can assume P_e to be one of the coordinates since $f(\alpha)$ is a continuous function. The remaining coordinate can be selected from one of the known moments. Then evaluating the upper and lower envelopes of the convex hull H in the 2-D space, the upper and lower bounds on P_e in terms of the known moment can be derived.

Since we need to know the convex hull H, the complexity of the problem depends on the complexity of the function $f(\alpha)$. If $f(\alpha)$ is of simple mathematical form as for linear channels, the bounding technique can be readily applied. But in nonlinear satellite channels, $f(\alpha)$ is not known in closed form for any of the models treated in this thesis, and for that matter, except for the hard-limiting channel, $f(\alpha)$ can be obtained only in the form of integrals. Therefore, it is extremely difficult to analyze the behaviour of $f(\alpha)$ to obtain the convex hull and the bounding technique cannot be easily applied. Therefore, in the following sections we consider only binary PSK signalling. The bounds are derived in terms of absolute moments of the ISI for the general TWT channel model. In the remaining sections, we apply these bounds to different channel models to obtain numerical results.

3.2 Derivation of the Bounds

A binary PSK modulated signal can be expressed, following the same notations as in section 2.2, as

$$S(t) = \sum_{k=-\infty}^{k=\infty} p(t-kT) \cos(\omega_c t + \phi_k) \qquad (3.1)$$

where $\phi_k = 0$ or π with equal probability.

Following the same arguments as in section 2.2, the input to the satellite transponder during the baud interval $(k-1)T \leq t < kT$ can be expressed as,

$$S_t(t) = A(t-kT) \cos(\omega_c t + \phi_k) + \{\sum_n A(t-nT) \cos(\phi_n+\phi_k)\} \cdot \cos(\omega_c t + \phi_k) + n_c^u(t) \cos(\omega_c t + \phi_k) - n_s^u(t) \cdot \sin(\omega_c t + \phi_k) \qquad (3.2)$$

where the summation is taken over all interfering terms in the baud interval under consideration.

Because we are using binary PSK modulation we note that no quadrature ISI component appears in (3.2). Then the signal at the receiver is

$$S_r(t) = f(R(t)) \cos[\omega_c t + \phi_k + \lambda(t) + \rho(R(t))] + n_c^d(t) \cos(\omega_c t + \phi_k) - n_s^d(t) \sin(\omega_c t + \phi_k) \qquad (3.3)$$

where

$$R(t) \triangleq \sqrt{x^2(t) + y^2(t)}; \qquad \lambda(t) \triangleq \tan^{-1}\left[\frac{y(t)}{x(t)}\right]$$

$$x(t) \triangleq A(t-kT) + \alpha(t) + n_c^d(t)$$

$$y(t) \triangleq n_s^d(t)$$

$$\alpha(t) \triangleq \sum_{\substack{n \\ n\neq k}}' A(t-nT)\ \text{Cos}\ (\phi_n + \phi_k) \qquad (3.4)$$

Because the ϕ_n are random variables, we note that α defines a random variable, which is the ISI term. At the receiver, $S_r(t)$ is coherently demodulated as described in section 2.2. In this case, we consider the in-phase sample conponent X_o only, which is given as

$$X_o = f(R(t_o))\ \text{Cos}\ \phi_k\ \text{Cos}[\lambda(t_o) + \rho(R(t_o))] + n_c^d(t_o) \qquad (3.5)$$

Since n_c^d is Gaussianly distributed, the probability of error conditioned on the random variables R and λ is

$$P_{e|\lambda,R} = \frac{1}{2} P_e\ [X_o<0 \mid \phi_k=0,\lambda,R] + \frac{1}{2} P_e\ [X_o>0 \mid \phi_k=\pi,\lambda,R]$$

$$= \frac{1}{2}\ \text{erfc}\ \left[\frac{f(R)\ \text{Cos}\ (\lambda + \rho(R))}{\sqrt{2}\ \sigma_d}\right] \qquad (3.6)$$

The time dependence of the variables is dropped in (3.6) for notational convenience.

Using the relations defined in (3.4), the probability of error conditioned only on α , i.e. the ISI random variable, can be shown to be,

$$P_{e|\alpha} = \frac{1}{2\pi\sigma_u^2} \int_{-\infty}^{+\infty}\int_{-\infty}^{+\infty} \frac{1}{2}\,\mathrm{erfc}\left[\frac{f(\sqrt{x^2+y^2})\cos\left(\tan^{-1}(y/x)+\rho(\sqrt{x^2+y^2})\right)}{\sqrt{2}\,\sigma_d}\right]$$

$$\cdot \exp\left[-\frac{(x-A-\alpha)^2}{2\sigma_u^2}\right] \cdot \exp\left(\frac{-y^2}{2\sigma_u^2}\right) dx\, dy \qquad (3.7)$$

Next, we try to give a useful interpretation for our present purpose of the expression given in (3.7). The term $(A+\alpha)$ is the sum of the wanted signal component and the unwanted ISI component α. Therefore $(A+\alpha)^2/2\sigma_u^2$ represents the effective carrier power to noise power ratio, when α is given. The effect of the component α is to either increase or decrease the CNR depending on the sign of α. Therefore when α is given, the expression $P_{e|\alpha}$ can be evaluated using the expressions derived for evaluating the probability of error in the absence of ISI. Defining this term by $P_g(A+\alpha)$, i.e. $P_g(A+\alpha) \triangleq P_{e|\alpha}$, we obtain the required probability of error as,

$$P_e = \int_{-I_m}^{+I_m} P_g(A+\alpha)\; d\,F(\alpha) \qquad (3.8)$$

where $I_m \triangleq \sum_n |q_n|$ is the worst case ISI magnitude or the peak value of the ISI. In general, the interference terms for $n > N$, become negligibly small and therefore I_m is always finite. In (3.8), $F(\alpha)$ denotes the cumulative probability distribution of the ISI random variable α. The

probability density function of α is a discrete function which assumes 2^{2N} values where 2N is the total number of interfering samples within any baud interval assuming the filter to have a symmetrical unit pulse response. Therefore, it is theoretically possible to evaluate P_e by computing 2^{2N} values of $P_g(A+\alpha)$ and then taking the average of these. Since the number of computations grows exponentially with N, when there is a large number of interference terms direct enumeration of P_e becomes impracticable.

Since (3.8) is in the form of (3.1), as mentioned in the introduction, we can use moment space bounding techniques. For this we need to know the shape of $P_g(A+\alpha)$ in the interval $\alpha \in [-I_m, I_m]$. One observation is that, when α varies from $-I_m$, to I_m, P_e decreases monotonically since the effect of α is either to increase or decrease the uplink CNR as explained before. With this observation, we can readily extract a convex region of $P_g(A+\alpha)$ under the restriction that $I_m < A - \sigma_u$. The proof of the convexity of $P_g(A+\alpha)$ under this restriction is given in Appendix B. The relation between I_m and σ_u when $A = 1$ is shown in Figure 3.1, which shows that in all practical systems of interest, this is not an undue restriction.

Next, we replace $P_g(A+\alpha)$ by an equivalent expression

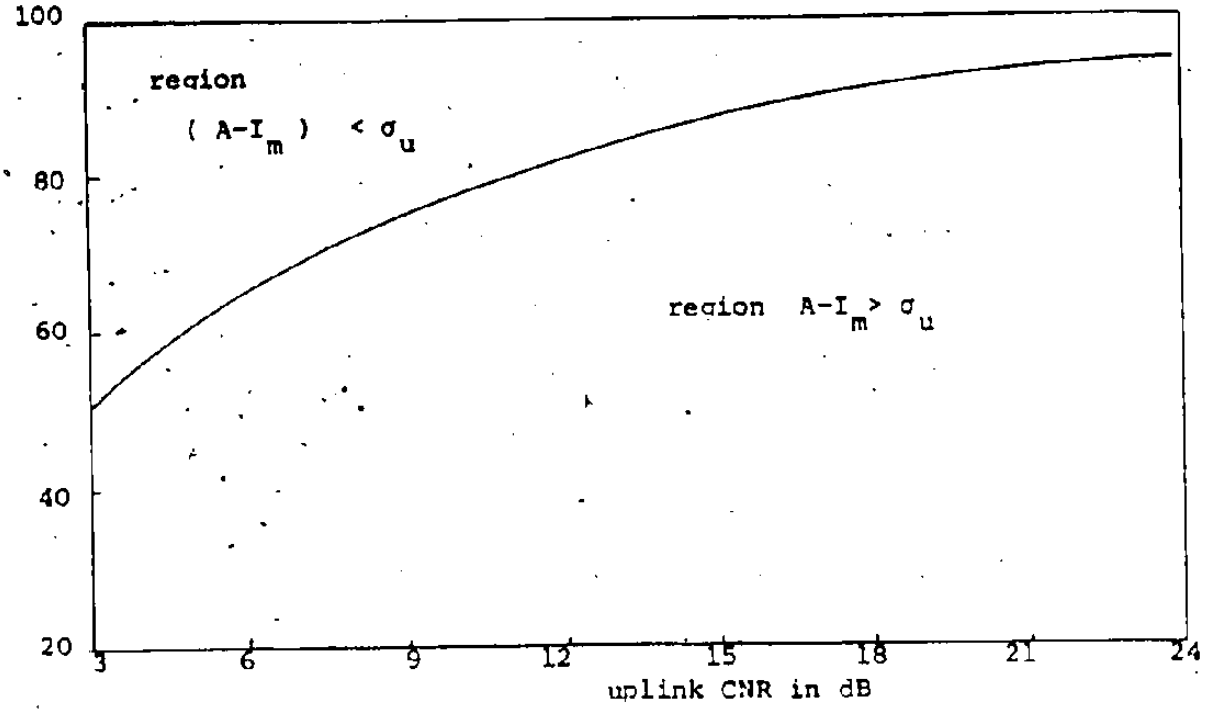

Fig. 3.1 Percentage eye closure vs. uplink CNR

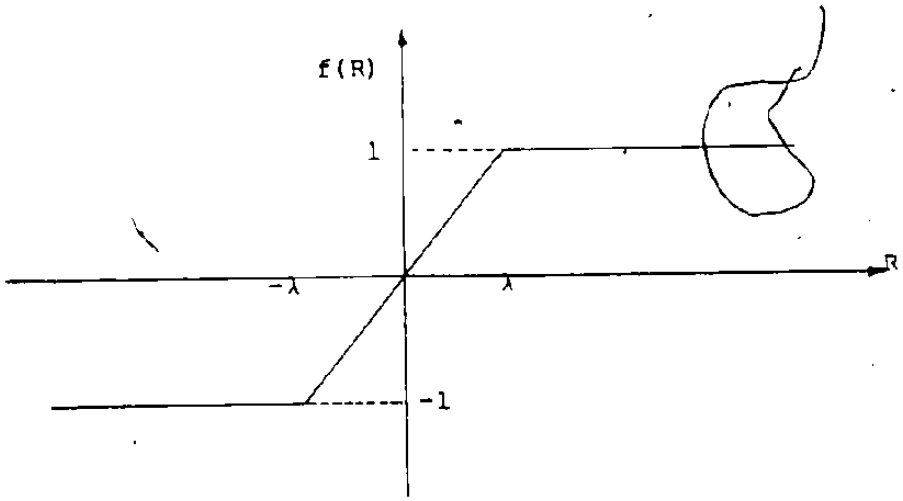

Fig. 3.2 Characteristics of a piece-wise smooth limiter

in terms of $|\alpha|$. We note that α is a discrete random variable taking 2^{2N} values. Hence, α can be separated into two disjoint sets $\{-|\alpha|\}$ and $\{+|\alpha|\}$ each having 2^{2N-1} discrete values. Therefore [30], we get

$$P_g(A+\alpha) = \frac{1}{2}\left[P_g(A+|\alpha|) + P_g(A-|\alpha|)\right] \triangleq f(|\alpha|) \qquad (3.9)$$

As explained in the introduction, if we select P_e as one of the coordinates in the 2-D moment space, we can select the first absolute moment of ISI as the other coordinate. We are then interested in the convex hull of $f(|\alpha|)$ as $|\alpha|$ varies from 0 to I_m. Since $f(|\alpha|)$ is strictly convex upward in this region, the upper envelope $H_u(|\alpha|)$ of the convex hull is,

$$H_u(|\alpha|) = \left\{\frac{1}{2}\left[P\ (A+I_m) + P\ (A-I_m)\right] - P_g(A)\right\}\frac{|\alpha|}{I_m} + P_g(A)$$

Then a upper bound on P_e is,

$$P_e \leq E\left[H_u(|\alpha|)\right]$$

$$= \frac{1}{2}\left[P_g(A+I_m) + P_g(A-I_m) - 2P_g(A)\right]\frac{m_1}{I_m} + P_g(A) \qquad (3.10)$$

where m_1 is the first absolute moment of α.

Since $f(|\alpha|)$ is convex upward, the lower envelope $H_L(|\alpha|)$ of the convex hull is the curve $f(|\alpha|)$ itself. Therefore, a lower bound on P_e can be expressed as

$$P_e \geq E[H_L(|\alpha|)]$$

$$= \frac{1}{2}[P_g(A+m_1) + P_g(A-m_1)] \qquad (3.11)$$

The inequality (3.11) can also be obtained through direct application of Jensen's inequality.

The next step is to evaluate the first absolute moment m_1 of ISI. But this is not easy to evaluate and therefore the following bounds are used for m_1 [30].

$$\sqrt{E[\alpha^2]} \leq m_1 \leq \frac{\{E[\alpha^2]\}^{3/2}}{\sqrt{E[\alpha^4]}}$$

The function $f(|\alpha|)$ increases monotonically when $|\alpha|$ varies from 0 to I_m. Therefore, when evaluating (3.11), the larger value of m_1 should be used and when evaluating (3.12), the lower value of m_1 should be used.

In the following sections, we apply these bounds to different nonlinear channel models to obtain numerical results. We use the 4-pole Chebyshev bandlimiting filter with $T/T_o = 2$, as given in Chapter 2.

3.3 Application to Different Channel Models

3.3.1 Hard-limiting Channel [55]

For a hard-limiting channel, the probability of error in the absence of ISI can be obtained from (2.34) by taking the m=0 term. Then (2.34) reduces to the series obtained by Jain and Blachman [11], which is

$$P_e = \frac{1}{2} - \frac{1}{\pi} \sum_{n=0}^{\infty} (-1)^n \frac{\Gamma(n/2+1)}{(2n+1)!} \rho_d^{2n+1} \, {}_1F_1\left(n+\frac{1}{2}, 2n+2, -\rho_d^2\right)$$

$$\cdot \frac{\Gamma(n+3/2)}{(2n+1)} q^{2n+1} \, {}_1F_1\left(n+\frac{1}{2}, 2n+2, -q^2\right) \qquad (3.12)$$

To evaluate the bounds given in (3.10) and (3.11), we need to evaluate P_e for uplink CNR values $(A+I_m)^2/2\sigma_u^2$, $(A-I_m)^2/2\sigma_u^2$, $(A+m_1)^2/2\sigma_u^2$, $(A-m_1)^2/2\sigma_u^2$ and $A^2/2\sigma_u^2$, for a given ρ_d using expression (3.12). The numerical results are shown in Figure 3.3.

3.3.2 Piece-wise Smooth Limiting Channel [56]

The characteristic function of a piece-wise smooth limiting channel is shown in Figure 3.2 and can be expressed mathematically as

$$f(R(t)) = \begin{cases} 1 & R(t) > \lambda \\ \dfrac{R(t)}{\lambda} & R(t) \leq \lambda \end{cases} \qquad (3.13)$$

$$\rho(R(t)) = 0$$

where λ is the limiter softness factor.

To evaluate the bounds for this channel, as for the hard-limiting channel, we need to know the probability of error in the absence of ISI. Even though the error probabilities have been evaluated previously [33], an enormous amount of numerical intergration needed to be performed to use these methods. Since our objective in this

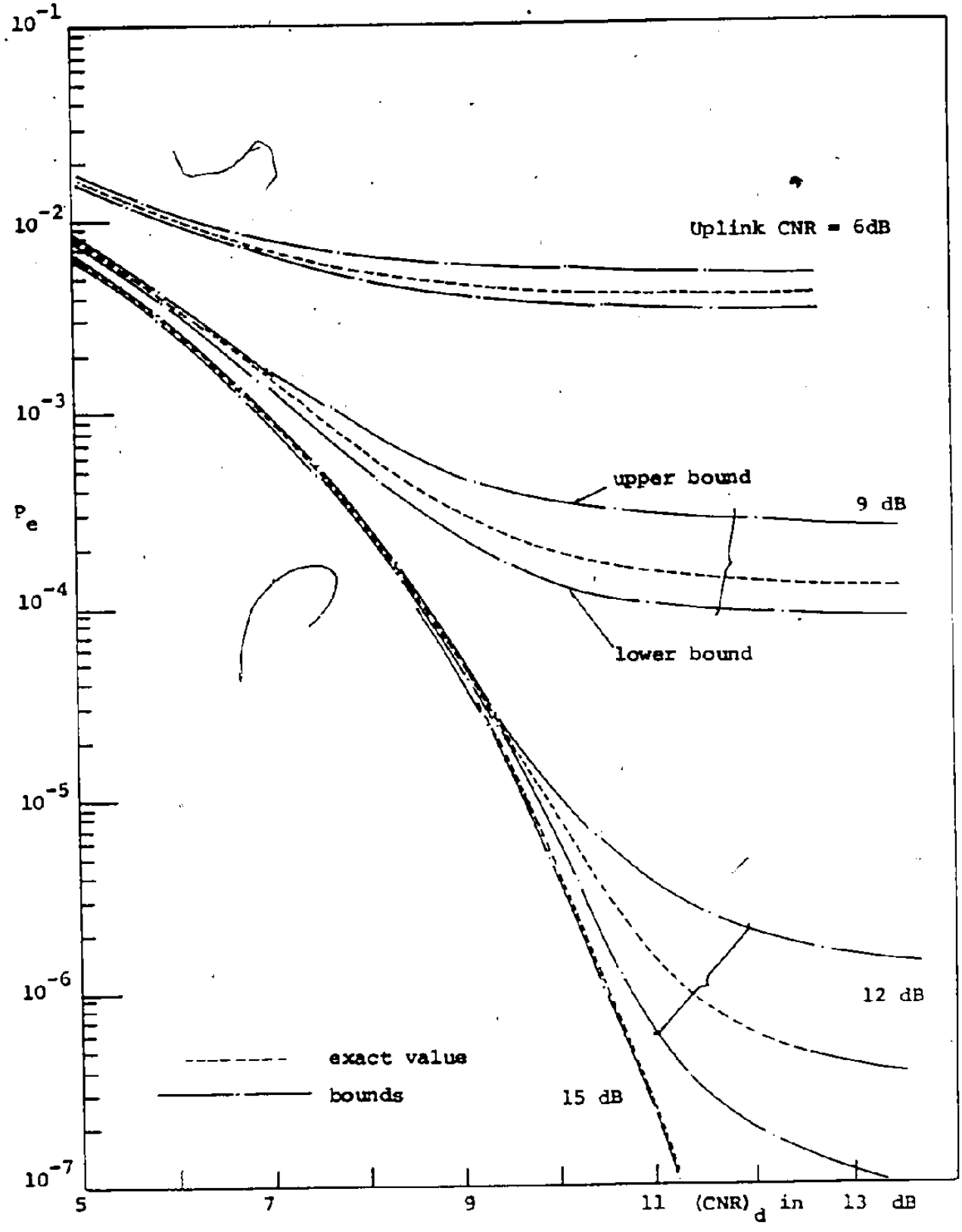

Fig. 3.3 Upper and lower bounds on probability of error for binary PSK system, hard-limiting channel, $T/T_0=2$

chapter is to derive bounds which can be easily computed, the use of these techniques is not justifiable. Therefore, we analyze this problem too, that is the evaluation of error proability in the absence of ISI, and an expression is derived in which the integrals are evaluated using recursive formulas.

In the absence of ISI, the probability of error can be obtained, from (3.6) as

$$P_e = E_{R,\lambda}\left[\frac{1}{2}\,\text{erfc}\,\left(\frac{f(R)\,\text{Cos}\,\theta}{\sqrt{2}\,\sigma_d}\right)\right] \tag{3.14}$$

where

$$R^2(t) \triangleq x^2(t) + y^2(t)$$

$$\theta(t) \triangleq \tan^{-1} y(t)/x(t)$$

$$x(t) \triangleq A(t-kT) + n_c^{(d)}(t)$$

$$y(t) \triangleq n_s^d(t)$$

Using the definition of R(t) given in (3.13), P_e in (3.14) becomes,

$$P_e = \int_0^{\lambda}\int_0^{2\pi} \frac{1}{2}\,\text{erf}\,\left(\frac{R}{\lambda}\,\frac{\text{Cos}\,\theta}{\sqrt{2}\,\sigma_d}\right)\,p(R,\theta)\,dR\,d\theta +$$

$$+\int_{\lambda}^{\infty}\int_0^{2\pi} \frac{1}{2}\,\text{erfc}\,\left(\frac{\text{Cos}\,\theta}{\sqrt{2}\,\sigma_d}\right)\,p(R,\theta)\,dR\,d\theta \tag{3.14}$$

where $p(R,\theta)$ is the joint probability density function of R and θ. The expression for $p(R,\theta)$ is given in [36] as,

$$P(R,\theta) = \frac{R}{2\pi\sigma_u^2} \exp\left(-\frac{R^2+A^2-2RA\cos\theta}{2\sigma_u^2}\right) \quad (3.15)$$

Substituting for $p(R,\theta)$ in (3.14), and evaluating the intergrals as shown in Appendix B, we obtain the probability of error as,

$$P_e = \frac{1}{4}\,\mathrm{erf}\,(\rho_\lambda)\,\mathrm{erf}\,(\rho_\lambda+\rho_u) + \frac{1}{4}\,\mathrm{erf}\,(\rho_\lambda)\,\mathrm{erf}\,(\rho_\lambda-\rho_u)$$

$$- \frac{1}{2\sqrt{\pi}}\,\mathrm{erf}\,(\rho_\lambda) \sum_{n=0}^{\infty} (-1)^n \frac{B_n X_n}{2n+1} + \frac{1}{2} Q(\sqrt{2}\,\rho_u, \sqrt{2}\,\rho_\lambda)$$

$$- \frac{e^{-\rho_u^2}}{2\pi} \sum_{n=0}^{\infty} (-1)^n \frac{\Gamma(n+1/2)}{2n+1} \rho_d^{2n+1}\, {}_1F_1\left(n+\tfrac{1}{2}, 2n+2, -\rho_d^2\right)$$

$$\sum_{r=0}^{\infty} B_{r,n}\, P_{r+n} \quad (3.16)$$

where $Q(.,.)$ is Marcum's Q function which can be evaluated recursively [37].

In (3.16)

$\rho_u^2 = \frac{A^2}{2\sigma_u^2}$ is the uplink CNR

$\rho_\lambda^2 = \frac{\lambda^2}{2\sigma_u^2}$ is a modified limiter softness factor

$\rho_d^2 = \frac{1}{2\sigma_d^2}$ is the downlink peak carrier power to noise power ratio $(PCNR)_d$

The advantage of the recursive formulas is that these can be easily used for numerical computation with little computational effort. We note that when $\lambda = 0$, i.e. for the hard-limiting channel, expression (3.16) reduces to the expression given by (3.12). The numerical results are shown in Figurea 3.4-3.7. Figures 3.6 and 3.7 show error rates for piece-wise smooth limiting channels in the absence of intersymbol interference. The exact values of probability of error in the presence of intersymbol interference are computed, using the technique developed in Chapter 2 in order to compare the accuracy of the bounds.

3.3.3 TWT Channel

The probability of error for the TWT channel model when there is no ISI can be obtained by setting $m = 0$ in (2.29), which also has been obtained previously by Forsey et al. [16] as

$$P_e = \frac{1}{2} - \frac{1}{\pi} \sum_{n=0}^{\infty} \frac{\Gamma(n+1/2)}{(2n+1)!} (-1)^n e^{-q^2}$$

$$\int_0^{\infty} {}_1F_1\left(n+\frac{1}{2}, 2n+2, -\frac{f^2(\sqrt{2}\sigma_u S)}{2\sigma_d^2}\right) s\, e^{-s^2} I_n(2Sq)$$

$$\cdot \cos n\rho(\sqrt{2}\,\sigma_u s) \cdot ds \qquad (3.17)$$

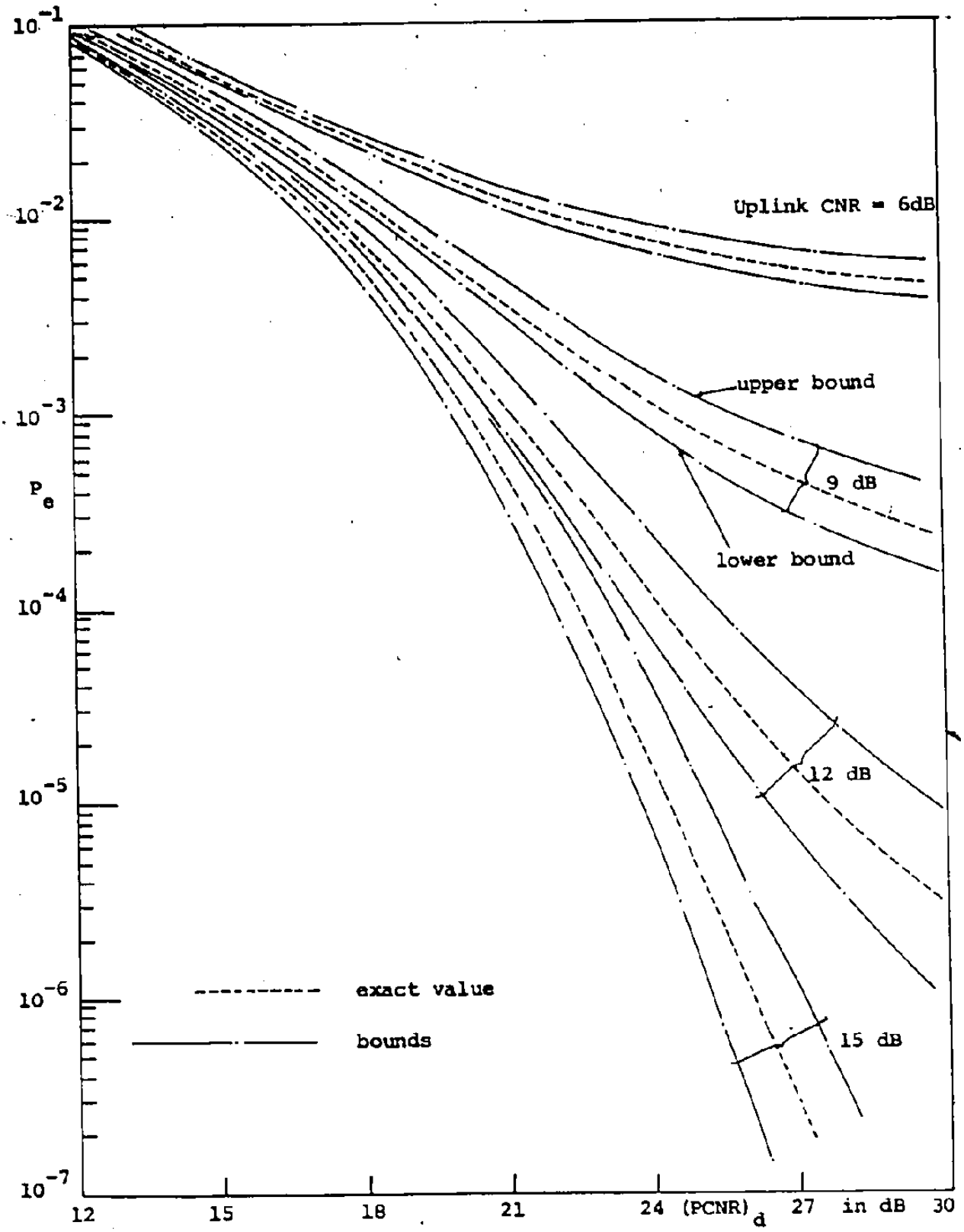

Fig. 3.4 Upper and lower bounds on probability of error for binary CPSK system, piece-wise smooth limiting channel (λ=4), T/T_0=2

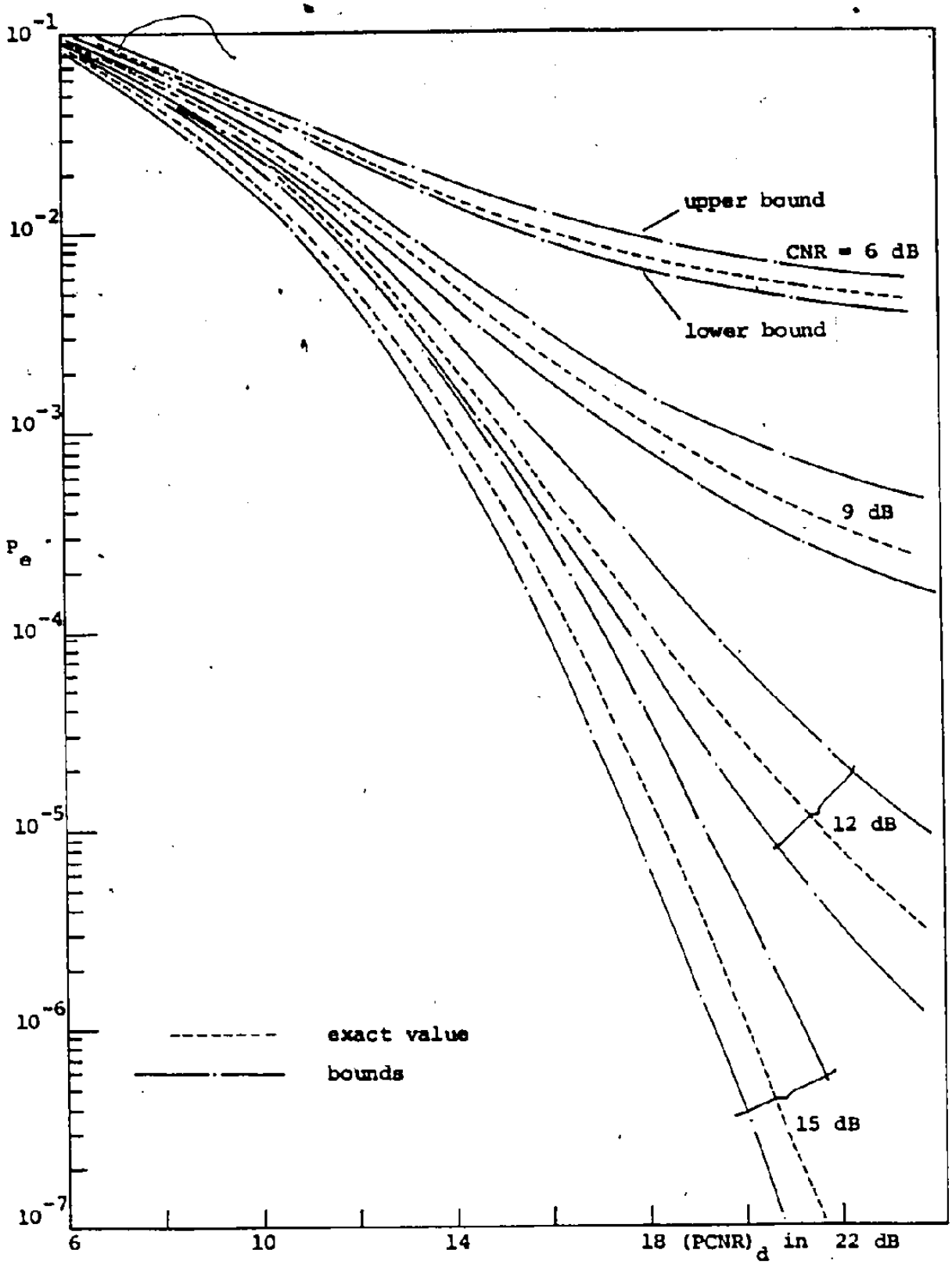

Fig. 3.5 Upper and lower bounds on probability of error for binary CPSK system, piece-wise smooth limiting channel (λ=2), T/T_0=2

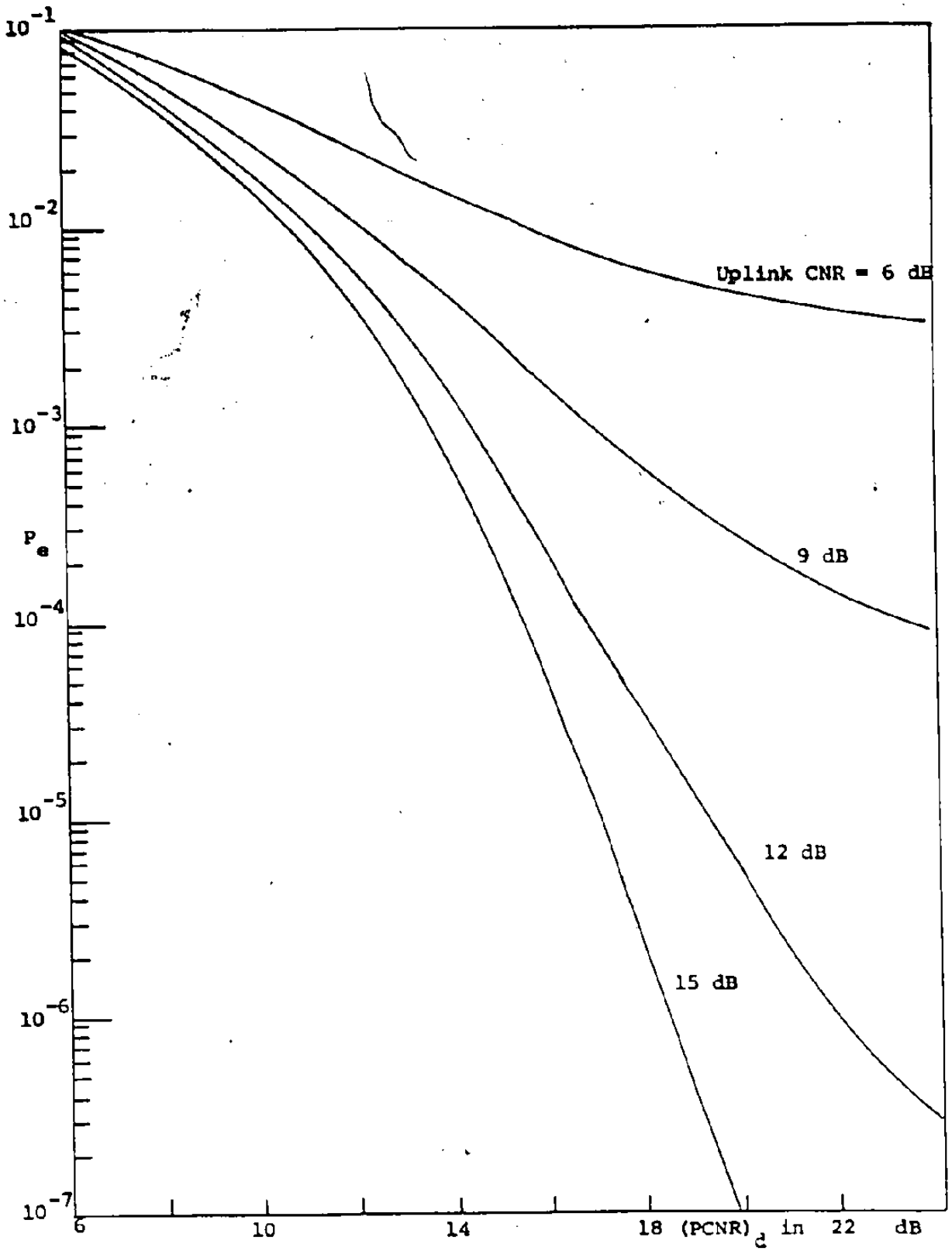

Fig. 3.6 Error probability of binary CPSK system, wide-band piece wise smooth limiting channel (λ=2)

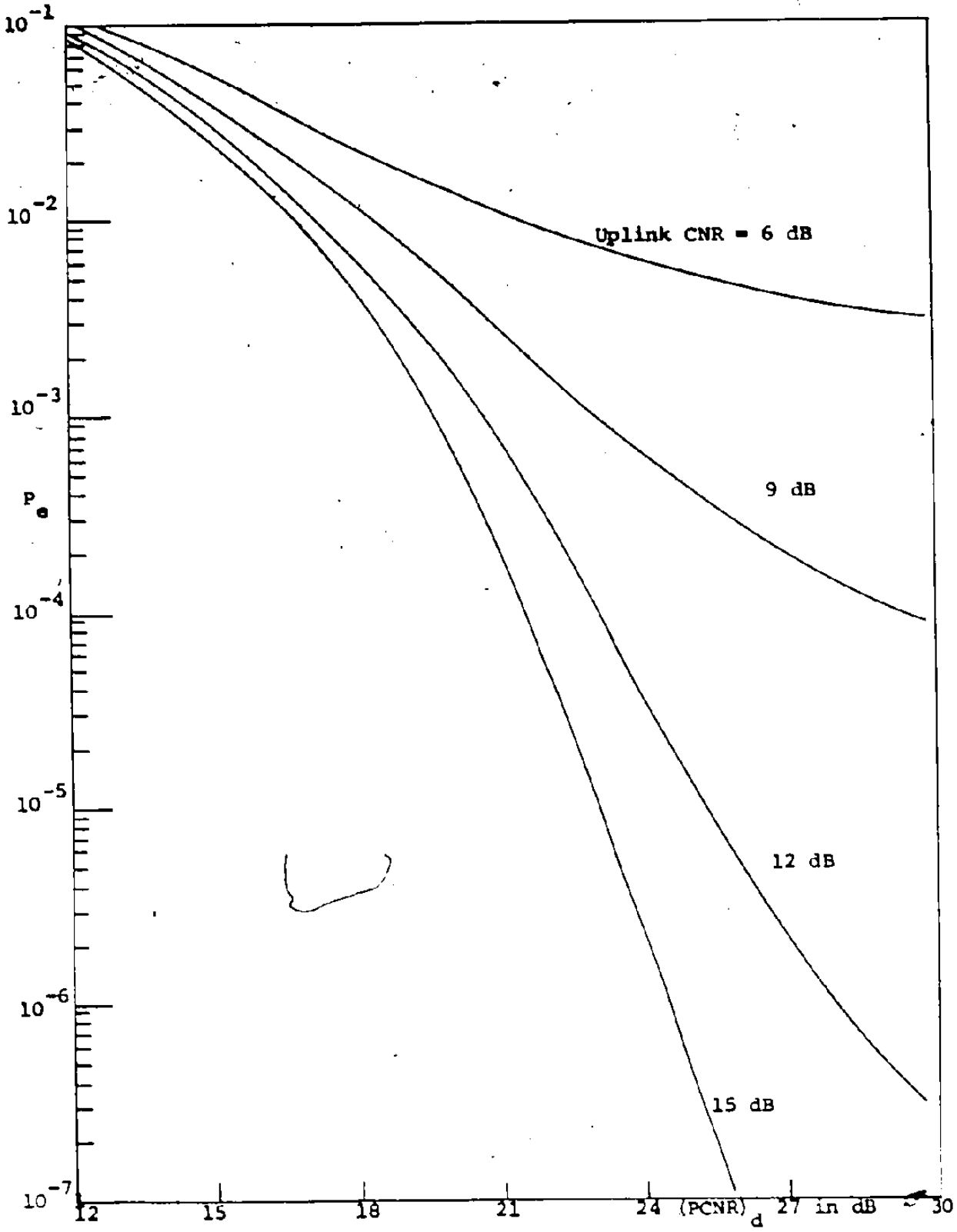

Fig. 3.7 Error probability of binary CPSK system, wide-band piece wise smooth limiting channel (λ=4)

This is readily evaluated and the results used to evaluate the bounds of (3.10) and (3.11). The numerical results are shown in Figure 3.8. Again in order to illustrate the utility of the bounds, we have included the exact values as computed in Chapter 2.

3.4 Conclusions

In this chapter we have derived upper and lower bounds on the probability of error in terms of the variance and fourth moment of the ISI. To evaluate these bounds, we need to know only the probability of error curves evaluated in the absence of ISI, i.e. for wideband channels. Therefore evaluation of the bounds is no more difficult than evaluating the error rates in the presence of additive Gaussian noise. From the numerical results, the bounds appear to be reasonably close to the exact results. The lower bound is tighter than upper bound.

Also, we have derived a technique to evaluate error rates for piece-wise smooth limiting channels in the absence of ISI which avoids numerical integration. Using this technique probability of error curves for a wideband piece-wise smooth limiting channel have been computed.

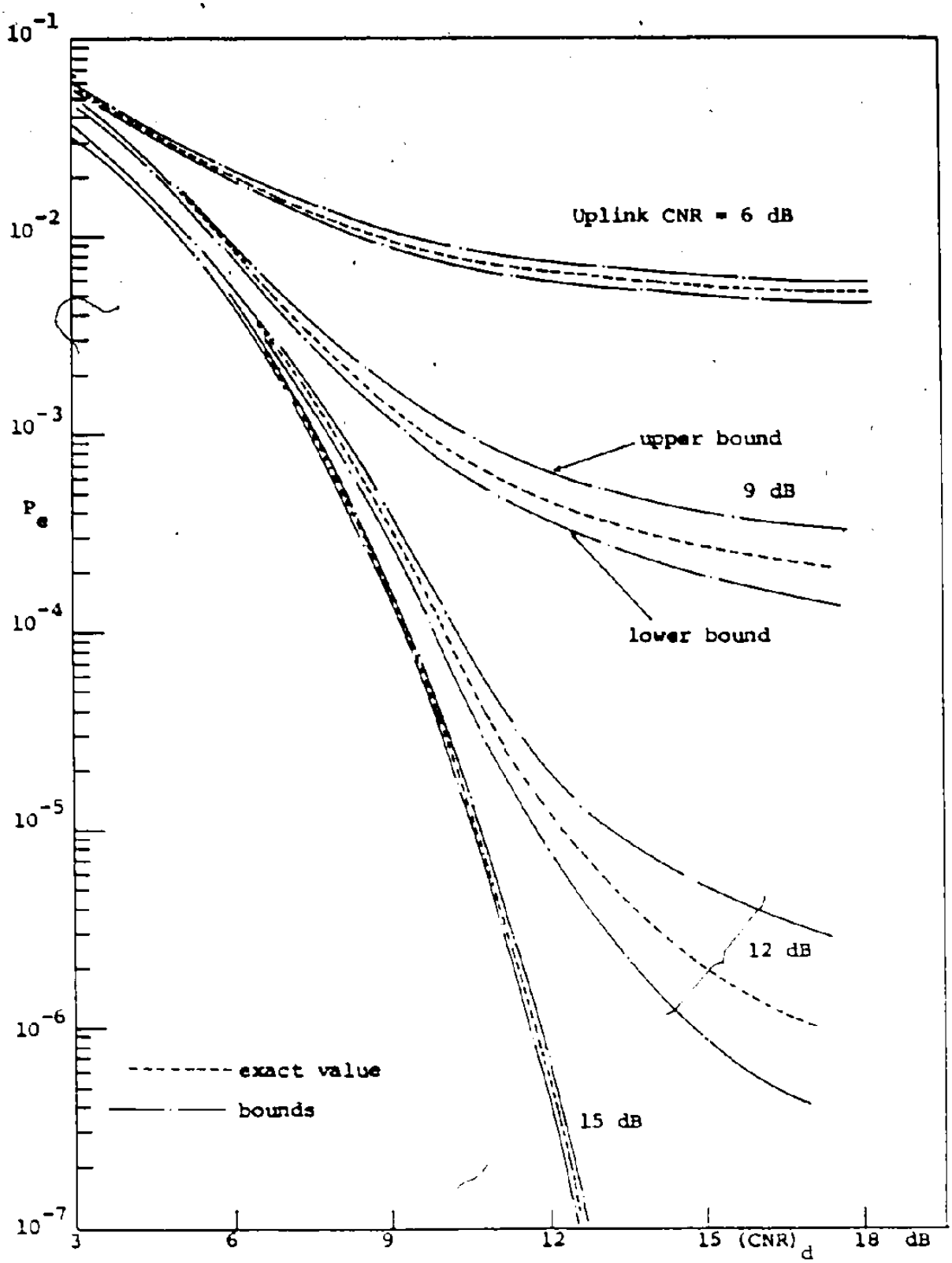

Fig. 3.8 Upper and lower bounds on probability of error for binary CPSK system, TWT channel (at saturation), $T/T_0=2$

CHAPTER 4

RECEIVER STRUCTURE FOR NONLINEAR BANDLIMITED BINARY CPSK CHANNELS

4.1 Introduction

The analyses in the previous chapters are limited to performance evaluation for bandlimited nonlinear satellite channels. In these analyses, we assumed the receiver to make decisions solely on the basis of samples taken once during each baud interval, regardless of the samples taken in other baud intervals. This receiver, commonly known as the single sample receiver, assumes that samples taken in one baud interval are statistically independent of the samples in other baud intervals. This is actually true only for memoryless wideband channels. In wideband channels, since there is no memory in the system, any one symbol carries information only about the data transmitted in that particular baud interval. Since bandlimiting introduces memory into the system, intuitively we would suspect that knowledge of the data in adjacent bauds may be effectively incorporated into the current decision process to increase the probability of correct decision.

This has been the basis for a great deal of research

work [41-46] on equalizers to compensate for ISI effects in both time invariant and time variant linear channels. But so far little attempt has been made to extend these well known ideas to nonlinear channels, perhaps due to the complexity of analysis introduced by the nonlinearity. Another reason for lack of activity in this area is due to the complexity and high cost of implementation of nonlinear receivers. With the rapid development of cheaper and faster digital processors, nonlinear receivers should become more practicable within the near future.

Reviewing the literature briefly, Lawless [45] has applied Voltera series techniques to synthesize receivers for bandlimited nonlinear telephone channels. His analysis is limited to quadratic nonlinearity having adjacent symbol interference only. The most recent work on the receiver synthesis is due to Mesiya and McLane [47]. In their work, Forney's [51] work on application of the Viterbi Algorithm for maximum likelihood sequence estimation for linear channels is extended to include binary CPSK transmission over nonlinear channels. Although the Viterbi Algorithm is theoretically appealing, its practical implementation for on-line processing is not feasible in high data-rate real time communication systems. On the other hand, decision feedback type receivers [41,42] are widely known and are actually in operation today in high speed digital

communication systems.

In this chapter, we derive a receiver structure similar to a decision feedback receivers for linear channels. We are concerned with the optimal processing of samples rather than the optimal processing or filtering of the baseband signal itself. The analysis is restricted to binary CPSK transmission and the channel model considered is a general TWT model. In section 4.3, we consider the application of this receiver to the hard-limiting channel, for the simple reason that it leads to tractable mathematical expressions. In section 4.4, we evaluate the performance of the receiver by Monte Carlo computer simulation techniques.

4.2 Derivation of the Receiver Structure

In the following analysis, we state only the major steps to avoid repetition from the previous chapters. We assume the bandlimiting filter to be time-invariant and to cause ISI at any time to be due only to previous data symbols. A typical filter impulse response is shown in Figure 4.1. The bandlimited binary CPSK signals can be expressed at the filter output as

$$S(t) = \{p(t-kT)*h(t)\}\ \mathrm{Cos}(\omega_c t+\phi_k)+\{\mathrm{Cos}\ \phi_k \sum_{i\neq k} [p(t-iT)*h(t)] \cdot \mathrm{Cos}\ \phi_i\}\ \mathrm{Cos}\ (\omega_c t + \phi_k) \qquad (4.1)$$

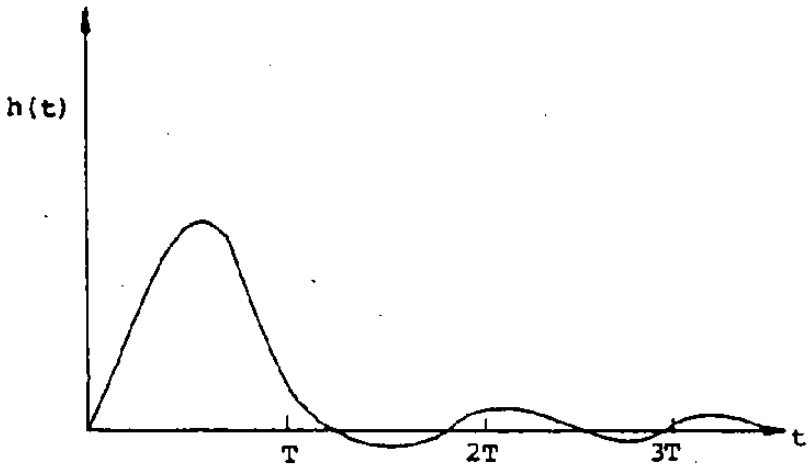

Fig. 4.1 Unit pulse response of the filter

The definitions of all notations are as in Chapters 2 and 3. Then the input signal to the satellite transponder during the kth baud interval is

$$S_i(t) = R_k(t) \text{ Cos } [\omega_c t + \phi_k + \lambda(t)] \qquad (4.2)$$

where

$$R_k^2(t) \triangleq [q_k + \text{Cos } \phi_k \sum_{i \neq k} q_i \text{ Cos } \phi_i + n_c^u(t)]^2 + [n_s^u(t)]^2$$

$$\lambda_k(t) \triangleq \tan^{-1} \frac{n_s^u(t)}{q_k + \text{Cos } \phi_k \sum_{i \neq k} q_i \text{ Cos } \phi_i + n_c^u(t)}$$

$$q_i \triangleq p(t-iT) * h(t) \qquad i = 0, 1, \ldots, k-1$$

The received signal during the kth baud interval is then

$$S_R(t) = f(R_k(t)) \text{ Cos } [\omega_c t + \phi_k + \lambda_k(t) + \rho(R_k(t))]$$
$$+ n_c^d(t) \text{ Cos } \omega_c t - n_s^d(t) \text{ Sin } \omega_c t \qquad (4.3)$$

where as before $f(\cdot)$ and $\rho(\cdot)$ represent the nonlinear effects of the satellite transponder.

At the receiver the signal $S_R(t)$ is coherently demodulated and sampled as shown in Figure 4.2. During any baud interval only one pair of samples (x_k, y_k) is taken. Our objective is to derive a processor which acts on the sample pairs (x_k, y_k), (x_{k-1}, y_{k-1}), ... to make a decision on the symbol transmitted in the kth baud interval $(k-1)T \leq t < kT$.

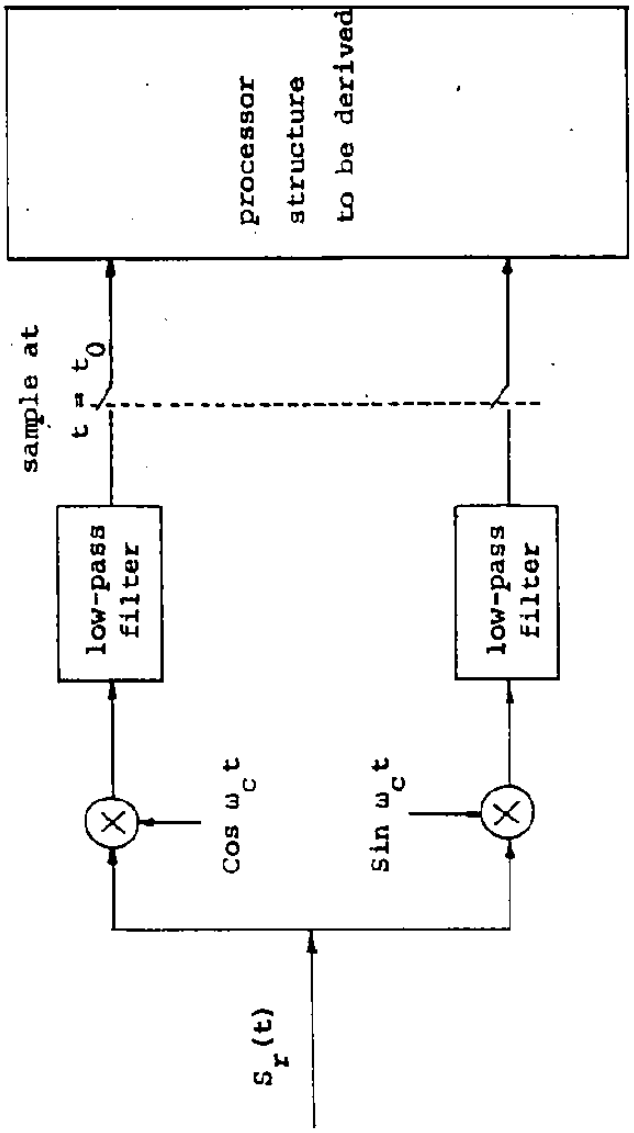

Fig. 4.2 Receiver under consideration

Because the bandlimiting filter has memory, we note that the samples x_k and y_k are dependent on the previous samples (x_{k-1}, y_{k-1}), ... etc. The inphase sample x_k and quadrature sample y_k are given, omitting the time dependence, as

$$x_k = f(R_k) \text{ Cos } [\phi_k + \lambda_k + \rho(R_k)] + n^d_{c,k} \tag{4.4}$$

$$y_k = f(R_k) \text{ Sin } [\phi_k + \lambda_k + \rho(R_k)] + n^d_{s,k} \tag{4.5}$$

where R_k and λ_k are as defined in (4.2). Since ϕ_k is either 0 or π, cos $\phi_k = 1$ when $\phi_k = 0$ and cos $\phi_k = -1$ when $\phi_k = \pi$.

Now let us define $a_k \triangleq \cos \phi_k$. We may then state the problem at hand as follows.

Problem:

We are given

$$\underset{\sim}{r} = (r_k, r_{k-1}, \cdots \quad)$$

$$\underset{\sim}{z} = (z_k, z_{k-1}, \cdots \quad)$$

where

$$r_{k-i} \triangleq (x_{k-i}, y_{k-i})$$

$$z_{k-i} \triangleq (R_{k-i}, \lambda_{k-i})$$

$$x_{k-i} \triangleq a_{k-i} \, f(R_{k-i}) \text{ Cos } [\lambda_{k-i} + \rho(R_{k-i})] + n^d_{c,k-i}$$

$$y_{k-i} \triangleq a_{k-i}\, f(R_{k-i})\, \mathrm{Sin}\,[\lambda_{k-i} + \rho(R_{k-i})] + n^{d}_{s,k-i}$$

$$R_{k-i} \triangleq \{[q_{k-i} + a_{k-i}\,(q_{k-i-1}\, a_{k-i-1} + \cdots + q_{k-i-M}\, a_{k-i-M})]^2 + [n^{u}_{s,k-i}]^2\}^{1/2}$$

$$\lambda_{k-i} \triangleq \tan^{-1} \frac{n^{u}_{s,k-i}}{q_{k-i} + a_{k-i}\,(q_{k-i-1}\, a_{k-i-1} + \cdots) + n^{u}_{c,k-i}}$$

$$i = 0, 1, \ldots, M$$

where M is the length of the memory of the filter in baud periods.

Then derive the decision statistics which yield the optimum decision on the value of a_k.

The solution to this is arrived at using the techniques of decision theory. We note that $S \triangleq \{a_{k-1}, \ldots, a_{k-M}\}$ is the past data. Since $a_k = +1$ or -1 with equal probability, the maximum likelihood ratio test yields the minimum probability of error [52]. Therefore, assuming that all past data are known, the composite likelihood ratio can be written as

$$\frac{\int p(\underset{\sim}{r}, \underset{\sim}{z} \mid a_k = +1, S)\, d\underset{\sim}{z}}{\int p(\underset{\sim}{r}, \underset{\sim}{z} \mid a_k = -1, S)\, d\underset{\sim}{z}} \quad \begin{matrix} >^{+1} \\ <_{-1} \end{matrix} \quad 1 \tag{4.8}$$

Since S is known z_k is independent of z_{k-i} $\quad i \geq 1$. This is clear from the definition of R_k and λ_k. Also, we have assumed that the noise samples are independent. Under the same assumptions, r_k is independent or r_{k-1}, r_{k-2}, $\cdots$,

r_{k-M}.

Therefore, the likelihood ratio (4.8) can be written as

$$\text{L.H.S.} = \frac{\int p(r_k, z_k | a_k=+1, S)\, dz_k}{\int p(r_k, z_k | a_k=-1, S)\, dz_k} \cdot \frac{\int p(r_{k-1}, \ldots, z_{k-1} \ldots | a_k=+1, S)\, dz_{k-1} \ldots}{\int p(r_{k-1}, \ldots, z_{k-1} \ldots | a_k=-1, S)\, dz_{k-1} \ldots} \tag{4.9}$$

Next we note that r_{k-1}, ... and z_{k-1}, ... are independent of a_k. Therefore, we may cancel out the second ratio in (4.9) to get equation (4.8) in the form,

$$\frac{\int p(r_k, z_k | a_k=+1, S)\, dz_k}{\int p(r_k, z_k | a_k=-1, S)\, dz_k} \begin{matrix} > \\ < \end{matrix} \begin{matrix} +1 \\ -1 \end{matrix} 1$$

$$\frac{\int p(r_k | a_k=+1, S, z_k)\; p(z_k | a_k=+1, S)\, dz_k}{\int p(r_k | a_k=-1, S, z_k)\; p(z_k | a_k=-1, S)\, dz_k} \begin{matrix} > \\ < \end{matrix} \begin{matrix} +1 \\ -1 \end{matrix} 1 \tag{4.10}$$

Since the noise samples are Gaussian random variables we can readily obtain the probability densities appearing in (4.10) as,

$$p(r_k | z_k, a_k=+1, S) = \frac{1}{\sqrt{2\pi}\ \sigma_d^2} \exp\{-\left[\frac{x_k - f_k \cos(\lambda_k+\rho_k)}{\sqrt{2}\ \sigma_d}\right]^2\} \cdot$$

$$\cdot \frac{1}{\sqrt{2\pi}\ \sigma_d^2} \exp\{-\left[\frac{y_k - f_k \sin(\lambda_k+\rho_k)}{\sqrt{2}\ \sigma_d}\right]^2\}$$

$$= \frac{1}{2\pi\ \sigma_d^2} \cdot \exp\frac{1}{2\ \sigma_d^2}\{-(x_k^2+y_k^2+f_k^2) + 2f_k[x_k \cos(\lambda_k+\rho_k) + y_k \sin(\lambda_k+\rho_k)]\} \tag{4.11}$$

Similarly we obtain,

$$p(r_k|z_k,a_k=-1,S) = \frac{1}{2\pi\sigma_d^2} \exp \frac{1}{2\sigma_d^2}\{-(x_k^2+y_k^2+f_k^2)-2f_k[x_k\text{Cos}(\lambda_k+\rho_k) + y_k \text{ Sin } (\lambda_k + \rho_k)]\} \quad (4.12)$$

$$p(z_k|a_k=+1,S) = p(R_k,\lambda_k|a_k=+1,S)$$

$$= \frac{R_k}{2\pi\sigma_u^2} \exp - \frac{1}{2\sigma_u^2} \{R_k^2+(q_k+\alpha)^2-2R_k(q_k+\alpha)\text{Cos}\lambda_k\} \quad (4.13)$$

$$p(z_k|a_k=-1,S) = \frac{R_k}{2\pi\sigma_u^2} \exp - \frac{1}{2\sigma_u^2} \{R_k^2+(q_k-\alpha)^2-2R_k(q_k-\alpha)\text{Cos}\lambda_k\} \quad (4.14)$$

where

$$\alpha \triangleq q_{k-1}\, a_{k-1} + \ldots + q_{k-M}\, a_{k-M}$$

$$f_k \triangleq f(R_k)$$

$$\rho_k \triangleq \rho(R_k)$$

Substituting (4.11) through (4.14) into (4.10), we obtain after simplification

$$\frac{\int_0^\infty \int_0^{2\pi} R_k \exp\{\frac{f_k}{\sigma_d^2}[x_k\text{Cos}(\lambda_k+\rho_k) + y_k\text{Sin}(\lambda_k+\rho_k)]\}\cdot\exp(\frac{-f_k^2}{2\sigma_d^2}) \cdot\exp\{-\frac{1}{2\sigma_u^2}[R_k^2+(q_k+\alpha)^2-2R_k(q_k+\alpha)\text{Cos}\lambda_k]\}dR_k d\lambda_k}{\int_0^\infty \int_0^{2\pi} R_k \exp\{-\frac{f_k}{\sigma_d^2}[x_k\text{Cos}(\lambda_k+\rho_k)+y_k\text{Sin}(\lambda_k+\rho_k)]\}\cdot\exp(\frac{-f_k^2}{2\sigma_d^2}) \cdot\exp\{-\frac{1}{2\sigma_u^2}[R_k^2+(q_k-\alpha)^2-2R_k(q_k-\alpha)\text{Cos}\lambda_k]\}dR_k d\lambda_k} \gtrless_{-1}^{+1} \quad (4.15)$$

We recall that in deriving the above likelihood ratio, we assumed all past data, i.e. the set S is known. Since in practice S is not known, we instead use the past decisions

$$\hat{S} \triangleq \{\hat{a}_{k-1}, \hat{a}_{k-2}, \ldots, \hat{a}_{k-M}\}$$

in place of the actual data in order to obtain a realizable receiver structure. This is the technique used in [41,46]. The implication of this is that the realizable receiver structure becomes a suboptimal receiver. However, provided the probability of decision error is fairly small this realizable structure will be close to optimum. In Figure 4.3, the general receiver structure is shown. As an application of the receiver structure, in the following sections we consider a hard-limiting channel which leads to tractable mathematical expressions.

4.3 Application to Hard-limiting Channel

4.3.1 Wideband Channel (No ISI)

With the usual definitions of $f(R_k)$ and $\rho(R_k)$ for a hard-limiting channel, we can evaluate the integrals in (4.15) (Appendix C). After some manipulation we obtain

$$\Lambda \triangleq \sum_{n=1}^{\infty} q_{2n-1}(q_k)\, I_{2n-1}\left(\frac{S_k}{\sigma_d^2}\right) \cos(2n-1)\gamma_k \;\underset{-1}{\overset{+1}{\gtrless}}\; 0 \qquad (4.16)$$

where

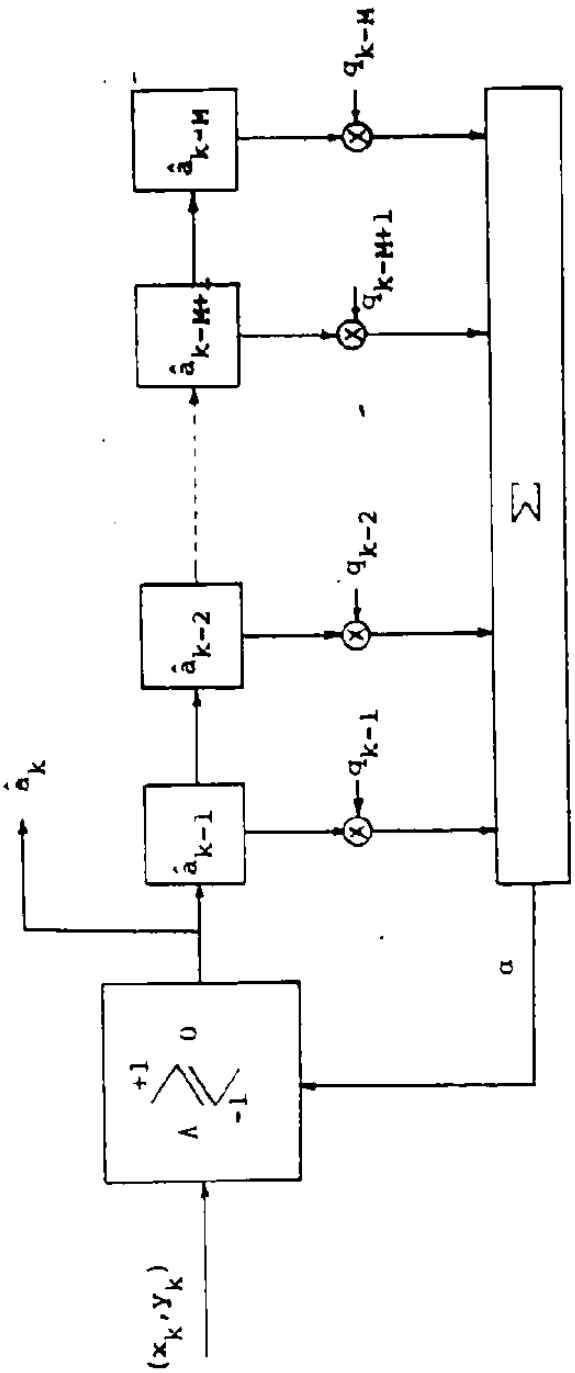

Fig. 4.3 Decision feed-back receiver structure

$$q_{2n-1}(q_k) \triangleq \frac{\Gamma(n+1/2)}{(2n-1)!}\left(\frac{q_k}{\sqrt{2}\sigma_u}\right)^{2n-1} {}_1F_1\left(n-\frac{1}{2},\ 2n,\ -\frac{q_k^2}{2\sigma_u^2}\right)$$

and (S_k, γ_k) represents the polar form of (x_k, y_k). We note that here Λ depends only on the present sample pair (x_k, y_k). Since the decision threshold is zero, we are interested in the zero crossings of the expression Λ. It can be easily shown that, because of the term $\cos(2n-1)\gamma_k$, the zero crossings are $\pi/2$ and $3\pi/2$ (or $-\pi/2$). Also, if we plot equation (4.16), it can be shown that (Figures 4.6-4.17)

$$\Lambda > 0 \qquad -\pi/2 < \gamma_k < \pi/2$$

$$\Lambda < 0 \qquad \pi/2 < \gamma_k < -\pi/2 \quad \text{for all } S_k$$

Since $\cos\gamma_k > 0$ for $-\pi/2 < \gamma_k < \pi/2$

and $\cos\gamma_k < 0$ for $\pi/2 < \gamma_k < -\pi/2$,

instead of computing the decision statistic (4.16) and testing for the sign of Λ, alternatively we may perform the test

$$x_k \gtrless_{-1}^{+1} 0 \qquad 4.17$$

regardless of y_k, to decide on a_k. In otherwords, in the absence of bandlimiting, i.e. for wideband channels, the single sample sign detector yields the optimum decision and no other processor which acts on the sample pair (x_k, y_k) would perform better than a sign detector. Of course, the

performance may be improved by suitably filtering the received signal before sampling, a factor we have not considered in this thesis. In the following section we consider the effect of ISI on the decision statistic.

3.2.1 Bandlimiting Channel

In this case, the likelihood ratio given in (4.15) can be simplified (Appendix C) to

$$\Lambda \triangleq \sum_{n=1}^{\infty} \{ f_n(q_k+a) - (-1)^n f_n(q_k-a) \} I_n\left(\frac{S_k}{\sigma_d^2}\right) \cos n\gamma_k \gtrless_{-1}^{+1} 0$$

where

$$f_n(q \pm a) \triangleq \frac{\Gamma(n/2+1)}{n!} \frac{(q_k \pm a)^n}{\sqrt{2}\,\sigma_u} F\left(\frac{n}{2}, n+1, -\left(\frac{q_k \pm a}{\sqrt{2}\sigma_u}\right)^2\right) \qquad 4.18$$

and (S_k, γ_k) denotes the polar form of (x_k, y_k).

Again, as in section 4.3.1, we are interested in the sign of Λ, and hence the zero crossings of Λ. Unlike in section 4.3.1, it is not possible to determine the zero crossings of Λ easily. Instead, Λ can be graphically plotted against γ_k keeping (S_k/σ_d^2), $(q_k/\sqrt{2}\sigma_u)$ and a as parameters to investigate the zero crossings of Λ. The results so obtained are shown in Figures 4.6-4.17. Instead of decision statistic Λ, we have plotted normalized Λ, i.e. $\Lambda_N = \Lambda/|\Lambda(\gamma_k=0)|$. This normalization is used simply for the convenience of plotting, and it is noted that the zero crossings and sign of Λ do not change by the normalization.

Even though the zero crossings are dependent on all the parameters given above, in general, the effect of α, that is the cumulative intersymbol interference due to past data is to adjust the zero crossings accordingly, when S_k/σ_d^2 and $q_k/\sqrt{2}\sigma_u$ are held constant.

We note that $S_k/\sigma_d^2 = 2\ S_k\ \rho_d^2$ where $\rho_d^2 = 1/2\sigma_d^2$ is the downlink CNR. Therefore, the effect of S_k is to modify the downlink CNR accordingly. Also, $q_k/\sqrt{2}\sigma_u$ is the uplink CNR. So that the threshold adjustment, i.e. the correction to the angle γ_k, basically depends on the uplink CNR, modified downlink CNR and the cumulative intersymbol interference due to past data. Since, in general, the uplink CNR and downlink CNR are known in satellite operation, we need to obtain nonlinear curves keeping only S_k and α as parameters. Since Λ is an even function of γ_k about π, we have shown the curves only for $\gamma_k = 0$ to π.

The effect of ISI on the decision regions is shown in Figure 4.4. By carefully examining this figure, an alternate receiver structure can be suggested as shown in Figure 4.5. Here the angle θ is the correction applied to angle γ_k in (4.18), to account for the ISI effect. The effect of θ is also shown in Figure 4.5.

The correction angle θ is the zero crossing of Λ for a given ISI value α, ρ_u^2 and $S_k\ \rho_d^2$ measured from $\pi/2$, which is the zero crossing in the absence of ISI as shown in

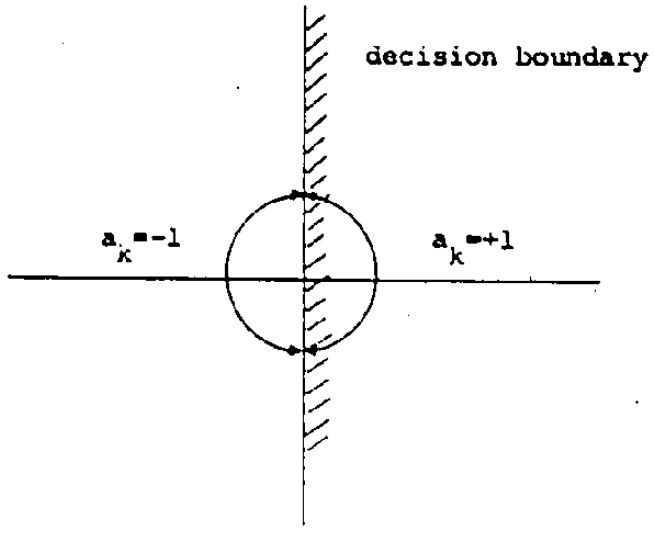

no intersymbol interference

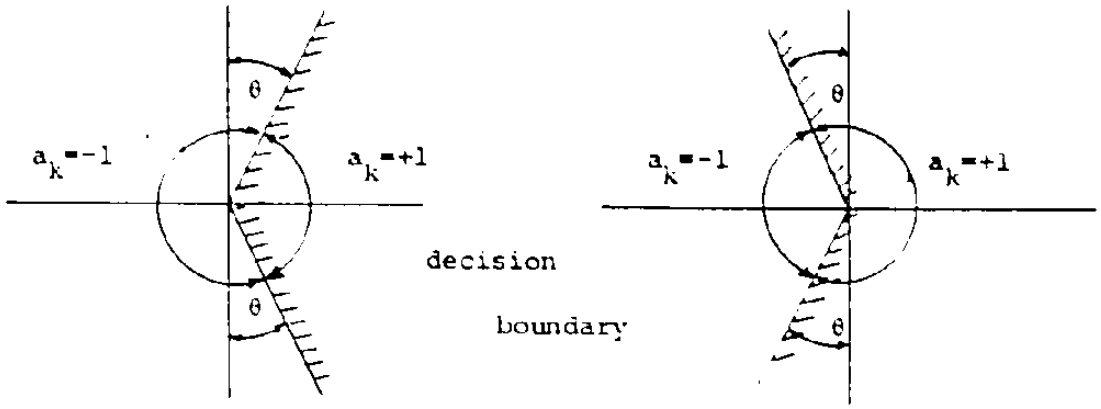

α >0 α <0

with intersymbol interference

Fig. 4.4 Effect on ISI on decision regions

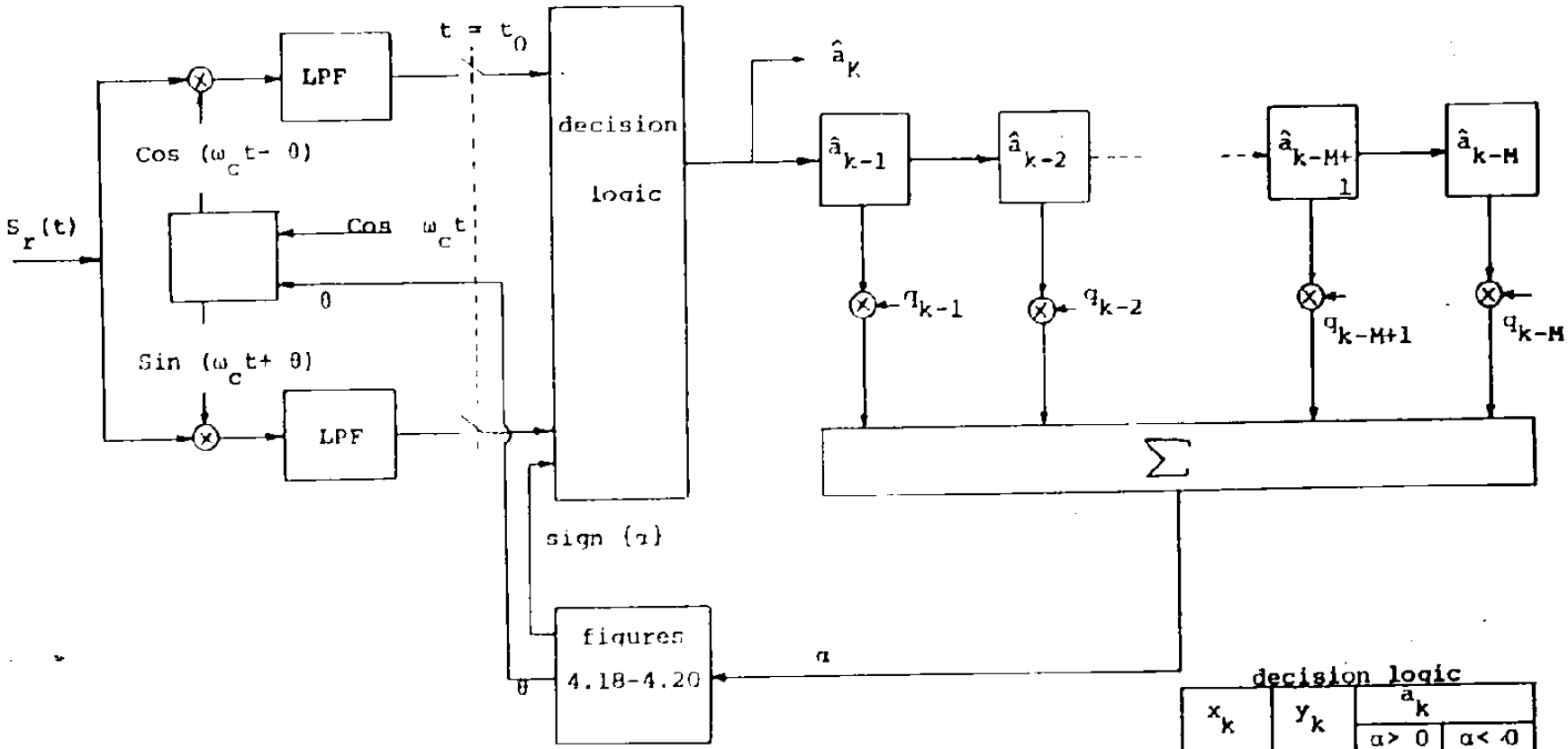

decision logic

x_k	y_k	$\hat{a}_k$	
		α> 0	α< 0
+1	+1	+1	+1
-1	-1	-1	-1
+1	-1	1	1
-1	+1	1	1

Fig. 4.5 An alternate implementation of the receiver

section 4.3.1. To implement the alternate receiver structure, we need to know the variation of θ with α. Since θ can be written as $\theta = f(\alpha, S_k \rho_d, \rho_u)$, we can obtain another set of curves from the previous set of curves shown in figures 4.6-4.17. The new set of curves so obtained are shown in figures 4.18-4.20. It can be seen that these curves are easier to implement than the former set of curves.

Though the general likelihood function Λ in (4.18) looks too complicated to reach any conclusions we can consider the form of the receiver in certain limiting cases of interest.

Case (a) High uplink CNR; i.e. $\sigma_u \to 0$

open eye $q_k > |\alpha|_{max}$

As $\sigma_u \to 0$ $\left(\frac{q_k \pm \alpha}{\sqrt{2}\ \sigma_u}\right) \to \infty$

Then it can be shown that $f_n(q_k \pm \alpha) \to 1$ as shown in Appendix C. Therefore the expression (4.18) reduces to

$$\Lambda = \sum_{n=1}^{\infty} I_{2n-1}\left(\frac{S_k}{\sigma_d^2}\right) \cos (2n-1)\, \gamma_k \underset{-1}{\overset{+1}{\gtrless}} 0 \qquad (4.19)$$

Because of the presence of the term $\cos(2n-1)\gamma_k$ in (4.19), we find, as in section 4.3.1, that the zero crossings are $\pi/2$ and $3\pi/2$. Therefore, using the same arguments as in section 4.3.1, it can be shown that the decision statistic

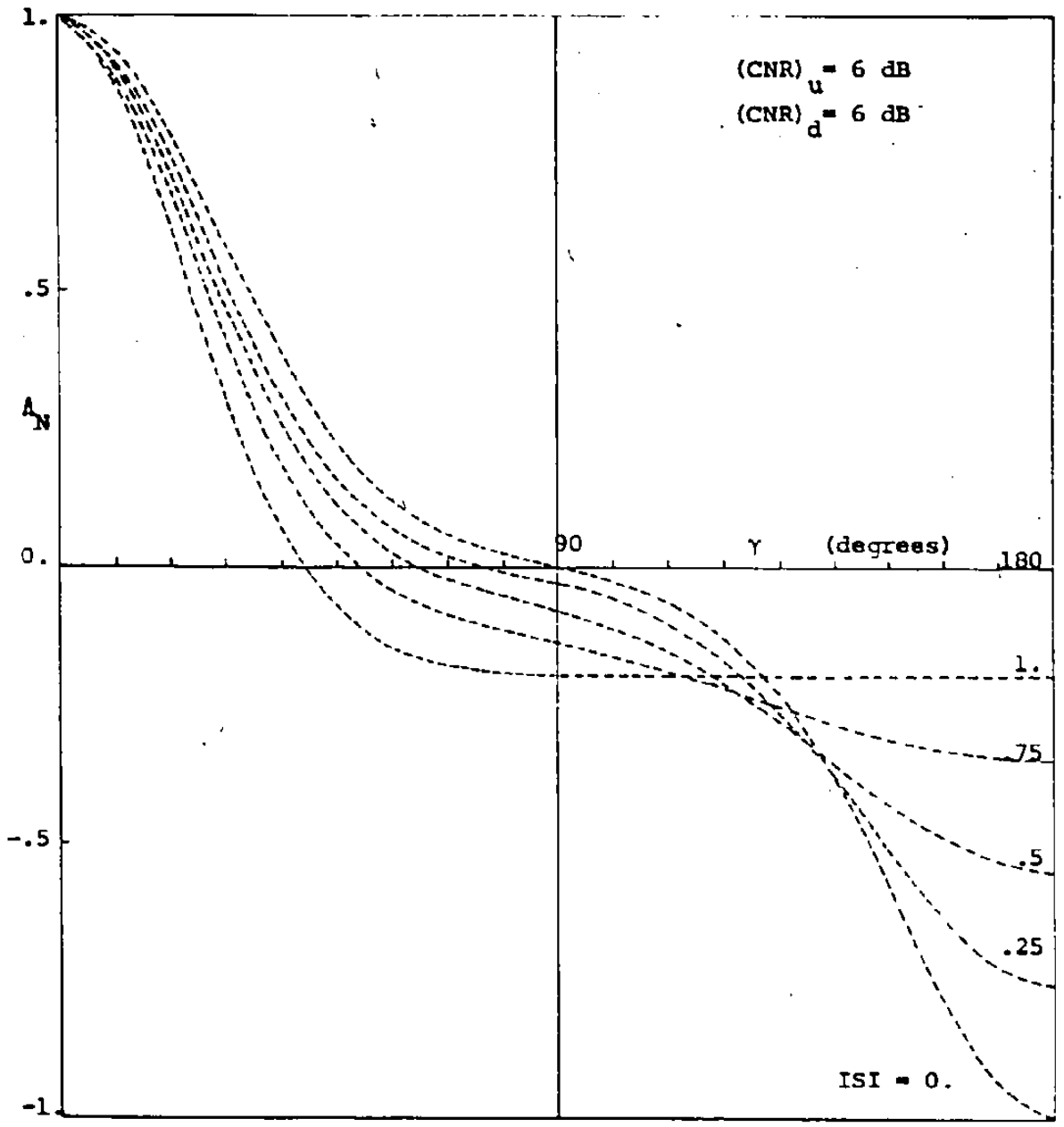

Fig. 4.6 Characteristics of decision statistics

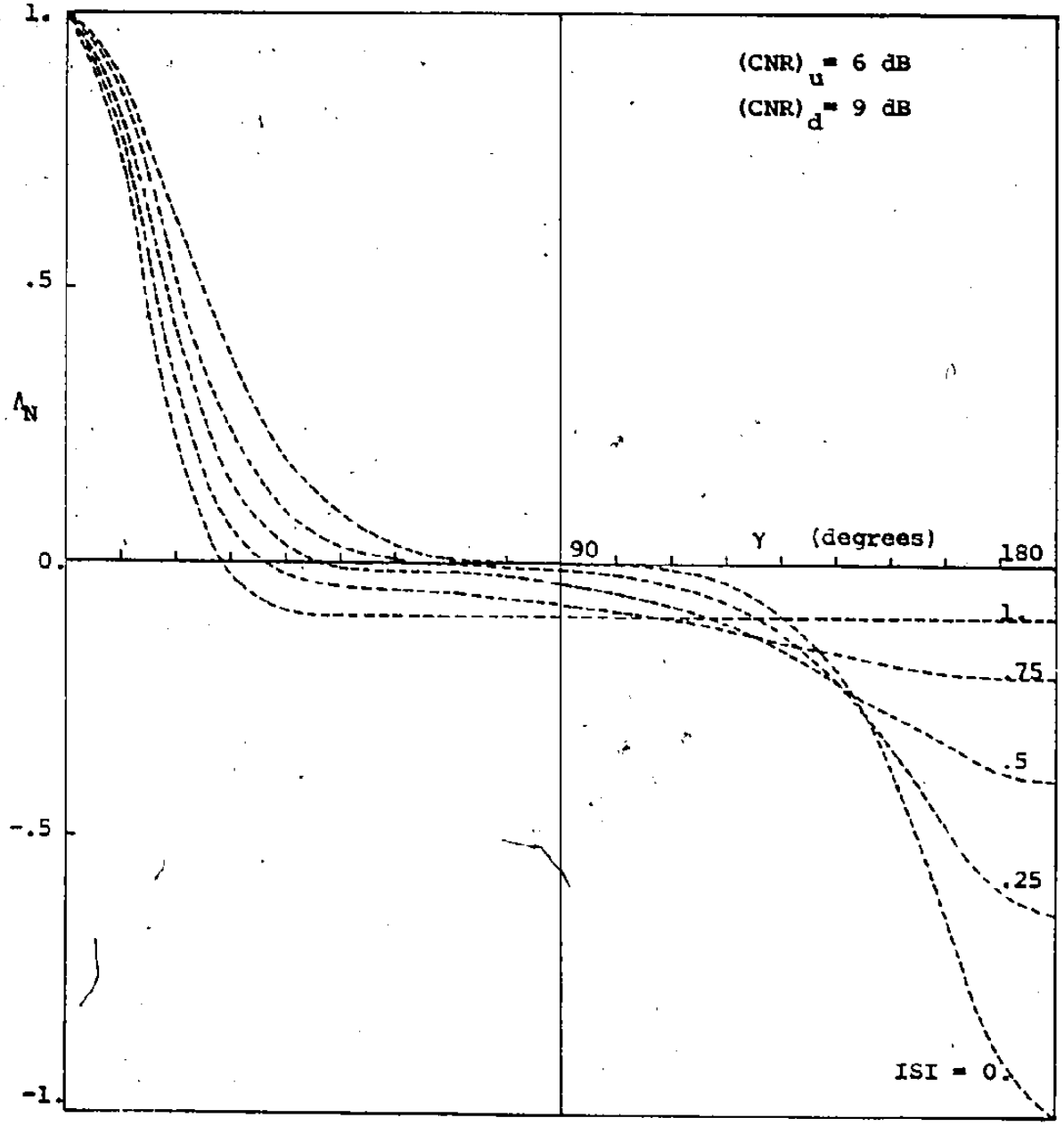

Fig. 4.7 Characteristics of decision statistics

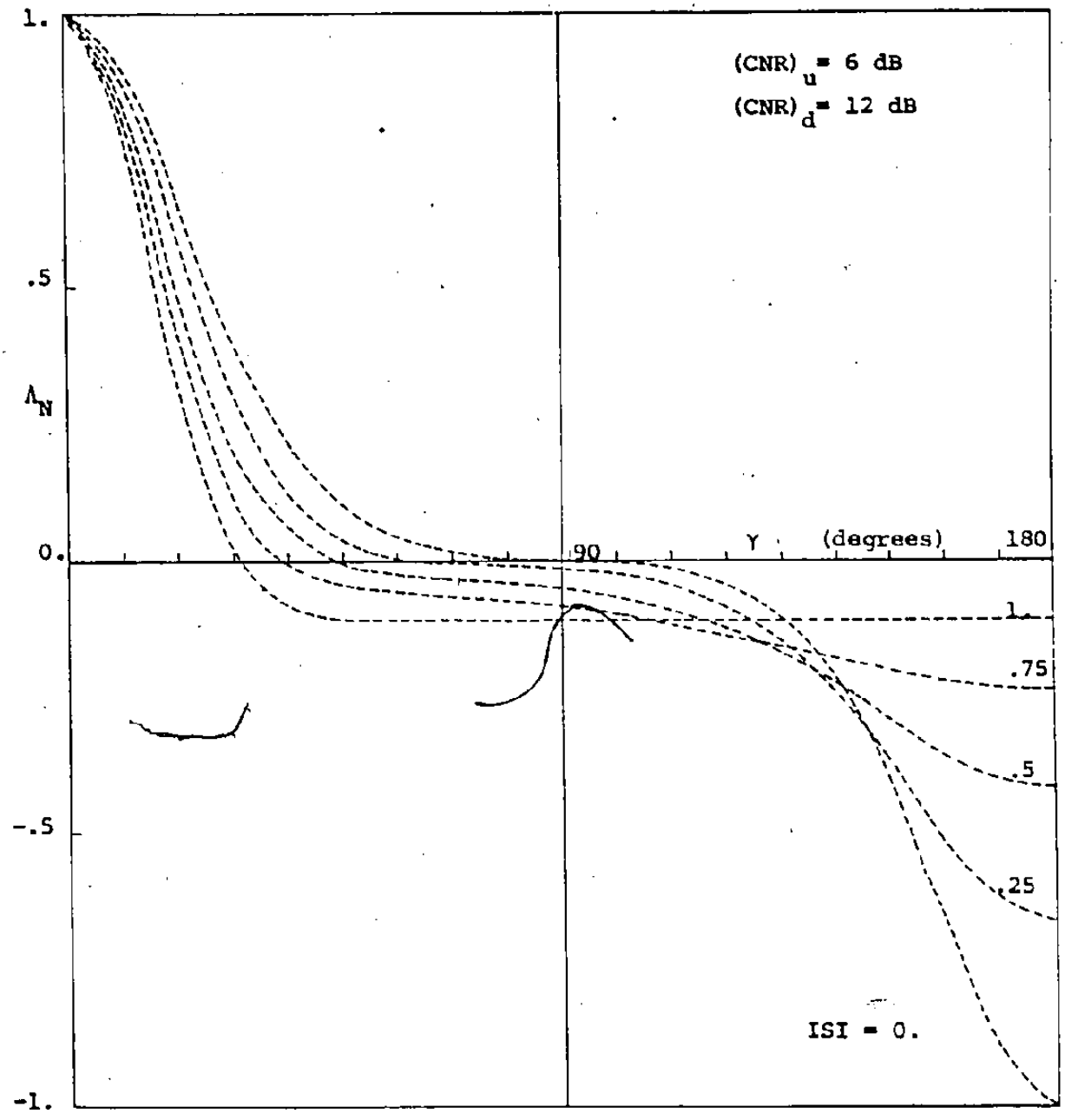

Fig. 4.8 Characteristics of decision statistics

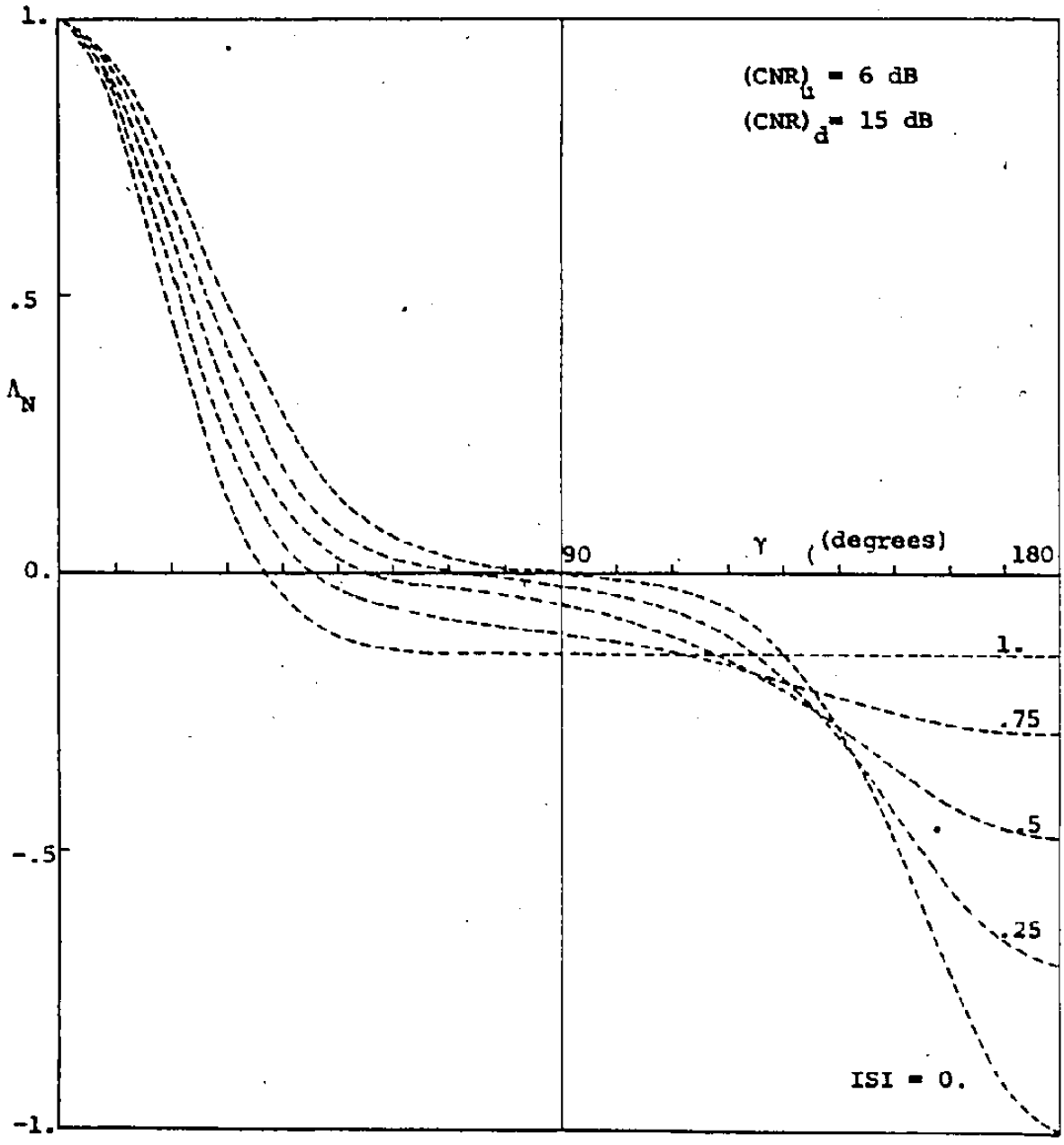

Fig. 4. 9 Characteristics of decision statistics

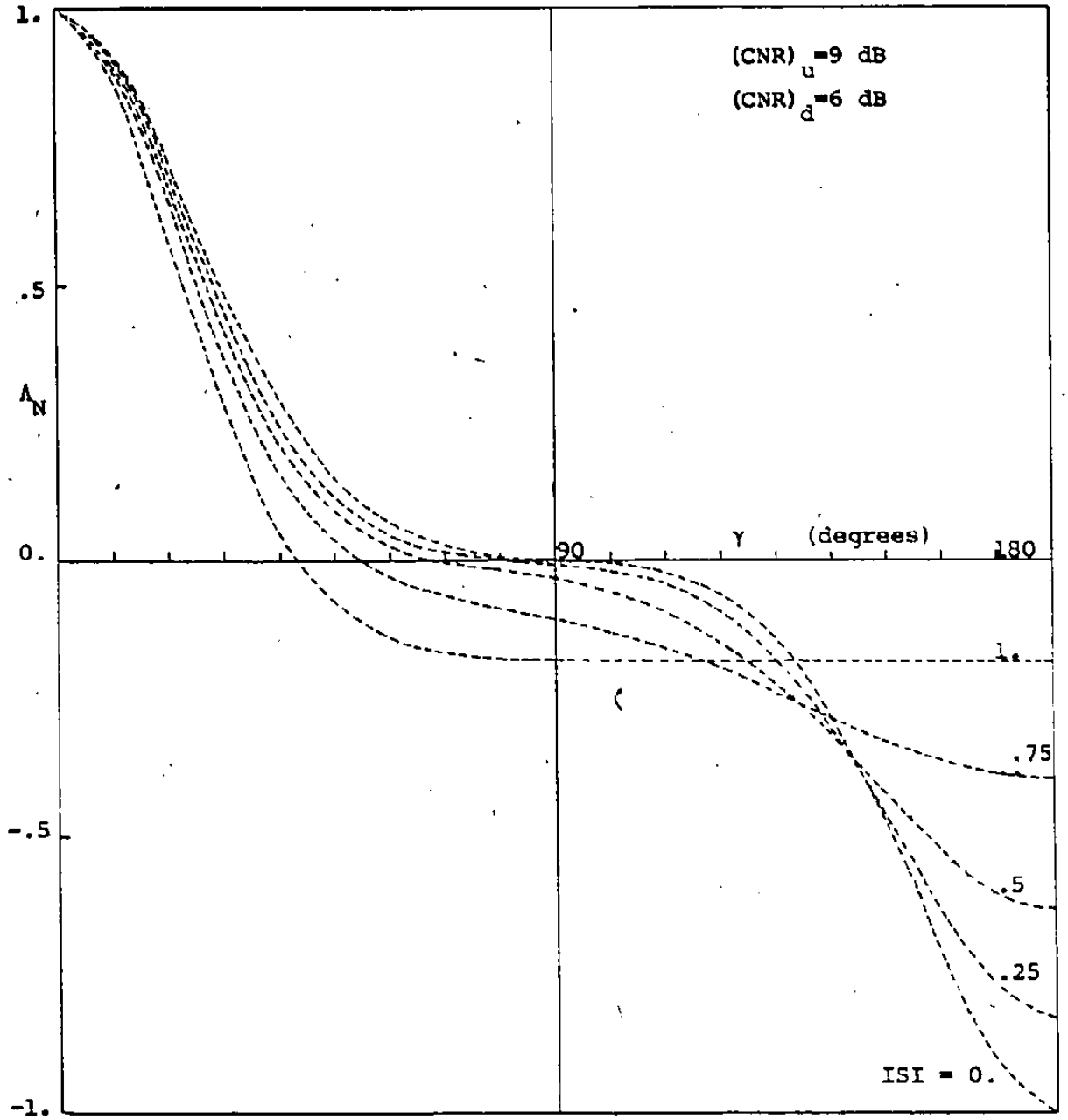

Fig. 4.10 Characteristics of decision statistics

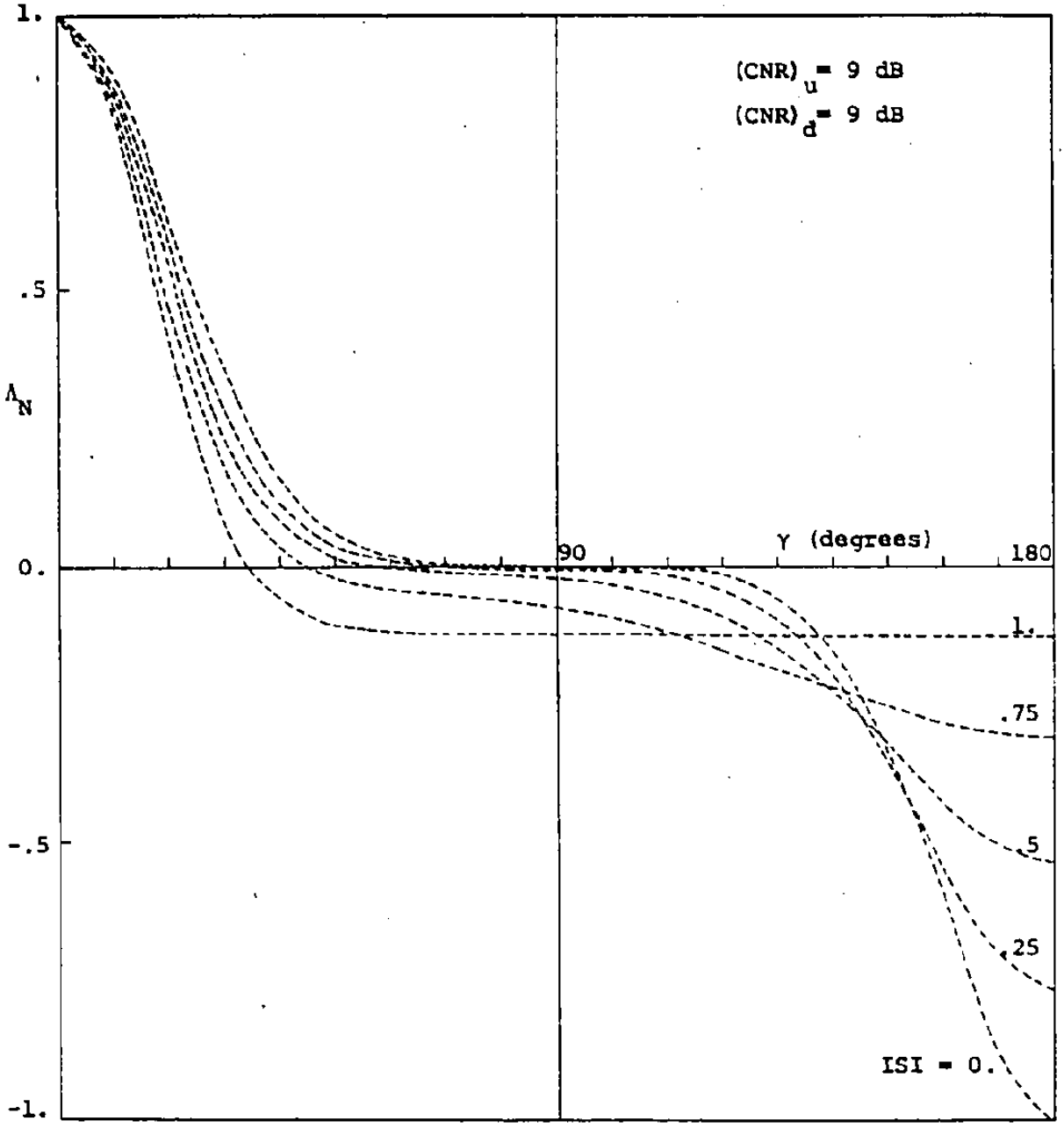

Fig. 4.11 Characteristics of decision statistics

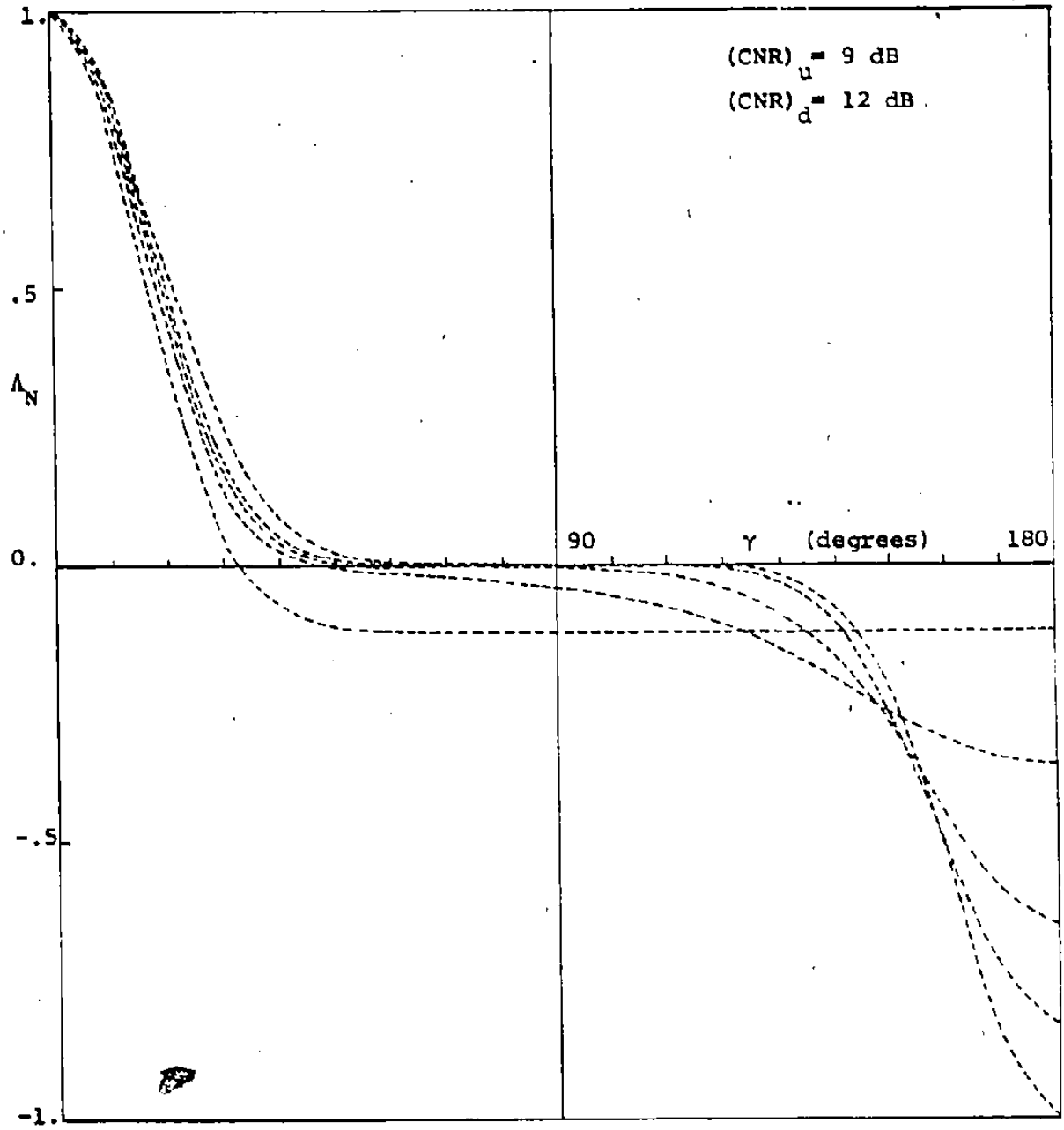

Fig. 4.12 Characteristics of decision statistics

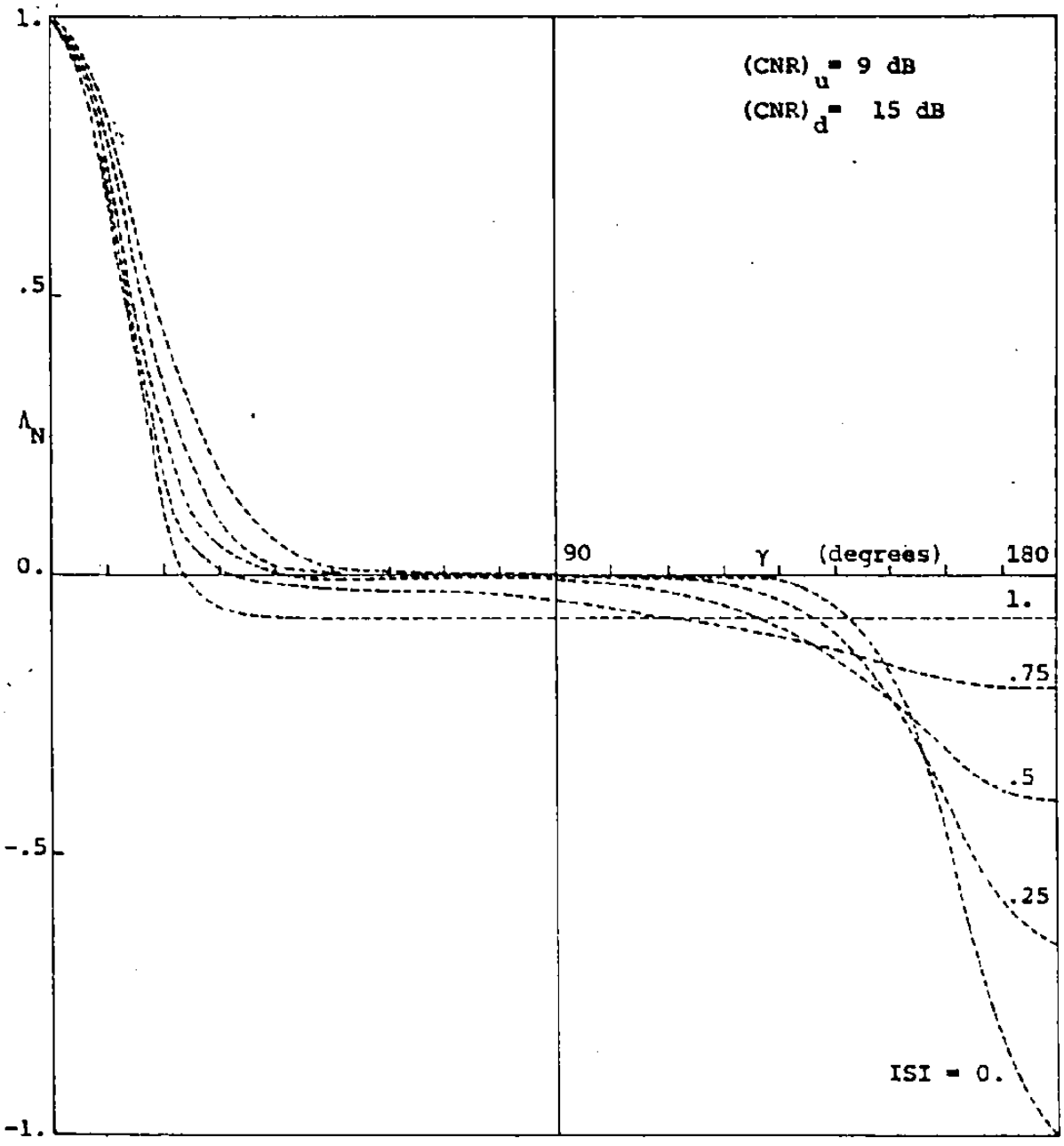

Fig. 4.13 Characteristics of decision statistics

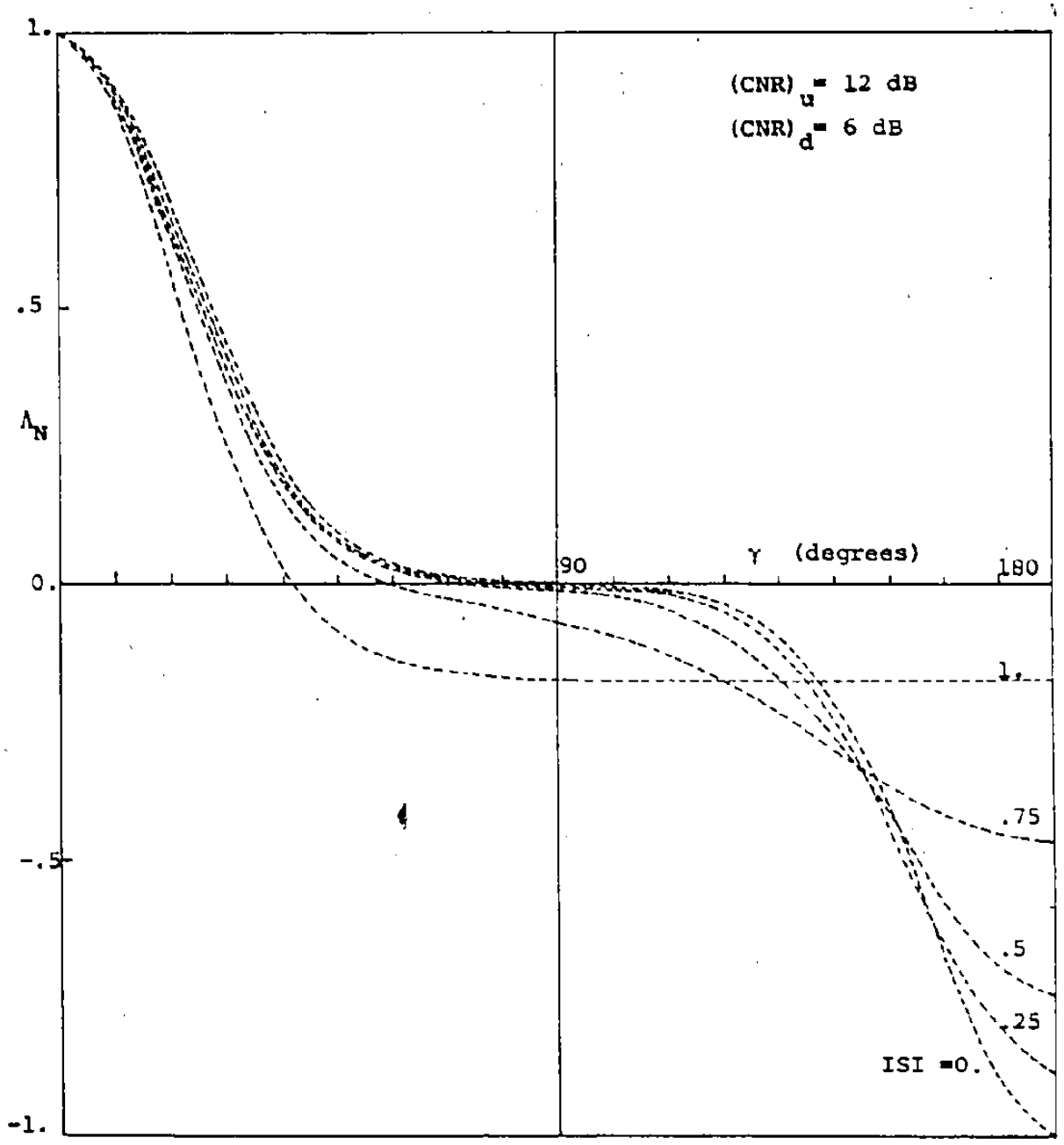

Fig. 4.14 Characteristics of decision statistics

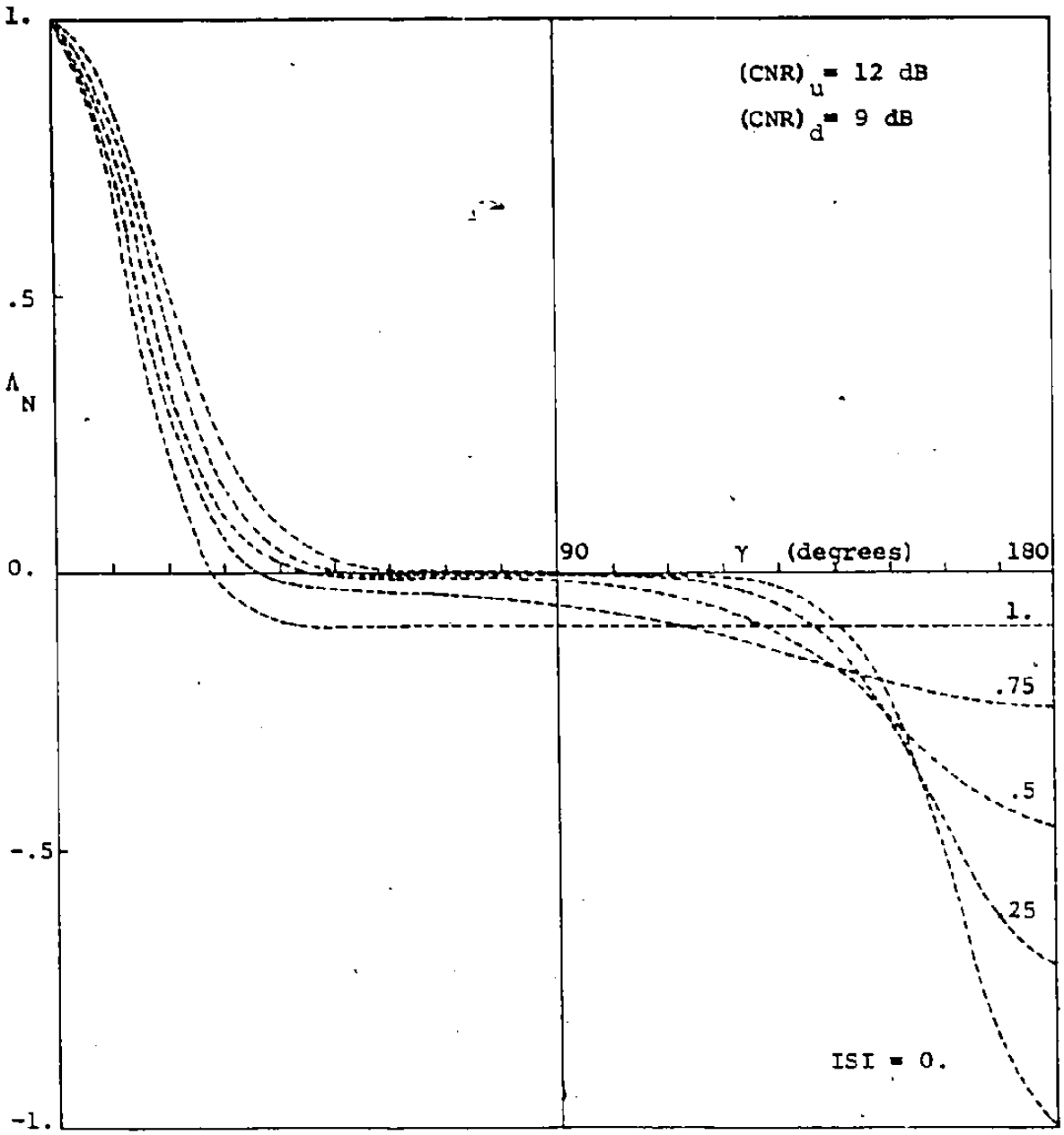

Fig. 4.15 Characteristics of decision statistics

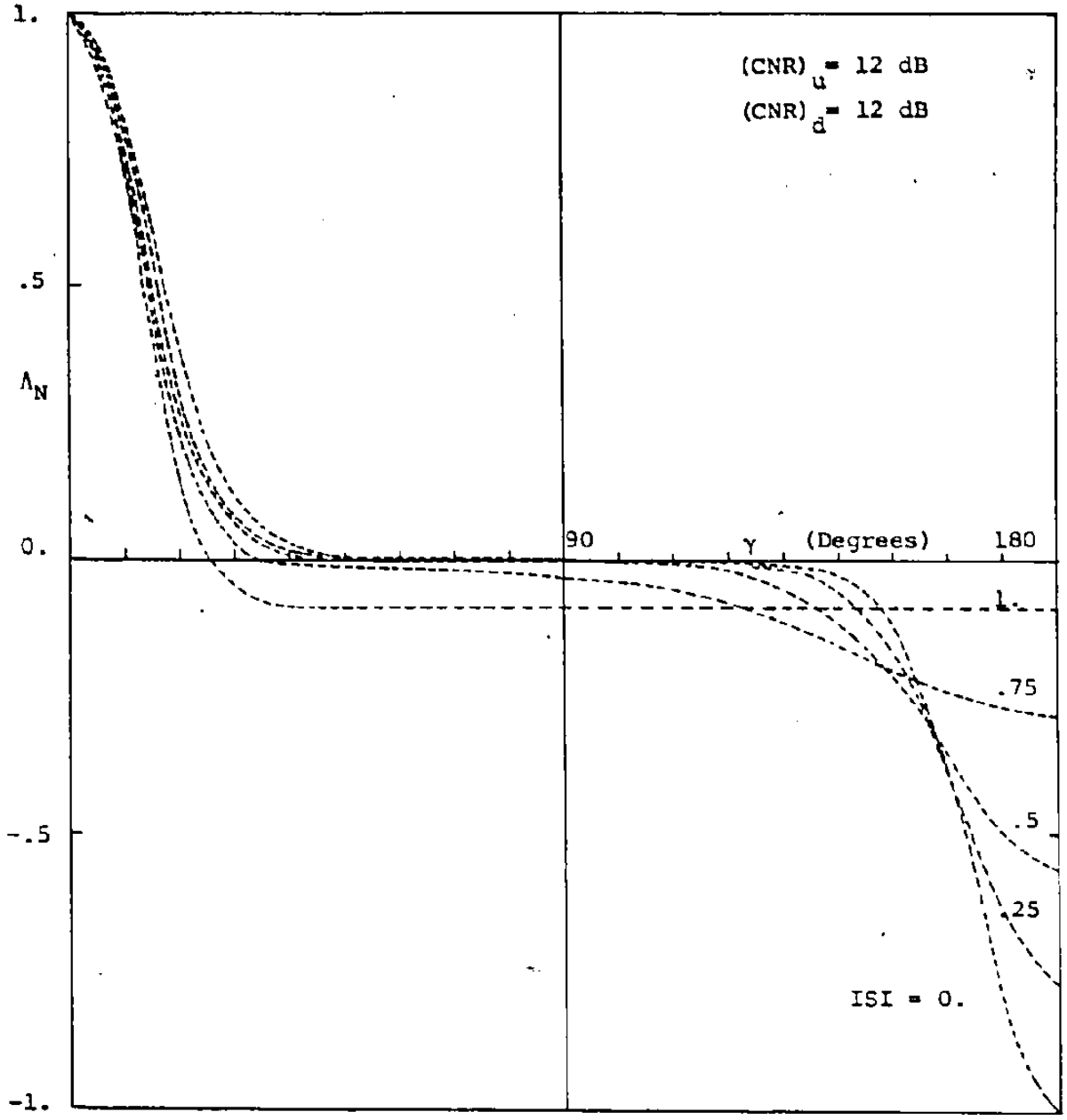

Fig. 4.16 Characteristics of decision statistics

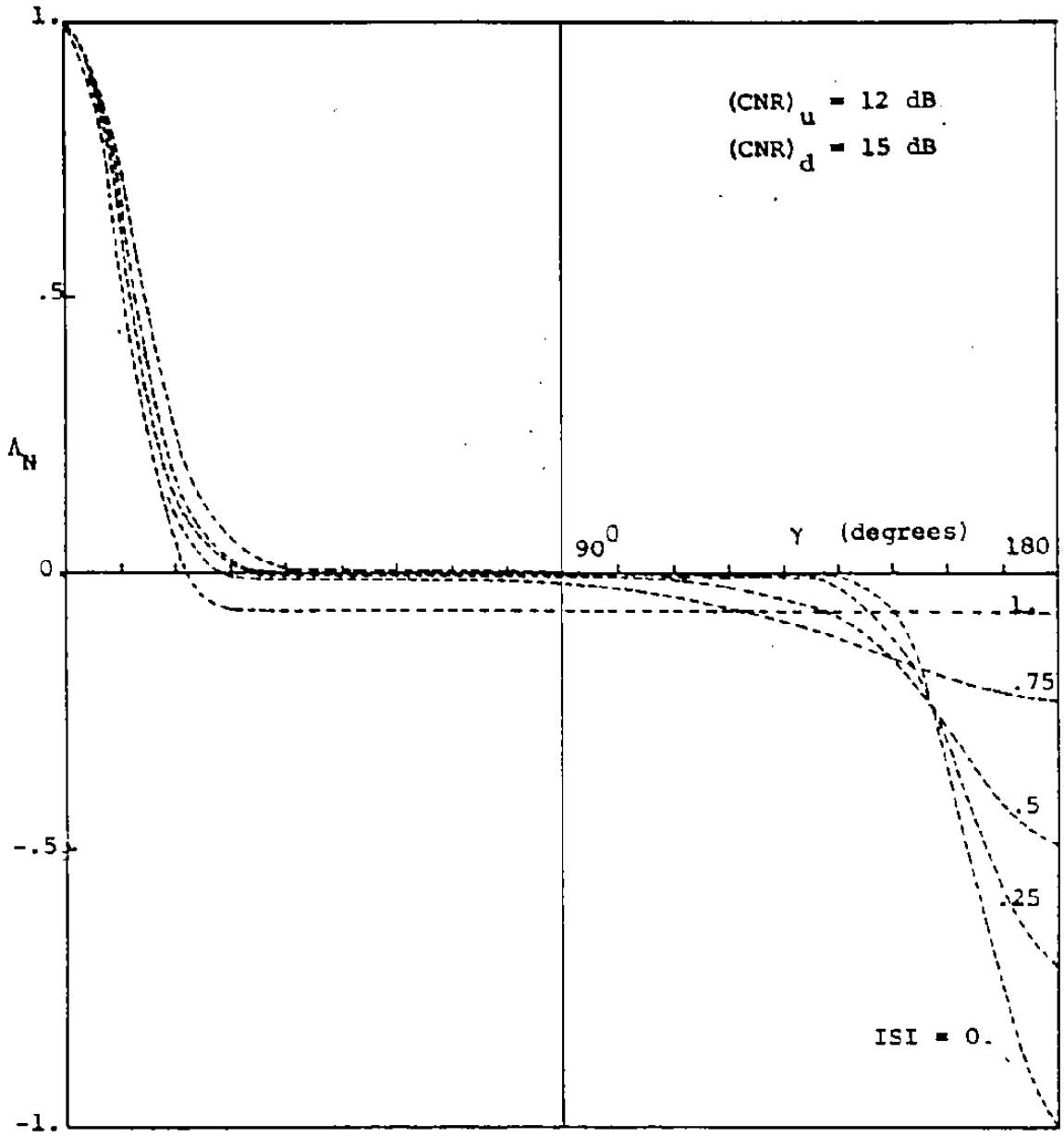

Fig. 4.17 Characteristics of decision statistics

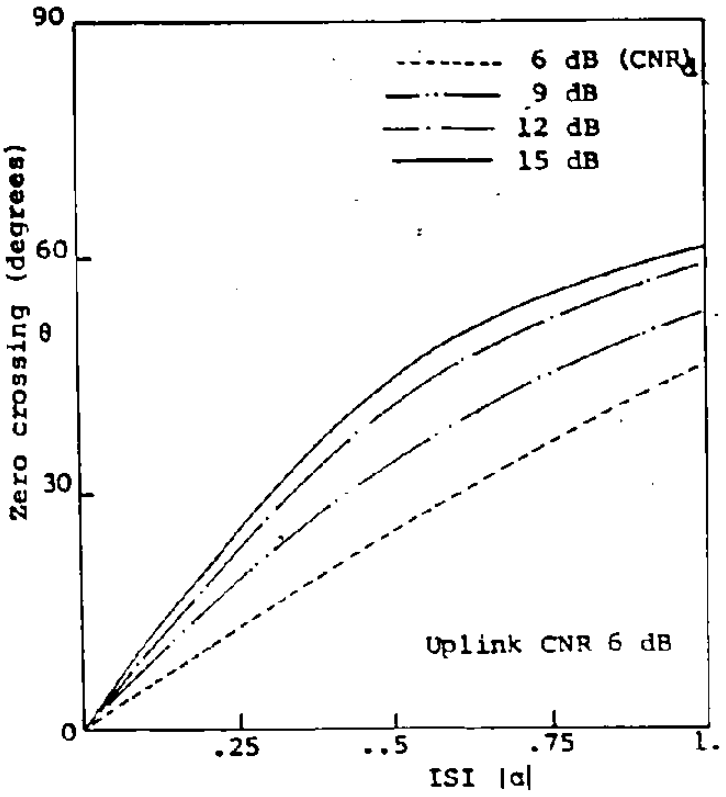

Fig. 4.18 Zero crossing adjustment vs. ISI

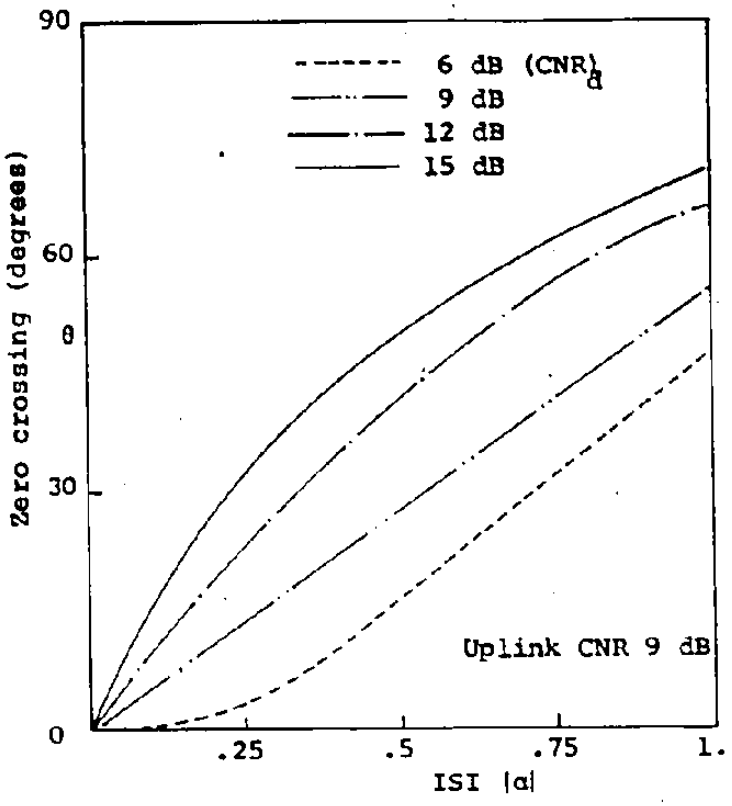

Fig. 4.19 Zero crossing adjustment vs. ISI

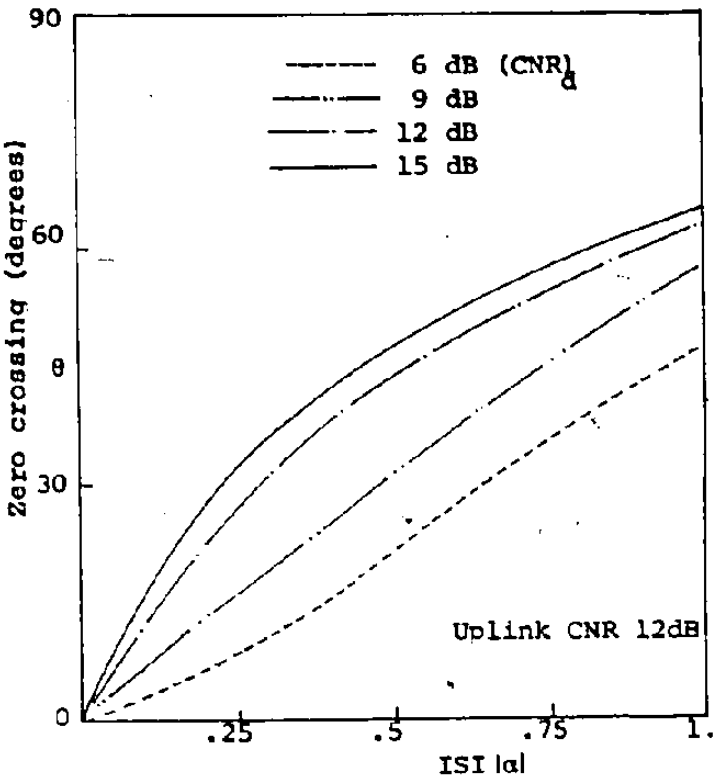

Fig. 4.20 Zero crossing adjustment vs. ISI

in this case is

$$x_k \gtrless_{-1}^{+1} 0$$

which is the single sample sign detector. This is in agreement with conclusions we reached in Chapter 2, since when there is no uplink thermal noise, the effect of the hard-limiter is to restore the original pulse shape without causing any errors, as long as $q_k > |a_m|$. Hence, ISI does not affect the received signal.

If $q_k < |a|_{max}$, i.e. the eye is closed, then it can be shown that (Appendix C)

$$\Lambda = 0$$

In this case the receiver makes an arbitrary decision to determine whether $a_k = +1$ or -1. The reason for this is that whenever a exceeds the magnitude of q_k, the hard-limiter regenerates wrong data if a has the opposite sign to that of the data. This is true even in the case of the complete absence of downlink noise. But we note that even in a closed eye system, the worst case ISI which causes the eye to close can happen only in certain baud intervals (for certain data sequences) and it is only in these baud intervals that receiver makes arbitrary decisions. Also, it is noted that in practical systems uplink noise is always present though possibly small and the limiting cases do not exactly apply.

Case (b)

High downlink CNR; i.e. $\sigma_d \to 0$

In this case making use of the approximate relation

$$I_m\left(\frac{S_k}{\sigma_d^2}\right) \approx \frac{e^{S_k/\sigma_d^2}}{\sqrt{2\pi(S_k/\sigma_d^2)}}$$

we can show that

$$\Lambda = \sum_{n=1}^{\infty} \{f_n(q_k+\alpha) - (-1)^m f_n(q_k-\alpha)\} \cos n\gamma_k \gtrless_{-1}^{+1} 0 \qquad (4.20)$$

The expression (4.20) in this case cannot be simplified further. But we note that the decision threshold is insensitive to the downlink noise and $S_k = \sqrt{x_k^2+y_k^2}$. Again, this in agreement with the results obtained in Chapter 2, where the probability of error curves tend to bottom out at high downlink CNR's, regardless of the ISI and uplink noise. We can not reach any further conclusions except for the fact that the ISI term α plays its role fully in deciding the zero crossings of Λ, that is in the location of the decision threshold.

4.4 Performance Evaluation

The difficulty in evaluating the performance of the receiver synthesized in the previous sections is due to the error propagation problem which is a common problem in all decision feedback receivers. Since past decisions are used

in making the current decision, any errors in the previous decisions tend to cause errors in the current decision. Even in the case of linear channels, the analysis becomes very difficult due to this error propagation problem and there are only three research papers published [48-50] so far which derive bounds on the error probability of the receiver. Therefore computer simulation techniques are commonly used to evaluate the performance of this type of nonlinear receiver. In our case because of the complexity of the decision statistic itself, even under the assumption that the ISI is known, it is not possible to obtain any approximation to the error probability. Hence, Monte Carlo simulation techniques are used in the following sections to evaluate the performance of the receiver.

4.4.1 Chebyshev Bandlimiting Filter

The 4-pole Chebyshev filter used in the numerical examples in Chapters 2 and 3 is used at the transmitter to bandlimit the binary PSK signals in this example. The channel is modelled in baseband form. To make a proper comparison with the performance of the single sample receiver considered in the previous chapters, the filtering of the received signal is considered to be ideal in the sense that no distortion is introduced. The envelope of the binary PSK modulated signal is considered to be rectangular,

i.e. refering to equation (4.1) in section 4.2

$$p(t) = \begin{cases} 1 & 0 \leq t < T \\ 0 & \text{elsewhere} \end{cases}$$

The number of past decisions used in the feedback path is taken as 10, because the filter coefficients beyond these become negligibly small. To generate equally probable data, uniformly distributed pseudo random numbers are generated which are distributed between 0 and 1. Then those numbers between 0 and .5 are taken as data corresponding to +1, and those between .5 and 1 are taken as data corresponding to -1.

The Gaussianly distributed noise components are generated using the subroutine GGNOR on the CDC 6400 computer. The number of errors counted in each test is 25. Since the number of computations grows rapidly, the simulation was limited to error rates 1×10^{-4} or greater. The results obtained are shown in Figure 4.21.

4.4.2 Butterworth Bandlimiting Filter

As the second example, a single pole Butterworth filter (RC filter) is chosen to bandlimit the PSK signals at the transmitter. The impulse response is given as

$$h(t) = \begin{cases} 4\pi B\, e^{-2\pi Bt} & t \geq 0 \\ 0 & t < 0 \end{cases}$$

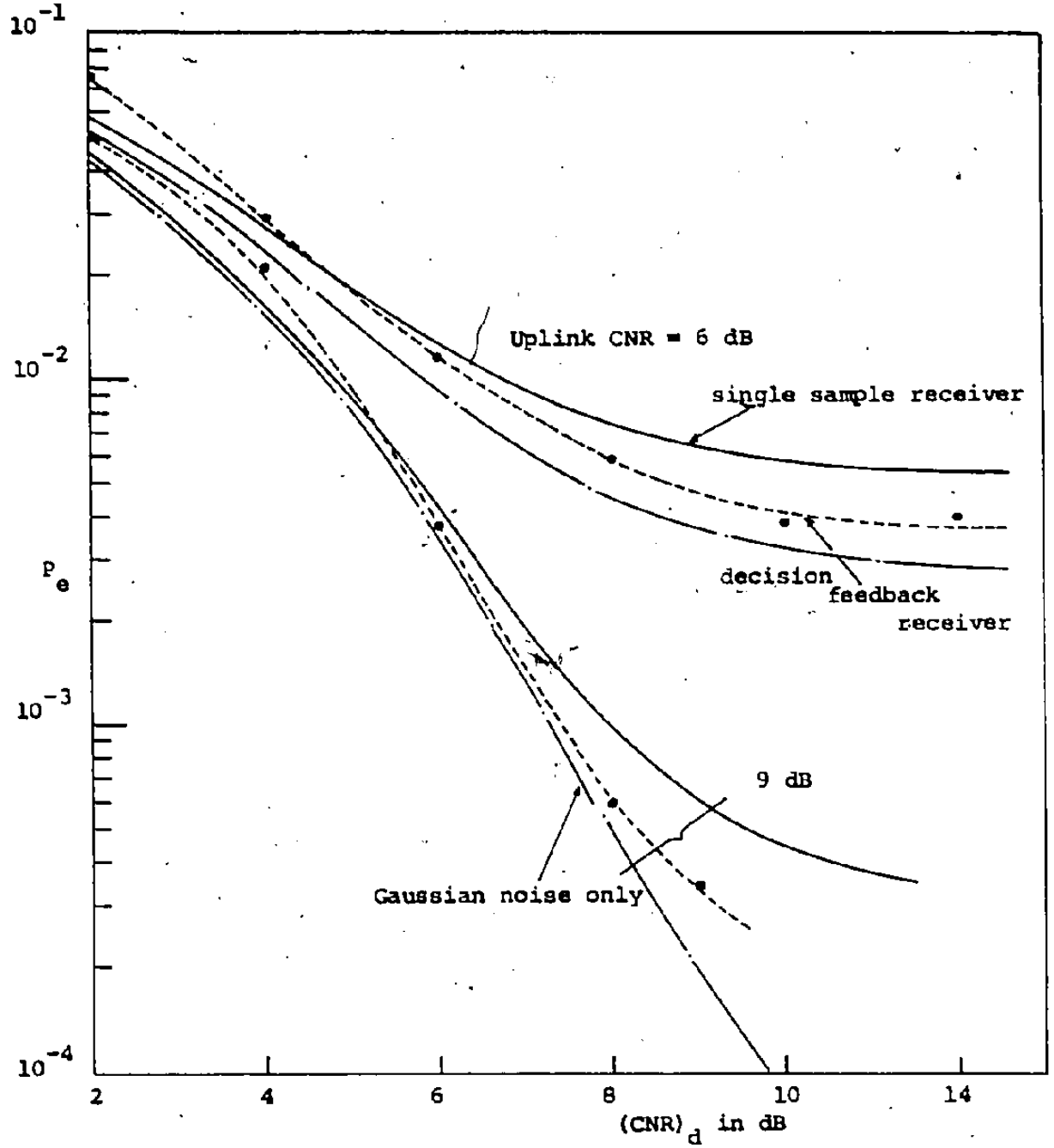

Fig. 4.21 Performance of the receiver, Chebyshev filter (T/T_0=2)

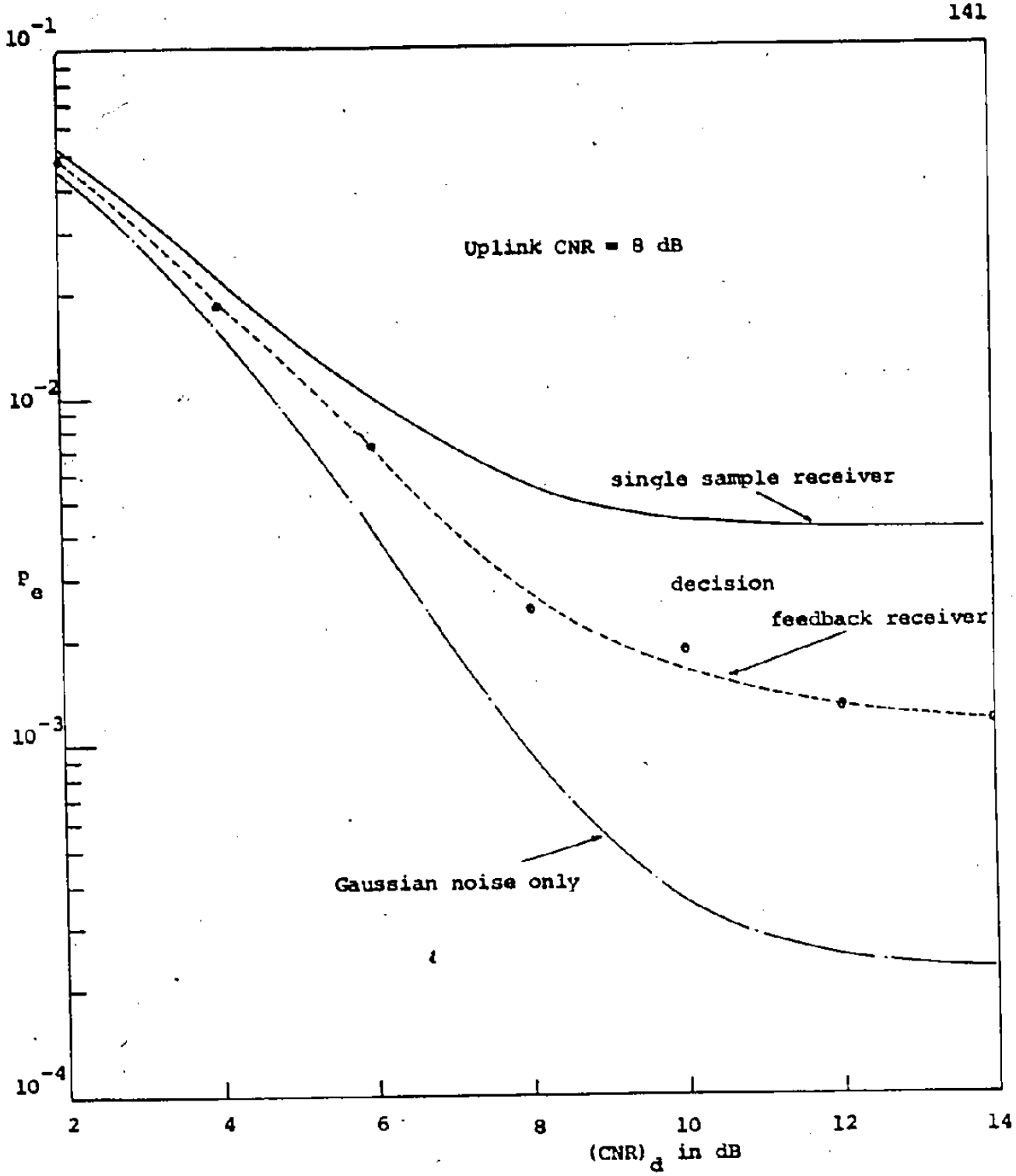

Fig. 4.22 Performance of the receiver, Butterworth filter (BT=.25)

where B is the bandwidth of the filter. In our example the time-bandwidth product (BT) is chosen as .25. The number of past decisions in the feedback path is taken as 10. The other details are as given in section 4.4.1. The results obtained are shown in Figure 4.22.

4.5 Conclusions

In both the examples we considered in our simulation study, the decision feedback receiver performed better than the single sample receiver for high downlink CNR's. Actually, when the error probability of the channel is less than 1×10^{-2}, the decision feedback receiver performs better. We were unable to perform the simulation study at lower error rates than 1×10^{-4}, because of the high computational cost. But at high uplink CNR's, i.e. at lower error rates, we can expect the receiver to perform better than the single sample sign detector, since there will be fewer errors in past decisions. At low downlink CNR's, i.e. when the error rate is high, the receiver becomes inferior to the sign detector. This is due to the fact that most of the past decisions fed back tend to be erroneous, thus causing the threshold to adjust in the incorrect direction.

Since the difference in performance of the sign detector in the presence of ISI and in the absence if ISI is significant in the range of high uplink CNR's and high

downlink CNR's, the receiver structure we have derived can be incorporated effectively in order to improve the performance in this range.

In addition, we have shown that for wideband hard-limiting channels, the single sample sign detector is optimal in the absence of prior signal processing. Also, if the uplink thermal noise is negligibly small, then even for bandlimiting channels, the sign detector will perform optimally, if the eye is open, since the hard-limiter restores the original pulse shape.

Although, we have performed the simulation study only for a hard-limiting channel, one can reasonably expect a receiver having this type of structure to perform better in other bandpass nonlinear channels.

CHAPTER 5

CONCLUSIONS AND SUGGESTIONS FOR FUTURE WORK

5.1 Conclusions

In this thesis we have investigated two major problems as follows: (a) the performance analysis of bandlimited CPSK signals transmitted over nonlinear bandlimited satellite channels, (b) a receiver synthesis for nonlinear bandlimited channels. The problems we have analyzed are in no way simple due to the inherent complexity of the nonlinearities, as well as the unknown distribution of the intersymbol interference. However we have attained the following objectives.

(a) Performance degradation of bandlimited M-ary CPSK signals due to satellite transponder nonlinearity, uplink thermal noise and downlink thermal noise is completely analyzed. The applicability of the technique is illustrated by considering numerical examples and different models for the transponder including a complex model of an actual TWT. The probability of error can be evaulated with reasonable computational effort using the technique given.

(b) Upper and lower bounds on the probability of error for bandlimited binary CPSK signals received over nonlinear channels are derived. These bounds can be evaluated with minimal computational effort using the previously evaluated error curves for wideband channels. When the intersymbol interference is small such as in well controlled practical satellite systems, these bounds yield reasonably close approximations to the exact probability of error.

(c) A receiver structure is derived to combat the degradation caused by intersymbol interference for bandlimited binary CPSK signals received over nonlinear satellite channels. The decision statistic is given in an integral form for a general class of nonlinearity, but is simplified to a series form in its application to a hard-limiting channel. It is shown that the single sample sign detection yields optimum results for wideband channels. Also, other special cases of interest are analyzed. Through the use of computer simulation, the performance of the receiver is evaluated. It is shown that the decision feedback receiver performs considerably better in the range of high downlink CNR's. Since the receiver structure is essentially the same regardless of the nonlinearity, we would expect to obtain similar

processing gain over single sample sign detector for other types of bandpass nonlinearities.

5.2 Suggestions for Future Work

Another worthwhile problem to be studied is the performance degradation caused in bandlimited nonlinear channels which use other modulation methods such as FFSK (Fast Frequency Shift Keying). These modulation methods are currently being considered for satellite communication because of their attractive spectral properties. But analysis of these problems will no way be easier to deal with and each case may have to be considered separately.

Secondly, one may attempt to derive tight bounds on the probability of error following the same arguments as given in Chapter 2. The difficulty here lies in analyzing the exact behaviour of the function whose expectation is to be evaluated. Also, another possibility is to extend the method to QPSK signal transmission, that is to evaluate error bounds by generalizing the single variate moment space techniques to multi-variate moment space. The major obstacle in this case is the difficulty of analysis and visualization of functions in three dimensions.

A possible extension to the study of the receiver structure is to find at least an approximate analytic method to evaluate its performance. Another useful extension will

be to generalize the analysis to include QPSK signal reception. It is also noted that we have not made any attempt to filter the received signal suitably to improve the receiver's performance. Virtually all real systems have significant filtering on the downlink path, and considerable effort is usually expended on experimentally adjusting these filters to obtain best performance. A very useful problem to investigate but a very difficult one to analyze is thus to develop means analyzing the effects of downlink filtering on error-performance of a system and eventually to develop a receiver structure when the communications systems model includes the effects of filtering following the nonlinear satellite transponder.

APPENDIX A

Derivation of Equations (2.15), (2.24), (2.29), (2.34) and Evaluation of the Power Series Coefficients

A.1 Derivation of Equation (2.15)

We rewrite equation (2.14) for completeness

$$P_{c|R,\lambda} = \frac{1}{2\pi\sigma_d^2} \int_0^{y'} \int_{x'}^{\infty} e^{-[x-f\cos(\lambda+\rho)]^2/2\sigma_d^2} e^{-[y-f\sin(\lambda+\rho)]^2/2\sigma_d^2} \cdot dx \cdot dy \qquad (A.1)$$

Transforming (x,y) to (R,θ) polar coordinates we get,

$$= \frac{1}{2\pi\sigma_d^2} \int_0^{\infty} \int_0^{2\pi/M} R\, e^{-(R^2+f^2)/2\sigma_d^2} e^{Rf\cos(\lambda+\rho+\theta)/\sigma_d^2} \cdot d\theta \cdot dR \qquad (A.2)$$

Next use the expansion [35],

$$e^{z\cos\gamma} = I_o(z) + 2 \sum_{n=1}^{\infty} I_n(z) \cos n\gamma \qquad (A.3)$$

Substituting (A.3) in (A.2), the integrals can be evaluated [23] to obtain the desired expression (2.15).

A.2 Derivation of Equation (2.24)

Substituting (2.23) in (2.22) we get

$$p(x,y) = \left(\frac{1}{2\pi}\right)^2 \sum_{\ell,m} b_{\ell,m} \int_{-\infty}^{+\infty}\int_{-\infty}^{+\infty} u^{\ell} v^{m} e^{j(a_o u + b_o v)} e^{-\sigma_u^2 (u^2+v^2)/2} \cdot e^{-j(ux+vy)}\, du \cdot dv$$

$$= \sum_{\ell,m} b_{\ell,m} (-1)^{\ell+m/2} \frac{\partial^{\ell}}{\partial x^{\ell}} \left\{\frac{1}{2\pi}\int_{-\infty}^{\infty} e^{-\sigma_u^2 v/2} e^{-ju(x-a_o)}\, du\right\} \cdot \frac{\partial^{m}}{\partial y^{m}} \left\{\frac{1}{2\pi}\int_{-\infty}^{+\infty} e^{-\sigma_u^2 v/2} e^{-ju(y-b_o)}\, dv\right\}$$

$$= \sum_{\ell,m} b_{\ell,m} (-1)^{\ell+m/2} \left\{\frac{\partial^{\ell}}{\partial x^{\ell}} \frac{1}{2\pi\sigma_u^2} e^{-(x-a_o)^2/2\sigma_u^2}\right\} \cdot \left\{\frac{\partial^{m}}{\partial y^{m}} \frac{1}{2\pi\sigma_u^2} e^{-(y-b_o)^2/2\sigma_u^2}\right\}$$

$$p(x,y) = \sum_{\ell,m} \frac{b_{\ell,m}}{(\sqrt{2}\sigma)^{\ell+m}} \frac{(-1)^{\ell+m/2}}{2\pi\sigma^2} H_{\ell_u}\left(\frac{x-a_o}{\sqrt{2}\sigma}\right) H_{m_u}\left(\frac{y-b_o}{\sqrt{2}\sigma}\right) \cdot e^{-(x-a_o/\sqrt{2}\sigma_u)^2} e^{-(y-b_o/\sqrt{2}\sigma_u)^2} \qquad (A.4)$$

The last expression (A.4) is obtained by using the relation

$$H_n(x) = (-1)^n \cdot e^{x^2} \cdot \frac{d^n}{dx^n} e^{-x^2}$$

A.3 Derivation of Equation (2.29)

When M = 2,

$$b_o = \overline{q_o}; \quad a_o = 0, \quad \alpha = 0, \quad \phi_\beta(v) = \sum_m b_m v^m$$

Therefore (A.4) can be written, after transforming $(x/\sqrt{2}\sigma_u, y/\sqrt{2}\sigma_u)$ rectangular co-ordinates to polar form (s,λ), as

$$p(s,\lambda) = \sum_m \frac{b_m}{(\sqrt{2}\sigma_u)^m} (-1)^{m/2} \frac{1}{\pi} \frac{\partial^m}{\partial q^m} s\, e^{-(s^2+q^2-2sq\cos\lambda)} \qquad (A.5)$$

The expression (2.15) can be written as

$$P_{c|R,\lambda} = \frac{1}{2} + \frac{1}{\pi} \sum_{n=0}^{\infty} \frac{\Gamma(n+1/2)}{(2n+1)!} \left(\frac{f(R)}{\sqrt{2}\sigma_d}\right)^{2n+1} {}_1F_1\left(n+\tfrac{1}{2}, 2n+2, -\frac{f^2(R)}{2\sigma_d^2}\right) \cdot \sin n(\rho(R)+\lambda) \qquad (A.6)$$

Then

$$P_c = E_{R,\lambda}\,[P_{c|R,\lambda}]$$

Combining (A.5) and (A.6) and evaluating the integral with respect to λ, we get the required expression

$$P_c = \frac{1}{2} + \frac{1}{\pi} \sum_{n=0}^{\infty} \frac{\Gamma(n+1/2)}{(2n+1)!} (-1)^n \sum_{m=0} \frac{b_m}{(\sqrt{2}\sigma_u)^m} (-1)^{m/2} \int_0^{\infty} \left[\frac{f(\sqrt{2}\sigma_u S)}{\sqrt{2}\,\sigma_d}\right]^{2n+1} {}_1F_1\left(n+\tfrac{1}{2}, 2n+2, -\frac{f^2(\sqrt{2}\sigma_u S)}{2\sigma_d^2}\right) s\, e^{-s^2} \cos n\rho(\sqrt{2}\,\sigma_u S) \frac{\partial^m}{\partial q^m} e^{-q^2} I_n(2sq)\, ds \qquad (A.7)$$

A.4 Derivation of Equation (2.34)

Substituting for

$$f(R(t)) = \begin{cases} a & R(t) \geq 0 \\ -a & R(t) < 0 \end{cases}$$

and

$$\rho(R(t)) = 0 \quad \text{for all } R(t).$$

in (A.7) we obtain the following expression for P_c.

$$P_c = \frac{1}{2} + \frac{1}{\pi} \sum_{n=0}^{\infty} \frac{\Gamma(n+1/2)}{(2n+1)!} (-1)^n \sum_{m=0} \frac{b_m}{(\sqrt{2}\sigma_u)^m} (-1)^{m/2}$$

$$\rho_d^{2n+1} \, {}_1F_1\left(n + \tfrac{1}{2}, 2n+2, -\rho_d^2\right) \frac{\partial^m}{\partial q^m} \int_0^{\infty} s \, e^{-s^2} e^{-q^2} I_n(2sq) \, ds \qquad \text{(A.8)}$$

where

$$\rho_d = \frac{a}{\sqrt{2}\,\sigma_u}$$

The integral in (A.8) can be evaluated to obtain the required expression for P_c as

$$P_c = \frac{1}{2} + \frac{1}{\pi} \sum_{n=0}^{\infty} \frac{\Gamma(n+1/2)}{(2n+1)!} (-1)^n \rho_d^{2n+1} \, {}_1F_1\left(n + \tfrac{1}{2}, 2n+2, -\rho_d^2\right)$$

$$\sum_{m=0} \frac{b_m}{(\sqrt{2}\sigma_u)^m} (-1)^{m/2} \frac{\partial^m}{\partial q^m} q^{2n+1} \, {}_1F_1\left(n + \tfrac{1}{2}, 2n+2, -q^2\right) \qquad \text{(A.9)}$$

A.5 Evaluation of Coefficients of Power Series Expansion

$M = 2$

For binary PSK, we recall that

$$\phi_\beta(v) = \prod_n \cos q_n v$$

Let

$$f_n(v) \triangleq \cos q_n v \tag{A.10}$$

Hence

$$\phi_\beta(v) = \prod_n' f_n(v) \tag{A.11}$$

$$h(v) \triangleq \log f_n(v) \tag{A.12}$$

Therefore

$$\theta(v) \triangleq \log \phi_\beta(v) = \sum_n' \log f_n(v) \tag{A.13}$$

Step 1: Obtain the coefficients of power series of h(v) in terms of the coefficients of power series of $f_n(v)$.

Let

$$f_n(v) = \sum_m c_{2m} v^{2m}; \quad b_o = 1 \tag{A.14}$$

$$h(v) = \sum_\ell a_{2\ell} v^{2\ell}; \quad a_o = 0 \tag{A.15}$$

From (A.12) we obtain, after differentiating with respect to v,

$$\frac{dh(v)}{dv} = \frac{1}{f_n(v)} \frac{\partial}{\partial v} f_n(v) \tag{A.16}$$

Substituting (A.13) and (A.14) in (A.15) we obtain

$$[c_o+c_2v^2+c_4v^4+\ldots]\ [2a_2v+4a_4v^3+\ldots] = 2c_2v+4c_4v^3+\ldots$$

Comparing the coefficients of v, v^2, v^3, ..., etc. it can be easily shown the following relation

$$a_{2\ell} = c_{2\ell} - \sum_{k=1}^{\ell} (2\ell-2k)\ c_{2\ell-2k}\ a_{2k} \tag{A.17}$$

and

$$a_o = 0$$

Step 2: Since the power series expansion for log $f_n(v)$ is known, summing over all the interference terms, we can obtain the series expansion of $\theta(v) \triangleq \log \phi_\beta(v)$ in equation (A.13). To obtain the power series expansion for $\phi_\beta(v)$ we proceed as follows.

Let
$$\theta(v) \triangleq \Sigma\, d_{2\ell}\, v^{2\ell}; \quad d_o = 0 \tag{A.18}$$

$$\phi_\beta(v) \triangleq \Sigma\, b_{2m}\, v^{2m} \tag{A.19}$$

From (A.13) we get

$$\phi_\beta(v)\, \frac{\partial}{\partial v}\, [\theta(v)] = \frac{\partial}{\partial v}\, [\phi_\beta(v)] \tag{A.20}$$

Subsitituting (A.18) and (A.19) in (A.20) we obtain,

$$[b_o+b_2v^2+b_4v^4+\ldots]\ [2d_2v+4d_4v^3+\ldots] = [2b_2v+4b_4v^3+\ldots]$$

Comparing the coefficients of v, v^2, v^3, ..., etc. it can be shown that

$$b_{2\ell} = \frac{1}{2\ell} \sum_{k=0}^{\ell} (2\ell-2k)\, d_{2\ell}\, c_{2k} \tag{A.21}$$

Using equations (A.13), (A.17) and (A.21), the required power series coefficients can be computed.

M=4; For QPSK,

we recall that

$$\phi_{\alpha,\beta}(u,v) = \prod_n' \cos\left(\frac{q_n u}{\sqrt{2}}\right) \cdot \prod_n' \cos\left(\frac{q_n v}{\rho 2}\right)$$

$$\sum_{\ell,m} b_{\ell,m}\, u^{\ell} v^{m} \triangleq \phi_{\alpha,\beta}(u,v) = \left[\sum_{\ell} b_{2\ell}\, u^{2\ell}\right]\left[\sum_{\ell} b_{2\ell}\, v^{2\ell}\right] \tag{A.22}$$

Since $b_{2\ell}$ can be evaluated using the relations (A.13), (A.17) and (A.21), the coefficient $b_{\ell,m}$ can be obtained from the above relation, (A.22).

APPENDIX B

Proofs of Convexity and Uniform Convergences and Derivation of Equation (3.16)

B.1 Proof of Convexity

We recall that,

$$P_g(A+\alpha) \triangleq \frac{1}{2}\int_{-\infty}^{+\infty}\int_{-\infty}^{+\infty} \operatorname{erfc}\left[\frac{f(\sqrt{x^2+y^2})\ \operatorname{Cos}\ (\tan^{-1}(y/x) + \rho(\sqrt{x^2+y^2})}{\sqrt{2}\ \sigma_d}\right]$$

$$\cdot \exp\left[-\frac{(x-A-\alpha)^2}{2\sigma_u^2}\right] \cdot \exp\left(\frac{-y^2}{2\sigma_u^2}\right) dx \cdot dy \qquad (B.1)$$

In this appendix we extract a convex region of $P_g(A+\alpha)$ under certain restrictions rather than exactly proving the convexity of $P_g(A+\alpha)$. We make the assumption that $P_g(A+\alpha)$ is monotonically decreasing when α varies from $-|I_m|$ to $+|I_m|$.

$$P' \triangleq \frac{\partial P_g(A+\alpha)}{\partial \alpha} = \int_{-\infty}^{+\infty}\int_{-\infty}^{+\infty} \operatorname{erfc}(g(x,y))\ \frac{(x-A-\alpha)}{2\sigma_u^2}\ e^{-(x-A-\alpha)^2/2\sigma_u^2}$$

$$\cdot\ e^{-y^2/2\sigma_u^2}\ dx\ dy$$

$$+ \frac{1}{\sigma_u^2} \int_{-\infty}^{+\infty} \int_{-\infty}^{+\infty} x \ \text{erfc}\ (f(x,y)) \cdot e^{-(x-A-\alpha)^2/2\sigma_u^2} \cdot e^{-y^2/2\sigma_u^2} \, dx \, dy \qquad (B.2)$$

where

$$g(x,y) \triangleq \frac{f(\sqrt{x^2+y^2}) \ \text{Cos}\ (\tan^{-1} y/x + \rho(\sqrt{x^2+y^2}))}{\sqrt{2}\ \sigma_d}$$

we know that $P' < 0$ for all $\alpha \in [-I_m, I_m]$. Also

$$k_1 \leq \text{erfc}\ (g(x,y)) \leq k_2 \quad \text{and} \quad k_1, k_2 \geq 0$$

Our next objective is to determine the values of erfc(•) dominant in the integrals of (B.2), so that $P' < 0$ always. To determine that, let us substitute k_1 in the first integral and k_2 in the second integral and evaluate the integrals.

$$P' = -\frac{(A+\alpha)}{\sigma_u^2} \int_{-\infty}^{+\infty} \int_{-\infty}^{+\infty} k_1 \frac{1}{2\pi\sigma_u^2} e^{-y^2/2\sigma_u^2} e^{-(x-A-\alpha)^2/2\sigma_u^2} \, dx \, dy$$

$$+ \frac{1}{\sigma_u^2} \int_{-\infty}^{+\infty} \int_{-\infty}^{+\infty} k_2 \frac{1}{2\pi\sigma_u^2} e^{-y^2/2\sigma_u^2} e^{-(x-A-\alpha^2)/2\sigma_u^2} \, dx \, dy$$

$$= -\frac{(A+\alpha)}{\sigma_u^2} k_1 + \frac{1}{\sigma_u^2} k_2 (A+\alpha)$$

$$= \frac{(A+\alpha)}{\sigma_u^2} (K_2 - k_1) \qquad (B.3)$$

But this is a contradiction of our assumption that $P' < 0$ since $k_2 > k_1$.

Therefore we conclude that in the first integral it is the upper bound on erfc(•) dominating and in the second integral it is the lower value of erfc(•) that dominates, so that $P' < 0$ always.

Therefore, in

$$\int_{-\infty}^{+\infty}\int_{-\infty}^{+\infty} \operatorname{erfc}(g(x,y)) \frac{1}{2\pi\sigma_u^2} e^{-y^2/2\sigma_u^2} e^{-(x-A-\alpha)^2/2\sigma_u^2} dx\, dy$$

upper bound k_2 dominates and in

$$\int_{-\infty}^{+\infty}\int_{-\infty}^{+\infty} \operatorname{erfc}(g(x,y)) \frac{1}{2\pi\sigma_u^2} e^{-y^2/2\sigma_u^2} e^{-(x-A-\alpha)^2/2\sigma_u^2} dx dy$$

lower bound k_1 dominates.

Out next objective is to investigate the second derivative of $P_g(A+\alpha)$.

$$P'' \triangleq \frac{\partial^2 P_g(A+\alpha)}{\partial\alpha^2} = \frac{(A+\alpha)^2}{\sigma_u^4}\int_{-\infty}^{+\infty}\int_{-\infty}^{+\infty} \operatorname{erfc}(g(x,y)) \frac{e^{-y^2/2\sigma_u^2}}{2\pi\sigma_u^2} e^{-(x-A-\alpha)^2/2\sigma_u^2} dx \cdot dy$$

$$- \frac{2(A+\alpha)}{\sigma_u^4}\int_{-\infty}^{+\infty}\int_{-\infty}^{+\infty} \operatorname{erfc}(g(x,y)) \frac{e^{-y^2/2\sigma_u^2}}{2\pi\sigma_u^2} x\, e^{-(x-A-\alpha)^2/2\sigma_u^2} dx\, dy$$

$$- \frac{1}{\sigma_u^2} \int_{-\infty}^{+\infty} \int_{-\infty}^{+\infty} \text{erfc}(g(x,y)) \frac{e^{-y^2/2\sigma_u^2}}{2\pi\sigma_u^2} e^{-(x-A-\alpha)^2/2\sigma_u^2} \, dx \, dy$$

$$+ \frac{1}{\sigma_u^4} \int_{-\infty}^{+\infty} \int_{-\infty}^{+\infty} \text{erfc}(g(x,y)) \frac{e^{-y^2/2\sigma_u^2}}{2\pi\sigma_u^2} x^2 e^{-(x-A-\alpha)^2/2\sigma_u^2} \, dx \, dy \qquad \text{(B.4)}$$

In (B.4), except for the last integral, all other integrals have appeared in expression (B.3). Therefore we know the dominating values of erfc(·). Since only in the last integral of (B.4) we do not know the dominating value of erfc(·), let us assume that k' dominates in this integral such that

$$k_1 \leq k' \leq k_2$$

Substituting appropriate values of erfc(·) in (B.4) and evaluating the integrals, we get

$$P'' = \frac{(A+\alpha)^2}{\sigma_u^4} k_2 - \frac{2(A+\alpha)^2}{\sigma_u^4} k_1 - \frac{k_2}{\sigma_u^2} + \frac{k'}{\sigma_u^2} + \frac{(A+\alpha)^2}{\sigma_u^4} k' \qquad \text{(B.5)}$$

In (B.5), we substitute $k' = k_1$ so that P'' is least positive.

Then we get

$$P'' = (k_2 - k_1) \left[\frac{(A+\alpha)^2}{\sigma_u^4} - \frac{1}{\sigma_u^2}\right]$$

Since $k_2 > k_1$, then for P'' to be positive, we need to satisfy the condition

$$\frac{(A+\alpha)^2}{\sigma_u^4} - \frac{1}{\sigma_u^2} > 0$$

$$(A+\alpha) > \sigma_u \tag{B.6}$$

Therefore we conclude that $P_g(A+\alpha)$ is convex upward if we satisfy the condition

$$(A+\alpha) > \sigma_u$$

We note that, if the above condition is not satisfied then $P_g(A+\alpha)$ can be either convex upward or downward.

B.2 Derivation of Equation (3.16)

We recall that

$$P_e = \frac{1}{2}\int_0^{\lambda}\int_0^{2\pi} \operatorname{erfc}\left(\frac{R\cos\theta}{\lambda\sqrt{2}\,\sigma_d}\right) p(R,\theta)\, d\theta dR + \frac{1}{2}\int_{\lambda}^{\infty}\int_0^{2\pi} \operatorname{erfc}\left(\frac{\cos\theta}{\sqrt{2}\,\sigma_d}\right) p(R,\theta)\, dR d\theta \tag{B.7}$$

The first term in (B.7) can be expressed as a product of two integrals in terms of rectangular coordinates x and y. We recall from (3.4), omitting the time dependence,

$$x \triangleq A + \alpha + n_c^d$$

$$y \triangleq n_s^d$$

Therefore, we get

$$P_e = \frac{1}{\sqrt{2\pi}\,\sigma_u^2} \int_{-\lambda}^{\lambda} \exp\left(\frac{-y^2}{2\sigma_u^2}\right) dy \int_{-\lambda}^{\lambda} \frac{1}{2}\,\mathrm{erfc}\left(\frac{x}{\lambda\sqrt{2}\,\sigma_d}\right) \frac{1}{\sqrt{2\pi}\,\sigma_u^2}$$

$$\exp\left[\frac{-(x-A)^2}{2\sigma_u^2}\right] dx$$

$$+ \frac{1}{2}\int_{\lambda}^{\infty}\int_{0}^{2\pi} p(R,\theta)\, dR d\theta - \frac{1}{2}\int_{\lambda}^{\infty}\int_{0}^{2\pi} \mathrm{erf}\left(\frac{\mathrm{Cos}\,\theta}{\sqrt{2}\,\sigma_d}\right) p(R,\theta)\, dR d\theta$$

$$= \frac{1}{2}\,\mathrm{erf}\left(\frac{\lambda}{\sqrt{2}\,\sigma_u}\right) \int_{-\lambda}^{\lambda} \mathrm{erfc}\left(\frac{\rho_d}{\rho_\lambda}\, u\right) \frac{1}{\sqrt{\pi}} \exp -(u-\rho_u)^2 du + \frac{1}{2}\int_{\lambda}^{\infty}$$

$$\cdot\, p(R)dR - \frac{1}{2}\int_{\lambda}^{\infty}\int_{0}^{2\pi} \mathrm{erf}\left(\frac{\mathrm{Cos}\,\theta}{\sqrt{2}\,\sigma_d}\right) p(R,\theta)\, dR\, d\theta \qquad (B.8)$$

where

$$\rho_u^2 = \frac{A^2}{2\sigma_u^2},\quad \rho_\lambda^2 = \frac{\lambda^2}{2\sigma_u^2},\quad \rho_d^2 = \frac{1}{2\sigma_u^2}$$

The expressions for $p(R,\theta)$ and $p(R)$ are [36],

$$p(R) = \frac{R}{\sigma_u^2} \exp\left(-\frac{R^2+A^2}{2\sigma_u^2}\right) I_o\left(\frac{RA}{\sigma_u^2}\right) \qquad (B.9)$$

$$p(R,\theta) = \frac{R}{4\pi\,\sigma_u^2} \exp\left(-\frac{R^2+A^2-2RA\,\mathrm{Cos}\,\theta}{2\sigma_u^2}\right) \qquad (B.10)$$

The last term in (B.8) can be simplified further in terms of the Confluent Hypergeometric functions, using the expansion for erf(·) [11],

$$\operatorname{erf}\left(\frac{\cos\theta}{\sqrt{2}\,\sigma_d}\right) = \frac{2}{\pi}\sum_{n=0}^{\infty}\frac{(-1)^n\,\Gamma(n+1/2)}{(2n+1)!}\,(\rho_d)^{2n+1}$$

$$,F,\left(n+\frac{1}{2},\,2n+2,\,-\rho_d^2\right)\cos(2n+1)\theta$$

$$\triangleq \frac{2}{\pi}\sum_{}^{\infty} f(n)\cos(2n+1)\theta \qquad \text{(B.11)}$$

The series (B.11) is uniformly convergent. Therefore, substituting (B.11) in (B.8) and evaluating the integral with respect to θ, we get,

$$P_e = \frac{1}{2}\operatorname{erf}(\rho_\lambda)\int_{-\rho_\lambda}^{\rho_\lambda}\frac{1}{\sqrt{\pi}}\operatorname{erfc}\left(\frac{\rho_d}{\rho_\lambda}u\right)\exp-(u-\rho_u)^2du + \frac{1}{2}\int_{\lambda}^{\infty}$$

$$.p(R)dR - \sum_{n=0}^{\infty} f(n)\int_{\lambda}^{\infty}\frac{R}{2\pi\,\sigma_u^2}\exp\left(-\frac{R^2+A^2}{2\sigma_u^2}\right)I_{2n+1}\left(\frac{RA}{\sigma_u^2}\right)dR \qquad \text{(B.12)}$$

In the above expression for P_e, the second term is in fact the Marcum's Q-function, which can be evaluated recursively as shown in reference [37]. The first integral and the last integral can be evaluated recursively as shown below.

Considering the first term in (B.12), we can write

$$\int_{-\rho_\lambda}^{\rho_\lambda}\frac{1}{\sqrt{\pi}}\operatorname{erfc}\left(\frac{\rho_\phi}{\rho_u}u\right)\exp-(u-\rho_u)^2du = \int_{-\rho_\lambda}^{\rho_\lambda}\frac{1}{\sqrt{\pi}}\exp-(u-\rho_u)^2du$$

$$-\int_{\rho_\lambda}^{\rho_\lambda} \operatorname{erf}\left(\frac{\rho_d}{\rho_u}\, u\right) \frac{1}{\sqrt{\pi}} \exp -(u-\rho_u)^2 du$$

$$= \frac{1}{2}\operatorname{erf}(\rho_\lambda-\rho_u) + \frac{1}{2}\operatorname{erf}(\rho_u+\rho_\lambda) - \int_{-\rho_\lambda}^{\rho_\lambda} \operatorname{erf}\left(\frac{\rho_d}{\rho_u}\, u\right) \frac{1}{\sqrt{\pi}} \exp -(u-\rho_u^2) du \tag{B.13}$$

We expand the erf(·) in terms of Hermite polynomials [34], as,

$$\operatorname{erf}\left(\frac{\rho_d}{\rho_u}\, u\right) = \frac{1}{\sqrt{\pi}} \sum_{n=0}^{\infty} \frac{(-1)^n}{2^{2n} n!} \left(\frac{\rho_d^2}{\rho_\lambda^2+\rho_d^2}\right) \frac{H_{2n+1}(z)}{2n+1} \tag{B.14}$$

The series (B.14) is uniformly convergent and therefore substituting it in (B.13), it can be shown that,

$$\int_{-\rho_\lambda}^{\rho_\lambda} \operatorname{erf}\left(\frac{\rho_d}{\rho_\lambda}\, u\right) \frac{1}{\sqrt{\pi}} \exp -(u-\rho_u)^2 du = \frac{1}{\sqrt{\pi}} \sum_{n=0}^{\infty} (-1)^n \frac{B_n X_n}{(2n+1)} \tag{B.15}$$

where

$$B_n = \frac{\rho_d^2}{\rho_\lambda^2+\rho_d^2} \frac{1}{n} \frac{1}{2^{2n}} B_{n-1}; \quad B_o = \frac{\rho_d^2}{\rho_\lambda^2+\rho_d^2}$$

$$X_{n+1} = \frac{-2\rho_u}{\sqrt{\pi}} \left[\exp -(\rho_\lambda-\rho_u)^2 + \exp -(\rho_\lambda+\rho_u)^2\right] H_{2n+1}(\rho_\lambda)$$

$$- \frac{1}{\sqrt{\pi}} \left[\exp -(\rho_\lambda-\rho_u)^2 - \exp -(\rho_\lambda+\rho_u)^2\right] H_{2n+2}(\rho_\lambda) + 4\rho_u^2 X_n$$

$$X_o = -\frac{1}{\sqrt{\pi}} \exp -(\rho_\lambda-\rho_u)^2 + \frac{1}{\sqrt{\pi}} \exp -(\rho_\lambda+\rho_u)^2 + \rho_u \operatorname{erf} (\rho_\lambda+\rho_u)$$

$$+ \rho_u \operatorname{erf} (\rho_\lambda-\rho_u)$$

The last term in (B.12) can be evaluated by using the power series expansion of Bessel functions [35]

$$I_{2n+1}\left(\frac{RA}{\sigma_u^2}\right) = I_{2n+1}(2\rho\rho_\lambda) = \sum_{r=0}^{\infty} \frac{\rho_\lambda^{2n+2r+1}}{r!(2n+2r+1)!} \rho^{2n+2r+1} \quad \text{(B.16)}$$

where $\rho \triangleq \frac{R}{\sqrt{2}\,\sigma_u}$

Substituting (B.16) in the last term of (B.12), it can be shown that

$$\int_\lambda^\infty \frac{R}{\sigma_u^2} \exp \frac{-(R^2+A^2)}{2\sigma_u^2} I_{2n+1}\left(\frac{RA}{\sigma_u^2}\right) dR = \sum_{r=0}^{\infty} B_{r,n} \cdot P_{r+n}$$

where

$$B_{r,n} = \frac{\rho_u^2(n+r+1/2)}{r(2n+r+1)} B_{r-1,n}$$

$$B_{o,n} = \frac{\rho_u^2(n+1/2)}{2n(2n+1)} B_{o,n-1}$$

$$B_{o,o} = \frac{\rho_u}{2\sqrt{\pi}} \exp(-\rho_u^2)$$

Combining (B.12), (B.15) and (B.17), we obtain the expression given in (3.16).

B.3 Proof of Uniform Convergences of Equations (B.11) and (B.14)

(a) Uniform convergence of (B.11)

Recall that

$$\operatorname{erf}\left(\frac{\cos\theta}{\sqrt{2}\,\sigma_d}\right) = \frac{2}{\sqrt{\pi}} \sum_{n=0}^{\infty} \frac{(-1)^n \Gamma(n+1/2)}{(2n+1)!}\, \rho_d^{2n+1}\, {}_1F_1\left(n+\tfrac{1}{2},\ 2n+2,\ -\rho_d^2\right) \cos(2n+1)\theta \qquad \text{(B.18)}$$

We use the Weirtrass M-test for testing the uniform convergence of the above series as given in reference [40]. Let

$$f(n) \triangleq \frac{(-1)^n \Gamma(n+1/2)}{(2n+1)!}\, \rho_d^{2n+1}\, {}_1F_1\left(n+\tfrac{1}{2},\ 2n+2,\ -\rho_d^2\right) \cos(2n+1)\theta$$

Then

$$|f(n)| \le \frac{\Gamma(n+1/2)}{(2n+1)!}\, \rho_d^{2n+1} \qquad \text{(B.19)}$$

because ${}_1F_1(a, b, -x) \le 1 \quad$ for $\quad 0 \le a \le b; \quad 0 \le x.$

Substituting $\Gamma(n+1/2) = \sqrt{\pi}\,\dfrac{2n!}{2^{2n}\, n!}$ in (B.19)

we get

$$f(n) \le \frac{\sqrt{\pi}}{2^{2n}} \frac{\rho_d^{2n+1}}{n!} \frac{1}{2n+1}$$

Since

$$\frac{\rho_d^{2n}}{n!} < e^{\rho_d^2}$$

for

$$f(n) \le \rho_d \frac{\sqrt{\pi}}{2^{2n}}\, e^{\rho_d^2} \frac{1}{(2n+1)} \qquad \text{(B.20)}$$

which is convergent for all finite ρ_d.

Therefore, the series (B.11) in uniformly convergent.

(b) Uniform Convergence of (B.14)

Recall that

$$\operatorname{erf}\left(\frac{\rho_d}{\rho_\lambda} u\right) = \frac{1}{\sqrt{\pi}} \sum_{n=0}^{\infty} \frac{(-1)^n}{2^{2n}\, n!} \left(\frac{\rho_d^2}{\rho_\lambda^2+\rho_d^2}\right) \frac{H_{2n+1}(u)}{(2n+1)} \tag{B.21}$$

$$|f(n)| \triangleq \left|\frac{(-1)^n}{2^{2n}\, n!} \left(\frac{\rho_d^2}{\rho_\lambda^2+\rho_d^2}\right) \frac{H_{2n+1}(u)}{2n+1}\right| \leq \frac{1}{2^{2n}\, n!} \frac{|H_{2n+1}(u)|}{2n+1}$$

We note that [35]

$$H_{2n+1}(u) \leq \sqrt{2}\, e^{2u\sqrt{n}}$$

Therefore

$$|f(n)| \leq \frac{\sqrt{2}}{2^{2n}} \frac{1}{2n+1} \frac{e^{2u\sqrt{n}}}{n!}$$

$$\leq \sqrt{2}\, \frac{1}{2^{2n}(2n+1)} \exp\left(e^{2u}\right)$$

The last step follows, because

$$\frac{(e^{2u})^{\sqrt{n}}}{n!} \leq \exp\left(e^{2u}\right)$$

The series

$$\frac{\sqrt{2}\, \exp\left(e^{2u}\right)}{2^{2n}(2n+1)}$$

is absolutely convergent.

Therefore, the series (B.21) is uniformly convergent.

APPENDIX C

Derivations of Equations (4.16), (4.18) and Approximate Expressions of Likelihood Ratio

C.1 Derivation of Equations (4.16) and (4.18)

Consider the numerator of expression (4.15), which we recall as

$$\int_0^{\infty}\int_0^{2\pi} R_k \exp\left\{\frac{f_k}{\sigma^2}\left[x_k \cos(\lambda_k+\rho_k) + y_k \sin(\lambda_k+\rho_k)\right]\right\} \exp\left(\frac{-f_k^2}{2\sigma_d^2}\right)$$

$$\exp\left\{-\frac{1}{2\sigma_u^2}\left[R_k^2 + (q_k+\alpha)^2 - 2R_k(q_k+\alpha)\cos\lambda_k\right]\right\} dR_k d\lambda_k$$

Noting that $f_k = 1$ and $\rho_k = 0$ for a hard-limiter, we get,

$$\int_0^{\infty}\int_0^{2\pi} R_k \exp\left\{\frac{S_k}{\sigma_d^2}\cos(\lambda_k-\gamma_k)\right\} \exp\left\{-\frac{1}{2\sigma_u^2}\left[R_k^2+(q_k+\alpha)^2-2R_k(q_k+\alpha)\right.\right.$$

$$\left.\left.\cos\lambda_k\right]\right\} dR_k d\lambda_k \qquad (C.1)$$

where

$$S_k = \sqrt{(x_k)^2+(y_k)^2};\ \gamma_k = \tan^{-1}(y_k/x_k)$$

Using the expansion of $\exp\left[S_k/\sigma_d^2 \cos(\lambda_k-\gamma_k)\right]$ in terms of Bessel functions as given in Appendix A, equation (A.3), and evaluating the integral with respect to λ_k we

get,

$$I_o\left(\frac{S_k}{\sigma_d^2}\right) + \sum_{n=1}^{\infty} \int_0^{\infty} R_k\, I_n\left(\frac{S_k}{\sigma_d^2}\right) I_n\left[\frac{R_k}{\sigma_u^2}(q_k+\alpha)\right]$$

$$\exp\{-\frac{1}{\sigma_u^2}[R_k^2 + (q_k+\alpha)^2]\}\ \mathrm{Cos}\ n\gamma_k\ dR_k$$

Then evaluating the integral with respect to R_k, we obtain

$$\left[I_o\left(\frac{S_k}{\sigma^2}\right) + 2\sum_{n=1}^{\infty} \frac{\Gamma(n/2+1)}{n!}\left(\frac{q_k+\alpha}{\sqrt{2}\sigma_u}\right)^n, F, \left(\frac{n}{2}, n+1, -\left(\frac{q_k+\alpha}{\sqrt{2}\sigma_u}\right)^2\right)\right]$$

$$I_o\left(\frac{S_k}{\sigma_d^2}\right)\ \mathrm{Cos}\ n\ \gamma_k$$

A similar expression can be obtained following the same method for the denominator of the likelihood ratio given in (4.15).

Then the likelihood ratio with these expressions become,

$$\frac{I_o\left(\frac{S_k}{\sigma_d^2}\right) + 2\sum_{n=1}^{\infty} \frac{\Gamma(n/2+1)}{n!}\left(\frac{q_k+\alpha}{\sqrt{2}\sigma_u}\right)^n, F, \left(\frac{n}{2}, n+1, -\left(\frac{q_k+\alpha}{\sqrt{2}\sigma_u}\right)^2\right)}{I_o\left(\frac{S_k}{\sigma_d^2}\right) + 2\sum_{n=1}^{\infty} \frac{\Gamma(n/2+1)}{n!}\left(\frac{q_k-\alpha}{\sqrt{2}\sigma_u}\right)^n, F, \left(\frac{n}{2}, n+1, -\left(\frac{q_k-\alpha}{\sqrt{2}\sigma_u}\right)^2\right)} \underset{-1}{\overset{+1}{\gtrless}}$$

$$I_n\left(\frac{S_k}{\sigma_d^2}\right)\ \mathrm{Cos}\ \gamma_k$$

$$I_n\left(\frac{S_k}{\sigma_d^2}\right)\ \mathrm{Cos}\ n\ \gamma_k$$

which is the general form of the L.R. for a hard-limiting channel.

After cross multiplying and taking all the terms to one side, we obtain the likelihood ratio as

$$\sum_{n=1}^{\infty} \{g_n (q_k+\alpha) - (-1)^n g_n (q_k-\alpha)\} I_n \left(\frac{S_k}{\sigma_d^2}\right) \text{Cos } n \gamma_k \gtrless_{-1}^{+1} 0$$

which is the expression given in (4.18) where

$$g_n(q_k \pm \alpha) \triangleq \frac{\Gamma(n/2+1)}{n!} \left(\frac{q_k \pm \alpha}{\sqrt{2}\sigma_u}\right)^n {}_1F_1\left(\frac{n}{2}, n+1, -\left(\frac{q_k \pm \alpha}{\sqrt{2}\sigma_u}\right)^2\right)$$

To obtain expression (4.16) for the case of no ISI, we set $\alpha = 0$ in the above expression. Since all even terms cancel out, we get

$$\sum_{n=1}^{\infty} g_{2n-1}(q_k) I_{2n-1} \left(\frac{S_k}{\sigma_d^2}\right) \text{Cos } (2n-1) \gamma_k \gtrless_{-1}^{+1} 0$$

C.2 Derivation of the Approximate Expressions

Case (a) $q_k > |\alpha|_{max}$; High uplink CNR

To derive the assymptotic value when $\sigma_u \to 0$ we use the assymptotic expansion of the Confluent Hypergeometric function [53] for large argument given as

$${}_1F_1(a,b,-x) = x^{-a} \frac{\Gamma(b)}{\Gamma(b-a)} \sum_{n=0}^{L} \frac{(a)_n (1+a-b)_n}{n!} x^{-n} + O(|x|)^{-a-L+1}$$

where $(a)_n = a(a+1)(a+2)\ldots(a+n-1)$

$(a)_o = 1$

Recall that

$$g_n(q_k \pm \alpha) = \frac{\Gamma(n/2+1)}{n!} \left(\frac{q_k \pm \alpha}{\sqrt{2}\sigma_u}\right)^n {}_1F_1\left(\frac{n}{2}, n+1, -\left(\frac{q_k \pm \alpha}{\sqrt{2}\sigma_u}\right)^2\right)$$

Then for large $(q_k \pm \alpha/\sqrt{2}\sigma_u)$, using the above assymptotic expansion we obtain,

$$g_n(q_k \pm \alpha) = 1 + \frac{n/2(-n/2)}{x} + \frac{(n/2)(n/2+1)(-n/2)(-n/2+1)}{2!\, x^2} + \ldots$$

where

$$x \triangleq \left(\frac{q_k \pm \alpha}{2\sigma_u^2}\right)^2$$

Therefore as $\sigma_u \to 0$, $x \to \infty$ and $g_n(q_k \pm \alpha) = 1$

next we consider the closed eye case $q_k < |\alpha|$ and $\alpha < 0$

Here we note that

$$g_n(q_k + \alpha) = \frac{\Gamma(n/2+1)}{n!} \left(\frac{q_k + \alpha}{\sqrt{2}\sigma_u}\right)^n {}_1F_1\left(\frac{n}{2}, n+1, -\left[\frac{q_k + \alpha}{\sqrt{2}\sigma_u}\right]^2\right)$$

$$= \frac{\Gamma(n/2+1)}{n!} (-1)^n \left(\frac{|\alpha| - q_k}{\sqrt{2}\,\sigma_u}\right)^n {}_1F_1\left(\frac{n}{2}, n+1, -\left[\frac{|\alpha| - q_k}{\sqrt{2}\,\sigma_u}\right]^2\right)$$

Therefore

$$g_n(q_k + \alpha) \to (-1)^n \text{ as } \sigma_u \to 0$$

Also,

$$g_n(q_k - \alpha) = g_n(q_k + |\alpha|)$$

Therefore

$$g_n(q_k - \alpha) \to 1 \text{ as } \sigma_u \to 0$$

Combining above relations we get

$$\{g_n(q_k+\alpha) - (-1)^n g_n(q_k-\alpha)\} \to 0 \text{ as } \sigma_u \to 0$$

Next consider the case $\alpha > 0$ and closed eye. i.e. $q_k < |\alpha|$. Again, we note that

$$g_n(q_k+\alpha) \to 1 \text{ as } \sigma_u \to 0$$

$$g_n(q_k-\alpha) = (-1)^n g_n(\alpha-q_k) \text{ where } (\alpha-q_k) > 0$$

Therefore

$$g_n(q_k-\alpha) \to (-1)^n \text{ as } \sigma_u \to 0$$

Combining above relations as before we get,

$$\{g_n(q_k+\alpha) - (-1)^n g_n(q_k-\alpha)\} \to 0 \text{ as } \sigma_u \to 0$$

REFERENCES

[1] Puente, J.G. and Werth, A.M., "Demand-assigned service for Intelsat global network", IEEE Spectrum, pp. 59-69, January 1971.

[2] Puente, J.G. and Schmidt, W.G. and Werth, A.M., "Multiple-access techniques for commerical satellites", IEEE Proceedings, Vol. 59, No. 2, pp. 218-229, February 1971.

[3] Gabbard, A. and Kaul, P., "Time division multiple access", Eascon' 74, Conference Record, pp. 179-184, 1974.

[4] Whelan, J.W., "Analog-FM vs Digital-PSK transmission", IEEE Trans. on Communications, Vol. COM-14, No. 3, pp. 275-282, June 1966.

[5] Chakraborty, D., "Intelsat IV satellite system (voice) channel capacity versus earth-station performance", IEEE Trans. on Commun. Technol. Vol. COM-20, pp. 355-362, June 1971.

[6] Gould, R.G. and Lum, Y.F., Communications satellite systems: An overview of the technology, IEEE Press, 1975.

[7] Satellite communications system technology, conference Publication No. 126, International Conf. On Satellite Commun. System Technol., IEE Publication, April 1975.

[8] Intelsat/IEE International Conference on Digital Satellite communication, November 1969.

[9] Dalgleish, D.I. and Reed, A.G., "Some comparisons of the traffic-carrying capacity of communication satellite using digital techniques with the capacity of satellites using frequency modulation", Intelsat/IEE International Conf. on Digital Satellite Communications, pp. 226-240, Nov. 1969.

[10] Hetrakul, P., CPSK Transmission through nonlinear channels, Ph.D. thesis, McMaster University, 1976.

[11] Jain, P.C. and Blackman, N.M., "Detection of a PSK signal transmitted through a hard-limited channel" IEEE Trans. Inform. Theory, Vol. IT-19, pp. 623-630, Sept. 1973.

[12] Lyons, R.G., "The effect of a bandpass nonlinearity on signal detectability", IEEE Trans. Commun. Technol., Vol. COM-22, pp. 51-60, Jan. 1973.

[13] Davisson, L.D. and Milstein, L.B., "On the performance of digital communication systems with bandpass limiters - Part I: One link systems", IEEE Trans. Commun. Technol., Vol. COM-20, pp. 972-975, Oct. 1972.

[14] Mizuno, T., Mornaga, N. and Namekawa, T., "Transmission characteristics of an M-ary Coherent PSK signal via a cascade of N bandpass hard-limiters", IEEE Trans. Commun., Vol. COM-24, pp. 540-545, May 1976.

[15] Hetrakul, P. and Taylor, D.P., "The effects of transponder nonlinearity on binary CPSK signal transmission", IEEE Trans. Commun., Vol. COM-24, pp. 546-553, May 1976.

[16] Forsey, R.J., Gooding, V.E., McLane, P.J. and Campbell, L.L., "M-ary PSK transmission via a coherent two-link channel exhibiting AM-PM and AM-PM nonlinearities", Conference Record, International Conference on Communications, pp. 16.2-335 - 16.2-339, June 1977.

[17] Jain, P., Huang, T.C., Woo, K.T., and Omura, J.K., "Detection of MPSK signals transmitted through a nonlinear satellite repeater", Conference Record NTC'77, National Telecommunications Conference, pp. 26:2-1 - 26:2-4, Dec. 1977.

[18] Shimbo, O., Fang, R.J. and Celebiler, M., "Performance of M-ary PSK systems in Gaussian noise and intersymbol interference", IEEE Trans. Inform. Theory, Vol. IT-19, pp. 47-58, Jan. 1973.

[19] Shimbo, O. and Celebiler, M., "The probability of error due to intersymbol interference and Gaussian noise in digital communication systems", IEEE Trans. Commun. Technol., Vol. COM-19, pp. 113-119, April 1971.

[20] Ho, E.Y. and Yeh, Y.S., "A new approach for evaluating the error proability in the presence of intersymbol interference and additive Gaussian noise", Bell Syst. Tech. J., Vol. 49, pp. 2249-2266, Nov. 1970.

[21] Stroud, A.H., Approximate Calculation of Multiple Integrals, Prentice Hall, Inc., 1971.

[22] Thomas, C.M., Weidner, M.Y. and Dunrani, S.H., "Digital Amplitude-Phase Keying with M-ary Alphabets", IEEE Trans. Commun. Technol., Vol. COM-22, pp. 168-180, Feb. 1974.

[23] Berman, A.L. and Mahle, C.E., "Nonlinear phase shift in travelling wave tubes as applied to multiple access communication satellites", IEEE Trans. Commun. Technol., Vol. COM-18, pp. 37-48, Feb. 1970.

[24] Lesh, J.R., "Signal to noise ratios in coherent Soft-limiters", IEEE Trans. Commun. Technol., Vol. COM-22, pp. 803-811, June 1974.

[25] Gradshteyn, I.S. and Ryzhek, I.M., Table of Integrals, Series, and Products, Translated by A. Jeffrey, New York; Academic Press 1965.

[26] Saltzberg, B.R., "Intersymbol interference error bounds with application to ideal bandlimiting signalling", IEEE Trans. Inform. Theory, Vol. IT-14, pp. 563-568, July 1968.

[27] Lugannani, R., "Intersymbol Interference and probability of error in digital systems", IEEE Trans. Inform. Theory, Vol. IT-15, pp. 682-688, Nov. 1969.

[28] Glave, F.E., "An upper bound on the probability of error due to intersymbol interference for correlated digital signals", IEEE Trans. Inform. Theory, Vol. IT-18, pp. 356-363, May 1972.

[29] Mathews, J.W., "Sharp error bounds for intersymbol interference", IEEE Trans. Inform. Theory, Vol. IT-19, pp. 440-447, July 1973.

[30] McLane, P.J., "Lower bounds for finite intersymbol interference error rates", IEEE Trans. Commun. Technol., Vol. COM-22, pp. 853-857, June 1974.

[31] Dresher, M., "Moment Space and inequalities", Duke Math. Jour., Vol. 20, pp. 261-271, June 1953.

[32] Yao, K. and Tobin, R., "Moment space upper and lower error bounds for digital systems with intersymbol interference", IEEE Trans. Inform. Theory, Vol. IT-22, pp. 65-74, Jan. 1976.

[33] Hetrakul, P., Taylor, D.P. and Haykin, S.S., "Effect of a soft-limiter on the error rate of an M-ary CPSK system", Conference Record ICC'74, International Conf. on Commun., pp. 44B-1, 44B-5, June 1974.

[34] Lebdev, N.N., Special Functions and Their Applications, pp. 68-76, Prentice Hall, Inc., N.J. 1965.

[35] Tranter, C.J. Bessel Functions with Some Physical Applications, Harf Publishing Comp., N.Y. 1968.

[36] Davenport Jr., W.B. and Root, W.L., An Introduction to the Theory of Random Signal and Noise, pp. 165-167, McGraw-Hill, N.Y. 1958.

[37] Brennan, L.E. and Reed, I.S., "A recursive method of computing the Q-function", IEEE Trans. Inform. Theory, Vol. IT-11, pp. 312-313, April 1960.

[38] Karlin, S. and Studden, W.J., Tchebyshev Systems: with Applications in Analysis and Statistics, New York Interscience, 1966.

[39] Godwin, H.J., Inequalities on Distribution Functions, Griffins Statistical Monographs - Hafner Publi. Comp. 1965.

[40] Rudin, W., Principles of Mathematical Analysis, pp. 147-149, McGraw-Hill, 1953.

[41] Austin, M.E., "Decision feedback equalization for digital communication over dispersive channels", MIT/R.L.E. Tech. Rep. 461, Aug. 1967.

[42] Lucky, R.W., "Automatic equalization for digital communication", BSTJ, Vol. 44, pp. 547-588, April 1965.

[43] George, D.A., "Match filters for interfering signals", IEEE Trans. Inform. Theory, Vol. IT-11, Jan. 1965.

[44] Lucky, J.W., Salz, J. and Weldon Jr., E.J., Principles of Data Communication, McGraw-Hill, N.Y. 1968.

[45] Lawless, W.J., Binary Signalling over Nonlinear Channels, Ph.D. Thesis, Polytechnic Institute of Brooklyn, 1971.

[46] Taylor, D.P., "The estimate feedback equalizer: A suboptimum nonlinear receiver", IEEE Trans. Commun., Vol. COM-21, pp. 979-990, Sept. 1973.

[47] Mesiya, M.F., McLane, P.J. and Campbell, L.L., "Maximum likelihood sequence estimation of binary sequences transmitted over bandlimited nonlinear channels", IEEE Trans. Commun., Vol. COM-25, pp. 633-643, July 1977.

[48] Duttweiler, D.L., Mazo, J.S. and Messerschmitt, D.G., "An upper bound on the error probability in decision-feedback equalization", IEEE Trans. Inform. Theory, Vol. IT-20, pp. 490-497, July 1974.

[49] Krishnamurthy, J. and Dante, H.M., "Bounds on probability of error in decision feedback equalizers", IEEE Trans. Aero. and Elect. Syst., Vol. AES-12, pp. 173-178, March 1976.

[50] Giovanni, Tamburelli, "On the exact error probability evaluation of a decision feedback and feedforward receiver for finite impulse response channel", Conference Record, NTC' 77, Nat. Telecom. Conf., pp. 11.3-7 to 11.3-5, Dec. 1977.

[51] Forney, G.D. Jr., "Maximum likelihood sequence estimation of digital sequences in the presence of intersymbol interference", IEEE Trans. Inform. Theory, Vol. IT-18, pp. 363-378, May 1972.

[52] Van Trees, H.L., Detection, Estimation and Modulation Theory, John Wiley Pub., N.Y. 1968.

[53] Slater, K.J., Confluent Hypergeometric Functions, Cambridge Univ. Press, 1960.

[54] Ekanayake, N. and Taylor, D.P., "CPSK signalling over hard-limited channels in additive Gaussian noise and intersymbol interference", IEEE Trans. on Inform. Theory, Vol. IT-25, pp. 62-68, Jan. 1979.

[55] Ekanayake, N. and Taylor, D.P., "Intersymbol interference error bounds for hard-limited satellite channels", Electronic Letters, Vol. 13, pp. 498-500, 1977.

[56] Ekanayake, N. and Taylor, D.P., "Binary CPSK performance analysis for saturating band-limited channels", To appear in IEEE Trans. on Commun., Vol. COM-27, March 1979.